# ABSTRACT

| | |
|---|---|
| Title of Dissertation: | DESIGN AND PILOT STUDY FOR AN EFFICIENT HIGH-THROUGHPUT AUTOMATED COMPUTER-VISION GUIDED INTELLIGENT DE-CALYXING MACHINE FOR POST-HARVEST STRAWBERRY PROCESSING |
| | John Lin, Doctor of Philosophy, 2016 |
| Dissertation Directed By: | Professor Yang Tao, Fischell Department of Bioengineering |

Strawberries harvested for processing as frozen fruits are currently de-calyxed manually in the field. This process requires the removal of the stem cap with green leaves (i.e. the calyx) and incurs many disadvantages when performed by hand. Not only does it necessitate the need to maintain cutting tool sanitation, but it also increases labor time and exposure of the de-capped strawberries before in-plant processing. This leads to labor inefficiency and decreased harvest yield. By moving the calyx removal process from the fields to the processing plants, this new practice would reduce field labor and improve management and logistics, while increasing annual yield.

As labor prices continue to increase, the strawberry industry has shown great interest in the development and implementation of an automated calyx removal system. In response, this dissertation describes the design, operation, and performance

of a full-scale automatic vision-guided intelligent de-calyxing (AVID) prototype machine. The AVID machine utilizes commercially available equipment to produce a relatively low cost automated de-calyxing system that can be retrofitted into existing food processing facilities.

This dissertation is broken up into five sections. The first two sections include a machine overview and a 12-week processing plant pilot study. Results of the pilot study indicate the AVID machine is able to de-calyx grade-1-with-cap conical strawberries at roughly 66 percent output weight yield at a throughput of 10,000 pounds per hour.

The remaining three sections describe in detail the three main components of the machine: a strawberry loading and orientation conveyor, a machine vision system for calyx identification, and a synchronized multi-waterjet knife calyx removal system. In short, the loading system utilizes rotational energy to orient conical strawberries. The machine vision system determines cut locations through RGB real-time feature extraction. The high-speed multi-waterjet knife system uses direct drive actuation to locate 30,000 psi cutting streams to precise coordinates for calyx removal.

Based on the observations and studies performed within this dissertation, the AVID machine is seen to be a viable option for automated high-throughput strawberry calyx removal. A summary of future tasks and further improvements is discussed at the end.

# DESIGN AND PILOT STUDY FOR AN EFFICIENT HIGH-THROUGHPUT AUTOMATED COMPUTER-VISION GUIDED INTELLIGENT DE-CALYXING MACHINE FOR POST-HARVEST STRAWBERRY PROCESSING

By

John Lin

Dissertation submitted to the Faculty of the Graduate School of the
University of Maryland, College Park, in partial fulfillment
of the requirements for the degree of
Doctor of Philosophy
2016

Advisory Committee:
Professor Yang Tao, Chair
Professor Yiannis Aloimonos
Professor Yu Chen
Professor Benjamin Shapiro
Professor Adel Shirmohammadi

## Preface

The production of foods is a globally competitive field. Processors are required to produce quality foods with the highest possible efficiency and lowest possible cost. As a result, the industrialization of food processing has replaced many traditional hand methods. This is seen in the agricultural industry through the wide use of semi-automated and fully automated pre- and post-harvest equipment. However, one area of limited automation is in the field of highly perishable delicate fruit. In particular, automating the processing of post-harvest strawberries has been a particularly difficult problem to solve for the industry. This can be attributed to the strawberry's easily bruised skin and extreme variation in firmness, size, shape, and color.

This dissertation focuses on developing a fully automated system that is able to quickly and efficiently perform post-harvest processing on conical strawberries. The technology used here can be adapted to other food applications.

**Acknowledgements**

I am extremely grateful to have had the opportunity to work with the University of Maryland and the California Strawberry Commission on this industry-changing technology. Specifically, I would like to express my gratitude towards my University of Maryland faculty advisors: Professor Yang Tao, Professor Benjamin Shapiro, Professor Adel Shirmohammadi, Professor Yiannis Aloimonos, and Professor Yu Chen, each of whom have had a critical role in making me the engineer I am today. I would also like to thank all the members and affiliates of the California Strawberry Commission. Without their assistance and collaboration, this project could not exist. In addition, I would like to thank my colleagues Xin Chen, Gary Seibel, Maxwell Holmes, Robert Vincent, Frank C. Pogoda, Luke Mahon, Ryan Gentry, Ben Krupsaw, and Eric Borrero, all of whom have been inspirational examples of hardworking, passionate engineers.

Finally, I would like to extend my deepest gratitude to my loving wife and to my parents, who have always supported and encouraged me in all my endeavors.

## Table of Contents

## List of Tables

## List of Figures

## List of Terms & Abbreviations

| | |
|---|---|
| ATP | Adenosine triphosphate |
| AVID machine | Automated Vision-guided Intelligent De-calyxing machine |
| *BcLp* vector | Berry center of gravity and Leaf pixel vector |
| Berry | The red fruit portion of the strawberry |
| Calyx | The green leaf portion of the strawberry |
| CCD | Charge-coupled device |
| CI | Confidence Interval |
| CNC | Computer Numerical Control |
| *Cog* | Center of gravity |
| CPSF | Cal Pacific Specialty Foods |
| CSC | California Strawberry Commission |
| HSI | Hue Saturation Intensity |
| IQF partial | A partial berry that is graded as Instant Quick Freeze |
| IQF whole | A whole berry that is graded as Instant Quick Freeze |
| Larger berry | A strawberry more than 1.25 inch in diameter |
| Medium berry | A strawberry between 5/8 inch and 1.25 inch in diameter |
| MOE | Margin of Error |
| OSHA | Occupational Safety and Health Administration |
| PCA | Principle Component Analysis |
| ROI | Region of Interest |
| Small berry | A strawberry less than 5/8 inch in diameter |
| SS304 | Austenitic 304 Stainless Steel |
| SS316 | Austenitic 316 Stainless Steel |
| UHMW | Ultra High Molecular Weight Polyethylene |
| UMD | University of Maryland |
| White shoulder | The white color region surrounding the calyx of some strawberries |

# Chapter 1: Overall Introduction

In 2014, processed strawberries in the U.S. reached annual evaluation of over $241 million, growing 30 percent over the previous year (Noncitrus Fruits and Nuts 2014 Summary, 2015). This represents over 550 million pounds of strawberries harvested for processing. These processed strawberries end up in foods such as ice cream, yogurt, juices, jams and jellies, and baked goods. However, before these strawberries reach the consumer, the calyx must be removed before each strawberry is individually quick-frozen to preserve taste and quality. According to the California Strawberry Commission (CSC), this especially labor-intensive process can more than double the time required for fruit picking. In addition, strawberry growers face significant challenges in finding field workers willing to use the sharp hazardous instruments for harvesting. Furthermore, the cutting tools are reused many times without sanitizing, which may serve as a vehicle for pathogen contamination (see Figure 1).


**Figure 1.** Field laborer using a cutting tool to manually remove strawberry calyx (Tao, California Strawberry Commission Annual Report 2012-2013, 2013).

This time-consuming and potentially hazardous process is raising the cost of processed strawberry products, reducing consumption, and jeopardizing American competitiveness in the world market. In 2012, the University of Maryland's Bio-imaging and Machine Vision Laboratory proposed a collaboration with the CSC to design and implement a technology for automated calyx removal on the processing line, thereby engendering significant cost savings, improving food safety, and enhancing the viability of strawberry processing in the U.S.

Our automated strawberry calyx removal system focuses on addressing four major concerns within today's frozen strawberry market. First, according to the CSC, it is difficult to find workers willing to harvest strawberries for processing, simply

because workers dislike handling sharp tools. To add to this concern, harvesting speed is incentivized, resulting in increased risk of both finger laceration and product contamination. Second, maintaining the sanitation of the cutting tools commonly used in-field during harvesting is a challenge. Decaying strawberry residue left on the cutting tools presents a potential for product contamination. With the warm weather and long hours of tool use, these conditions can create a serious health and food-safety risk. Third, the post-harvest quality and safety of the strawberry harvest is directly related to the speed with which the cut fruit can proceed from field to freezer. The strawberry industry's current manual labor-based system greatly limits the field-to-freezer speed. Fourth, due in part to comparatively high labor costs, U.S. frozen strawberry producers are facing severe challenges from lower-cost international competitors such as Mexico, China, and Chile (FAOSTAT, 2013). To combat this labor cost disadvantage and compete effectively in the world market, the U.S. processed strawberry industry must seek advanced technologies that increase efficiencies in the harvesting process. Consequently, strawberry growers and processors have a strong interest in an innovative, rapid, and safe automated calyx removal method that can be performed inside the processing facility rather than the field. Such an innovation would improve worker efficiency, safety, and job satisfaction, while also improving food safety, increasing product throughput, and enabling the U.S. industry to mitigate its labor cost disadvantages and compete effectively with international competitors on the world market.

This project's long-term goal is to revolutionize strawberry post-harvesting practices through the introduction of a new automated technology that will relegate

in-field calyx cutting to the dustbins of history. This goal of moving the calyx removal process from the field to the processing plant will be accomplished by developing an automated, optical-guided calyx cutting technology featuring a bladeless high-pressure thin waterjet knife. This new technology will have a 100+ strawberries/sec per machine processing capacity and will significantly reduce field labor and strawberry exposure to in-field heat and contaminants. Each of our proposed de-calyxing machines yields a production equivalent to a minimum of 30 laborers.

This dissertation is organized into the following chapters. Chapter 2 details the overall objectives of this dissertation research. Chapter 3 provides background and significance around the processed strawberry industry and its current concerns. Chapter 4 reviews relevant literature and technology used during the design process of the AVID machine. Chapter 5 provides an overview of the AVID machine. Chapter 6 presents the results of a 12-week pilot study. Chapters 7, 8, and 9 describe in detail the three main components of the AVID machine: material handling, machine vision, and waterjet cutting system. These chapters focus on each subsystem's design methodology and efficacy. Chapter 10 follows with overall conclusions. Chapter 11 provides an overview of the AVID machine's potential economic impact, and Chapter 12 describes suggestions for future improvements and studies.

# Chapter 2: Overall Objective

The main goal of this research was to design, build, and implement a commercially viable automated machine capable of de-calyxing strawberries at a throughput and accuracy that exceeds industry expectations. This research utilized three main components to achieve this goal: a material handling method, a machine vision algorithm, and a waterjet cutting system. The material handling method first oriented and singulated the strawberries through the use of rotational energy. Once the strawberries were oriented and evenly spaced from one another, the color-based real-time machine vision algorithm identified key features that could determine an appropriate cut location. The multi-waterjet cutting system used these coordinates to quickly position waterjet cutting streams to remove the calyx. Specifically, the objectives of Chapters 7, 8, and 9 were to:

1. Design and determine the efficacy of a field-ready material handling system that is able to orient a vast majority of conical strawberry cultivars.
2. Develop and quantitatively assess a real-time segmentation algorithm to identify strawberry features and locate an appropriate cut-line position.
3. Develop and investigate the use of a high-speed waterjet cutting system for calyx removal.

Ultimately, the goal of this dissertation is to present a method for developing a fully automated strawberry calyx removal technology for retrofitting existing or new

food processing lines. This would decrease the likelihood of food contamination, while increasing overall quality and yield.

# Chapter 3: Background and Significance

This chapter provides a basic understanding of the frozen strawberry industry. This includes an overview of how product is produced and sold, the variability of strawberry size and shape, current labor issues faced by the industry, and a snapshot of the global frozen strawberry economy.

## 3.1 Frozen Strawberry Industry

Strawberries consist of two markets: fresh and processed. The growth of both markets is dependent on each other's success. It is estimated that the typical strawberry farmer allocates 80 percent of his strawberries to the fresh market and 20 percent to the frozen market (Noncitrus Fruits and Nuts 2014 Summary, 2015). The delicate and perishable nature of fresh strawberries requires that when markets are saturated, any excess berries be quickly frozen. This allows frozen strawberries to gradually be introduced into the market according to demand. Freezing strawberries also allows the fruit to be exported globally. Therefore, the processed strawberry market provides economic stability and diversification to the industry.

Trailing only grapes and apples, fresh strawberries are the 3rd largest non-citrus fruit crop in the U.S., with annual production valued at $2,623,625,000 (Noncitrus Fruits and Nuts 2014 Summary, 2015). Strawberry production involves repeated fruit bearing and multiple harvests per season, making strawberries the highest tonnage per acre (25 tons/acre) crop among all non-citrus fruits (Noncitrus Fruits and Nuts 2015 Summary, 2015). The labor costs to harvest this fruit can comprise up to 60 percent of overall production costs (Chase, 2012). It is estimated

that twice the amount of labor is necessary to prepare a strawberry for processing compared to picking for the fresh market.

The current method of calyx removal involves in-field use of cutting blades. The strawberry is picked from the vine, de-calyxed on the spot, and then tossed into a bin. This bin is then transported to a nearby processing facility, where berries are stored in refrigerated areas until enough quantity is accumulated for the instant quick freezing (IQF) process. De-calyxed berries can at times be stored for up to two days in refrigerated areas before they are sent to IQF. This can result in yield loss, decreased quality, and increased nutrient decline (Daming Dong, 2013) (Youngjae Shina, 2007) (Mohammad Ali Sahari, 2004).

### 3.2 Production and Utilization

Frozen strawberry processors in general categorize strawberries designated for processing as IQF whole, IQF partial, and juice quality. These categories are then further broken down into grades and sizes. Each variation has an associated price, with the most valuable typically being medium sized IQF whole. The main distinguishing factors between the three categories are the size and quality of berry retained after de-calyxing (Grading Manual for Frozen Strawberries, 1992). A depiction of the strawberries and their expected categorization is shown in Figure 2.

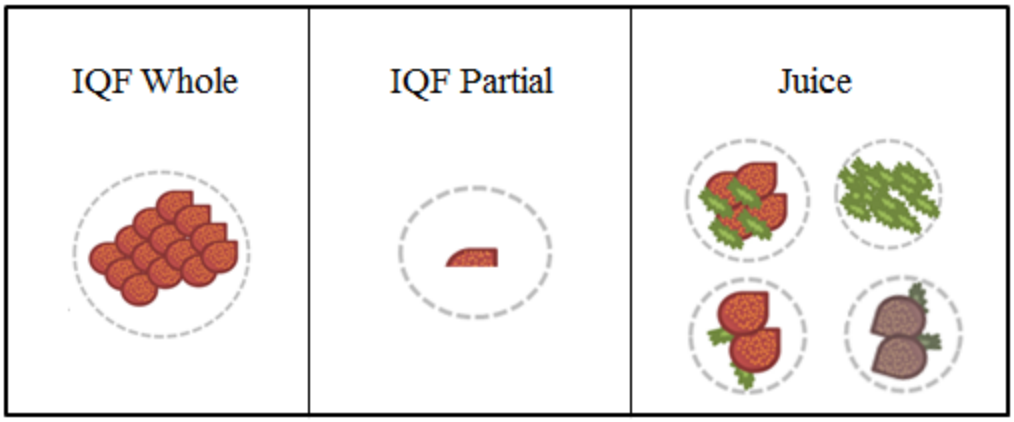


**Figure 2.** Cartoon depiction of the features associated with IQF whole, IQF partial, and juice berries are illustrated.

A high grade IQF whole berry must consist of at least 3/4 of the original strawberry after being de-calyxed and must be free of damage, discoloration, and calyx. A high grade IQF partial berry consists of less than 3/4 of the original strawberry after being de-calyxed and must be free of damage, discoloration, and calyx. A high quality juice berry must only be free of mold and rot. IQF whole and IQF partial berries are significantly more valuable than juice berries (Wahl, Liegel, & Seavert, 2014).

### 3.3 Variability in Strawberry Size and Shape

Strawberry sizes and shapes of all varieties typically follow a seasonal growth pattern. Early in the season, strawberries are large in size. As the season tapers off and multiple bearings of fruit have been harvested, strawberry size tends to decrease. Berry and leaf color can vary depending on weather, fertilizer, pesticides, humidity, air salinity, and many other environmental factors.

The best looking strawberries are first sold to the fresh market, which is more lucrative for farmers. What is left on the vines is then harvested for the processing

market. As a result, the variations in size, shape, firmness, and degree of damage are far more extreme in the processed market than the fresh.

### 3.4 Harvest

Strawberries are one of the most labor-intensive row crops. They are risky and expensive to grow, but can yield high revenue per acre (Ara, Haydar, Mahmud, Khalequzzaman, & Hossain, 2009). From 1974 to 2012, California strawberry output increased nearly six fold, and consumer demand continues to grow (Janick, Brecht, & Saltveit, 2010). Strawberries are considered one of the fastest-growing and most profitable segments of California's farm economy to date. Annual strawberry sales exceeded $2.4 billion in 2012. American farmers now receive more money for fresh strawberries each year than for any other fresh fruit grown in the U.S. besides apples and grapes (Iowa State University, 2014).

Although lucrative, there are many difficulties in profiting from strawberry farming. Adverse weather conditions can quickly and irreversibly damage crops. A strong wind can cause leaves to rub against the berries, marring their skin with brown streaks, while a heat wave can stunt growth and soften the fruit. A heavy rain can break the skin and create small tears, which will quickly become infected with mold. Even a few days of rain can destroy an entire harvest of strawberries (Schlosser, 1995).

The market for strawberries can also be just as unpredictable as the weather. Wholesale prices for fresh strawberries fluctuate widely from 34 cents to 2 dollars per

pound, depending on the quality of the fruit, the time of year, and the supply (Daugovish, Klonsky, & De Moura, 2011).

The perishability of fresh produce also exposes growers to considerable risk. Ten days after a strawberry is picked, it begins to spoil. When including transportation time, this leaves a short window to pick and pack strawberries for the fresh market. This pressures growers to accept the prevailing market price for those berries.

One of the main solutions to help stabilize the unpredictable nature of strawberry farming is to harvest strawberries quickly after they bloom and then freeze any excess berries. In 2014, frozen berries sold for an average of 42 cents per pound (Noncitrus Fruits and Nuts 2014 Summary, 2015). However, the increased amount of labor needed to prepare strawberries for freezing presents a major difficulty, because these strawberries must first have their calyxes removed before they can be frozen. This additional step can more than double the amount of labor necessary to harvest the same acreage of land. The cost of labor to harvest strawberries constitutes roughly 60 percent of the total costs in strawberry production (Wu, Guan, & Whidden, 2012). Therefore, an increase in labor expenses can easily be the differentiating factor between a profitable harvest year and a net loss.

### 3.5 Labor Shortage

As reported by *The Atlantic* magazine and confirmed with our talks with growers and processers along the California coast, strawberry picking is some of the lowest paid, most difficult, and therefore least desirable farm work in California

(Schlosser, 1995). Strawberries are fragile and easily bruised, so they must be picked with great care. Workers must select only strawberries of the proper size, firmness, shape, and color. Rotting strawberries must be tossed away, or they will spoil their neighbors. Workers move down the furrows pushing small wheelbarrows; they pause, bend over, brush aside leaves to their left and right, pick berries, place them in boxes, check the plants, and move on, all in one continuous motion. Once their boxes are filled, they rush to have them tallied at the end of the field, rush back, and begin the process again.

Strawberry plants are 4 or 5 inches tall and grow from beds 8 to 12 inches high. Workers must bend at the waist to pick the fruit, making this a strenuous task. Repeatedly bending over for one hour can cause a stiff back; doing so for ten to twelve hours a day, weeks at a time, can cause excruciating pain and lifelong disabilities. It is not uncommon for strawberry pickers to suffer from chronic back pain.

Cultivating the fruit is so labor intensive that the strawberry industry now employs more farm workers than the industries of all vegetables grown in California Valley combined (Schlosser, 1995). Most strawberry pickers hope to find jobs in the nearby vegetable fields, where wages are better and the work is less grueling. As a result, turnover rates are extremely high in the strawberry work force (Labor: US Fruits and Vegetables, 2011).

### 3.6 Commodity Profile

The U.S. is the largest producer of strawberries in the world. In 2011, the U.S. accounted for 28 percent of the world's production (see Figure 3). At a distant second, Spain accounted for 11 percent, followed by Turkey, Egypt, Mexico, and Poland (ERS, 2013).

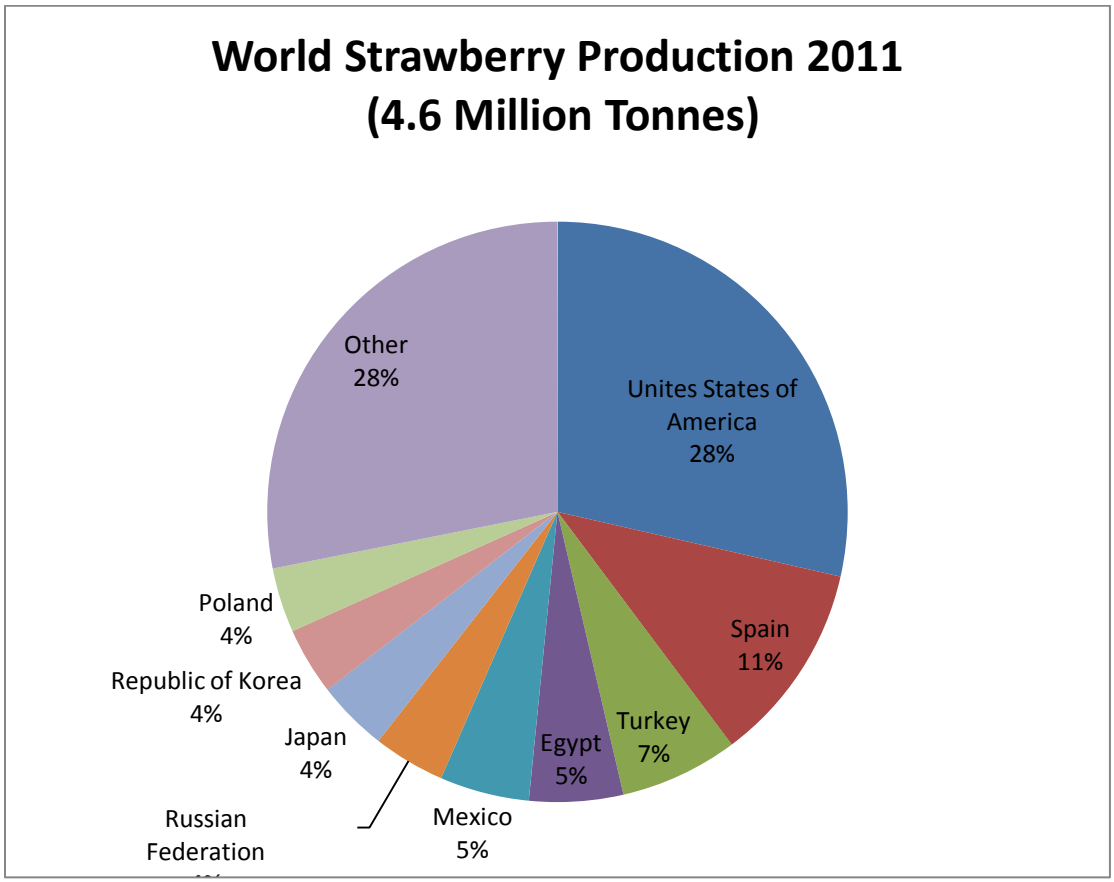


**Figure 3.** Share of world production of strawberries by country, 2011 (ERS, 2013).

Although the U.S. is the largest producer of strawberries in the world, the majority of U.S. strawberries are consumed domestically. As a result, the U.S. is also the fourth largest importer of strawberries. Imports of fresh strawberries make up less than 10 percent of U.S. fresh strawberry consumption, but imports of frozen strawberries account for over 60 percent of U.S. frozen strawberry consumption and

continues to rise. This illustrates the growing reliance on foreign exports as well as the need for technological advancements in the processed strawberry industry.

Furthermore, in the last decade, U.S. consumption of frozen strawberries has almost doubled (see Figure 4). As a result, frozen strawberry imports have increased, while exports have decreased. The frozen strawberry industry has been placing a great deal of effort and resources in developing the technology to increase production capacities and create a more sustainable system.

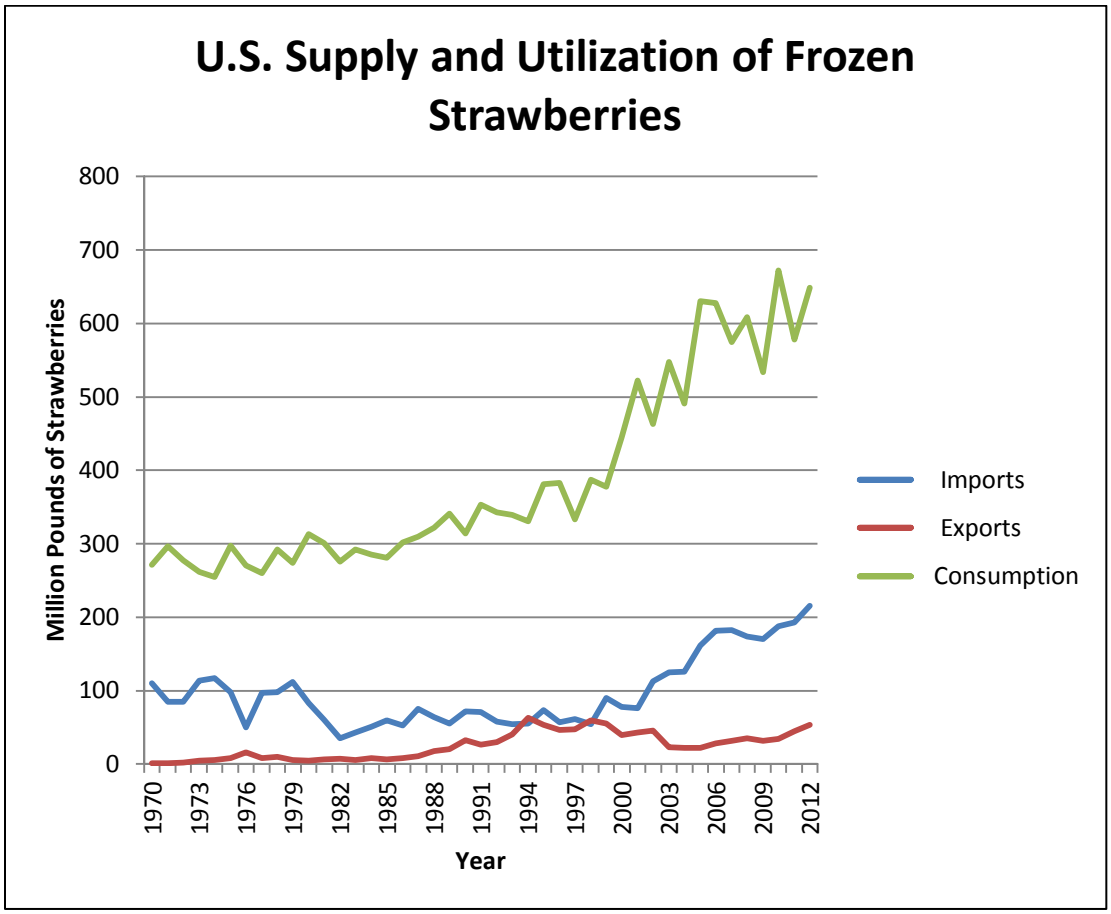


**Figure 4.** U.S. supply and utilization of frozen strawberries (FAOSTAT, 2013).

# Chapter 4: Review of Literature

This chapter provides a review of literature and technology related to food processing. This includes methodologies, apparatuses, and up-and-coming techniques used for cutting foods.

## 4.1 Design Considerations for Food Processing Equipment

The food processing environment consists of a wide range of harsh conditions. This can include large changes in temperature, pressure, and pH, as well as continuous mechanical abrasion. Furthermore, the choice of engineering materials is limited due to food hygiene considerations (Kress-Rogers & Brimelow, 2001). Materials must not have a rough surface, nor should they absorb water or leach substances.

It is typical for frozen strawberry processors to operate machinery 16 hours a day, 7 days a week. The machines may be thoroughly cleaned with high-pressure steam on a weekly basis, while the food processing systems may be periodically flushed with hot caustic soda solutions throughout the day. In addition, ambient humidity can reach 100 percent, and all water used on-site contains high levels of chlorine. As a result, the typical machines designed for such environments comprise of stainless steel (SS304 or SS316) and UHMW plastic whenever possible. An additional consideration is the accumulation of debris, bacteria, and other containments in corners and crevices. Ideally, machines should not have areas where water can pool.

A food processing system's reliability is considered paramount to the industry. The perishability of food items makes each minute a machine is out of operation a very costly liability. If a component breaks, replacement parts must be readily available and interchangeable within minutes.

Many considerations are taken into account when designing machinery for use within a food processing environment. The design of the prototype AVID machine discussed in this dissertation focuses on being food contact compliant and easy to adjust, repair, and sanitize. Additional hygienic design elements can be found in the 3-A sanitary guidelines (3-A Sanitary Standards, Inc., 2015).

### 4.2 Past Automated Strawberry Calyx Removal Machines

Inventors have been developing apparatuses for automatically orienting and removing unwanted portions of strawberries since the 1960s. All of these devices use some sort of vibrational, rotational, pinch, or suction-driven orientation method, along with a metal blade to cut the strawberry. Some of these machines are quite elaborate, as shown in Figure 5.

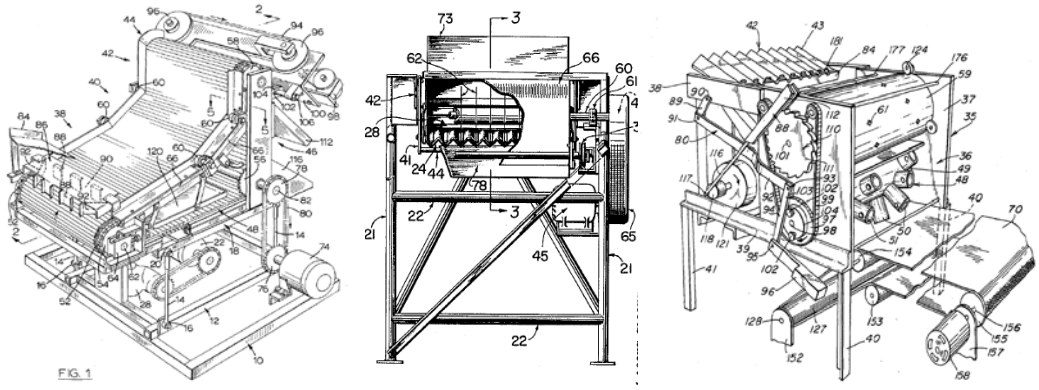

**Figure 5.** Illustrations of past automated strawberry calyx removal systems are shown. The inventors of these machines are (Ledebuhr, Hansen, & Patterson, 1978), (Hartman & Gerrans, 1963), and (Leban, 1976) from left to right, respectively.

Although clever, some drawbacks to these devices are their low throughput, high maintenance, and potential metal hazards if the cutting tool were to be chipped and lost within the food stream. To our knowledge, our proposed machine will run at speeds 10 to 15 times that of current processing systems and use bladeless technology for calyx removal. Furthermore, the simple design of our machine significantly minimizes annual maintenance.

Recently, there have been multiple commercially available strawberry calyx removal systems placed on the market (Turatti, 2013) (Seditec S.A., 2016) (PND Fruit Processing Machinery, 2016). An example of one is shown in Figure 6. The machine requires a minimum of four individuals to operate at full capacity and relies on a bladed cutting system.

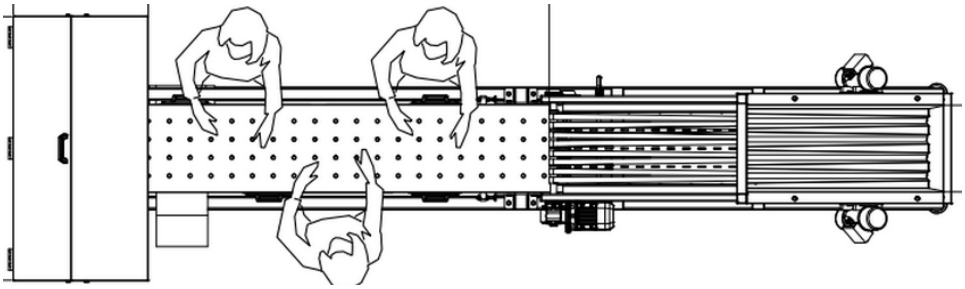

**Figure 6.** A diagram of a strawberry calyx removal assistant marketed and sold by Turatti. Workers orient and place the strawberries on a marked conveyer that is fed into a bladed cutting area (Turatti, 2013).

### 4.3 Calyx Identification Vision Algorithms

In the last decade, there has been an increased amount of research focused on the development of a machine vision calyx identification algorithm for robotic harvesting (see Figure 7). The algorithms use sophisticated image transformations and blob analysis to determine fruit and calyx location. Some examples of these techniques are OHTA color space transformations, region growing algorithms, *k*-

means clustering, BP neural networks, and histogram pattern matching (Zhang, 1996), (Omid, Khojastehnazhand, & Tabatabaeefar, 2010) (Brosnan & Sun, 2002). Although useful for segmenting strawberries and their calyxes from backgrounds found in nature, these techniques are computationally expensive. This places a bottleneck on the throughput of strawberries to be analyzed and processed. Furthermore, this increases the hardware and operating costs of the machine.

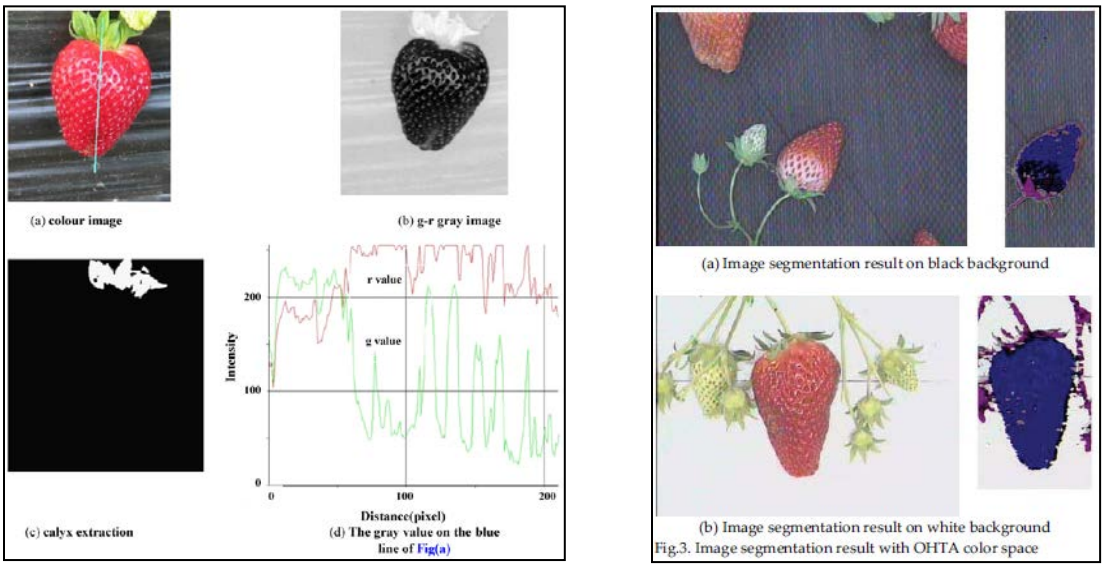


**Figure 7.** An example of a *k*-means clustering method used to locate the strawberry calyx and fruit regions is shown in the four figures on the left (Liming & Yanchao, 2010). An example of an OHTA color space-based segmentation algorithm is shown in the four figures on the right (Feng, Qixin, & Masateru, 2008). The computation speed of both algorithms, along with their blob analysis, is 3 seconds and 1 second, respectively.

### 4.4 Waterjet Cutting Technology

In the last 20 years, water-only waterjet cutting technology has been incrementally replacing processes typically performed by metal cutting blades. This has been seen in the textile, cardboard, rubber, plastic, and more recently food

processing industries. Food applications now include cakes, string beans, spinach, celery, and more (Walker & Bansal, 1999), (Robertson, 1974), (Jordan, 1988).

In waterjet cutting, water is directed through an orifice as small as 0.003 inch at a pressure level of up to 120,000 psi and aimed at a material in much the same way as a bandsaw or laser. There are three major components in an ultrahigh-pressure waterjet cutting system: the pump, the nozzle, and the cutting fluid.

### 4.4.1 The High-Pressure Pump

The pump is the heart of the waterjet system (see Figure 8). The pump pressurizes the water and delivers it continuously through a small orifice nozzle that concentrates the water into a supersonic knife-like waterjet stream. Two main types of pumps can be used for waterjet applications: an intensifier-based pump and a direct drive-based pump. Because our application uses the former, we will focus the discussion on intensifier-based pumps.

An intensifier pump's water circuit consists of the inlet water filters, booster pump, intensifier, and shock attenuator. Ordinary tap water is filtered by the inlet water filtration system consisting of a 5, 1, and 0.45 micron cartridge filter. The filtered water then travels to the booster pump, where the inlet water pressure is maintained at approximately 90 psi, ensuring that the pump has a constant supply of water. The filtered water is then sent to the intensifier pump and is pressurized up to 60,000 psi. Before the water leaves the pump unit to travel through the plumbing to the cutting head, it first passes through the shock attenuator. This large vessel

dampens the pressure fluctuation to ensure that the water exiting the cutting head is steady and consistent.

The hydraulic circuit consists of an electric motor, hydraulic pump, oil reservoir, manifold, and piston plunger. The electric motor powers the hydraulic pump, which pulls oil from the reservoir and pressurizes it to up to 3,000 psi. This pressured oil is sent to the manifold, where the manifold's valves create the stroking action of the intensifier by sending hydraulic oil to one side of the plunger or the other. The hydraulic oil is then cooled during the return back to the reservoir.

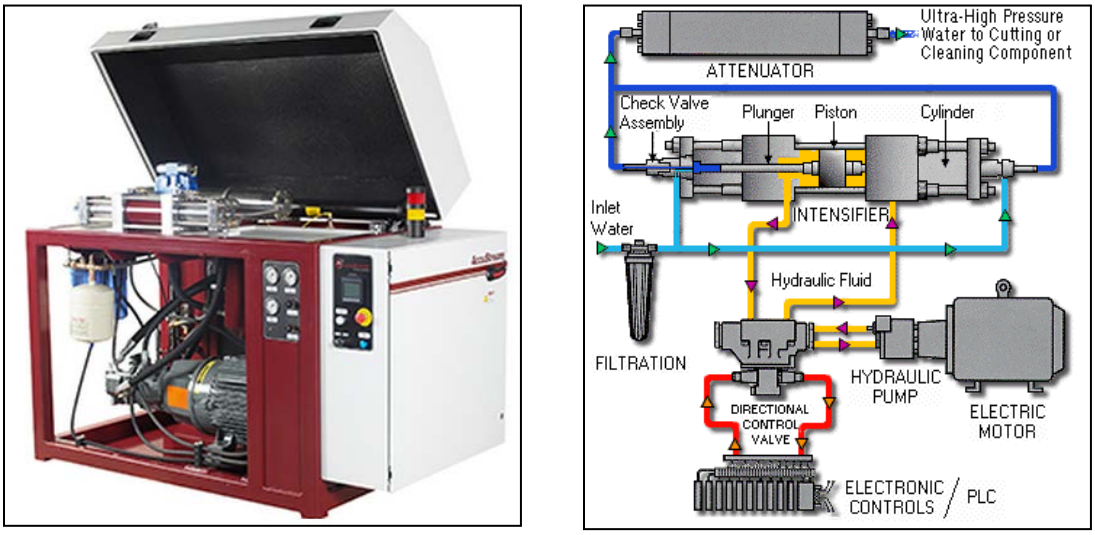


**Figure 8.** A commercially available high-pressure intensifier pump is shown on the left (AS-6050, 2014). The water and hydraulic circuits are shown on the right (How a Water Jet Machine Works, 2013).

This project uses a custom high-flow 30,000 psi pump to remove the calyxes from strawberries. The high flow increases the pressurized water output and therefore the number of cutting nozzles that can be used. Furthermore, the relatively low pressure prolongs the wear-life of the components and increases the overall safety of the machine.

### 4.4.2 Nozzle

This project uses a custom 0.005-inch diamond orifice nozzle assembly to create a long and coherent high-pressure cutting stream, which is necessary for knife-like cut quality to remove the calyx. In addition, diamond orifices are the lowest maintenance orifice type that can be used in waterjet cutting systems. Other types of orifices include ruby and sapphire. While their upfront costs are significantly less expensive than diamond orifices, they have a low coherent cutting stream and must be changed every 10 to 15 hours.

### 4.4.3 Cutting Fluid

This project uses filtered chlorinated water as the cutting fluid, which allows for a safe and sanitary method of removing the strawberry calyx. The total dissolved solids within the water are kept in the range of 50 – 150. This decreases the possibility of water-facing internal components prematurely failing due to solvation or mineral abrasion.

# Chapter 5: Overview of Study

## 5.1 Innovation

The AVID machine combines an efficient strawberry orientation and singulation method with real-time calyx identification and subsequent removal to create the first automated high-throughput de-calyxing system. The handling system takes strawberries of random orientation and organizes them into a uniform grid pattern. This allows the machine vision system to use a simple but fast CIELAB-based feature identification algorithm to determine calyx locations. The calyxes can then be removed through the use of a custom-designed high-speed precision waterjet knife positioning system.

## 5.2 Approach

The major goal of this research was to develop a fully automated strawberry calyx removal system to be retrofitted into existing processing lines. The components of this system have been quantitatively analyzed and iteratively modified to optimize production capacity and quality. With the assistance of the CSC, we developed a robust ergonomic field-ready strawberry processing machine.

All three of the proposed machine's components are essential for each individual component to operate at maximum efficiency. The material handling system picks strawberries up from a water tank and simultaneously orients and singulates each strawberry. The result is a uniform grid of strawberries, which is then fed into a vision chamber where the strawberries are quickly imaged. The machine vision system uses a series of feature recognition and segmentation algorithms to

identify the strawberry calyx location in real-time. The optimal calyx removal location will then be sent to the waterjet actuation system, which precisely moves the waterjet knife to the cutting position, and as a result, the strawberry calyx is removed.

This machine has the potential to significantly increase strawberry yield and quality. In addition, the techniques explored here can be adapted for other fruits and vegetables. Ultimately, this research will further advance agricultural technology and bring the target of food sustainability closer to fruition.

### 5.3 Machine Summary

The machine summary is divided into two sections. The first section describes an overview of the design and operation of the AVID machine's three main components. The second section outlines the sequence of communication between the machine vision and the waterjet actuation system.

#### 5.3.1 AVID Components

The AVID machine consists of three main components: a strawberry loading and orientation conveyor, a machine vision system for calyx identification, and a synchronized multi-waterjet knife removal actuation system (see Figure 9).

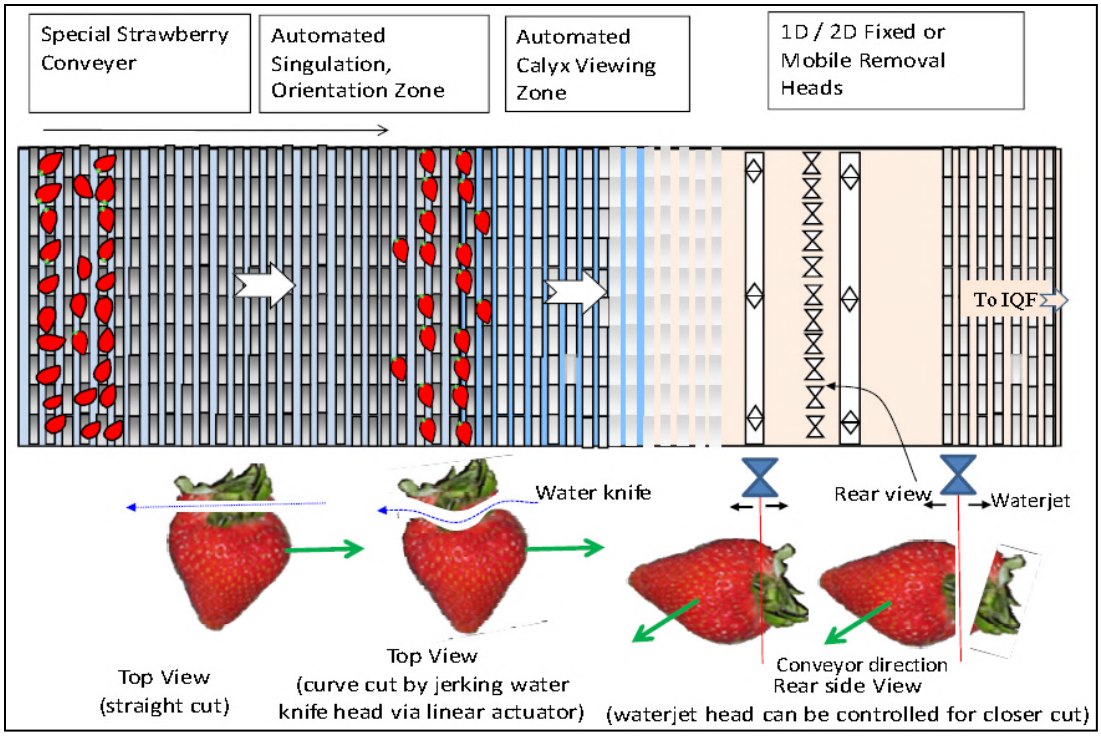


**Figure 9.** An overview of the automated strawberry calyx removal system components is shown (Tao, California Strawberry Commission Annual Report 2012-2013, 2013).

The AVID machine is designed for conical strawberries to be first loaded into a water tank. The strawberries are immersed in a sanitation bath and float to the water's surface to form a single layer. An elevating conveyor consisting of specially designed parallel roller rods then lifts the floating strawberries from the water by the valley of adjacent rods. This common technique enables one layer of fruit to be processed. The roller rods then begin rotating; due to the strawberries' conical or polarized shape, the berries will orient themselves such that the direction of their symmetrical axes aligns parallel with the axes of the roller rods. In addition, the roller rods are molded to cup individual strawberries, creating an evenly spaced grid of oriented strawberries along the conveyor.

When the fruit comes into the optical section, an industrial camera will take an image of the fruit's surface. By the time the strawberries exit the viewing area, all calyx positions will have been precisely located. At this time, all strawberries remain in their stationary locations as they move to the calyx removal section.

The strawberry position on the conveyor is known through the use of a synchronized conveyor shaft encoder. The computer will register each calyx's position as coordinates with respect to the conveyor, thereby locating the calyx at any given time with sub-millimeter precision. While there are several calyx removal mechanisms and options, we will use a non-metal, blade-free waterjet knife approach. By using the machine vision guided waterjet knife cutting technique, the automated calyx removal machine will take the coordinates from the vision system and remove each calyx with millimeter precision. The interactions of all three components are depicted in Figure 10.

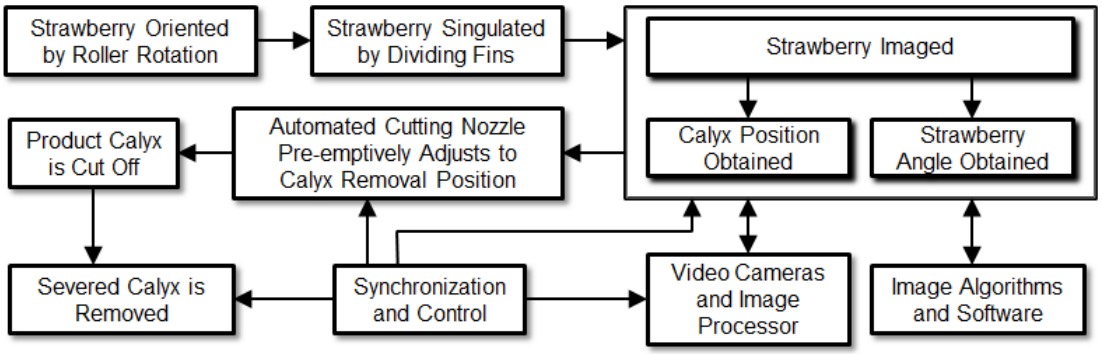


**Figure 10.** A flow diagram illustrating the interactions between the main components of the AVID machine is shown.

### 5.3.2 AVID Communication

The heartbeat of the AVID machine is the conveyor's encoder pulse, as seen in Figure 11. This pulse is physically synchronized to the conveyor's roller rods so

that at each falling edge, an image of a strawberry is taken, the key features extracted, and the cut location sent to the waterjet cutting nozzles.

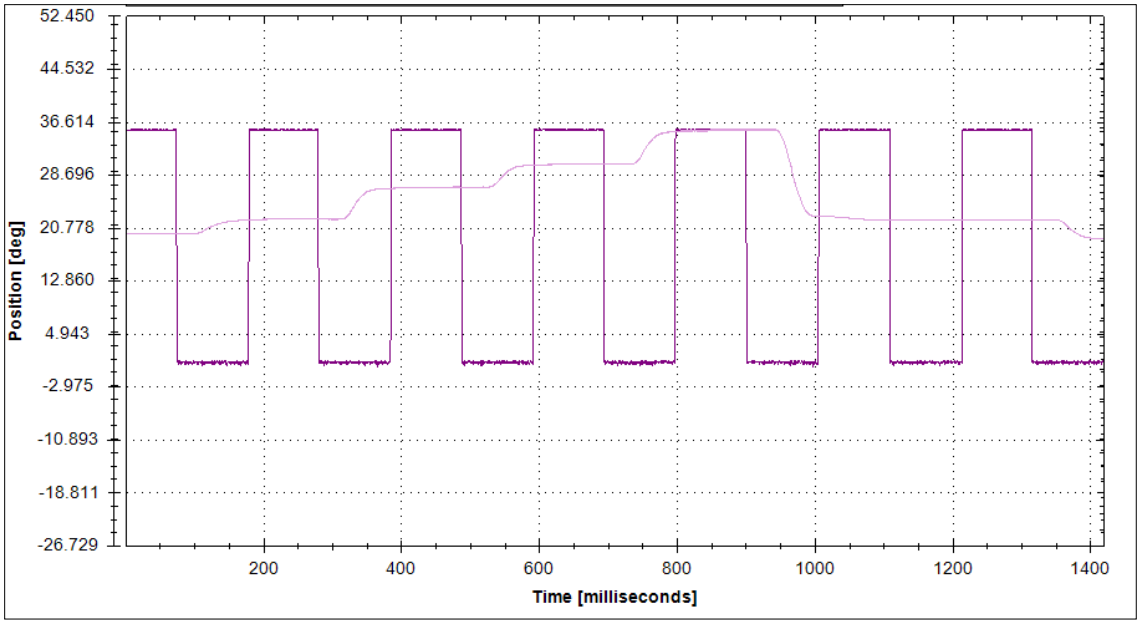


**Figure 11.** The AVID machine's conveyor encoder pulse is shown as the square purple signal train. The position of the waterjet cutting nozzle is shown as the pink trace.

Specifically, the sequence of communication follows 10 steps. An overview of these steps is detailed below:

1) The falling edge of the encoder acts as an interrupt signal that triggers the frame grabber hardware, which acquires the color image from the camera.
2) This also triggers the motors to move to the cut-line position determined from the previous image. If this is the first image (i.e. there were no previous images), the motors are set to a default position.
3) Image processing is performed on the acquired color image.
4) Critical features of the strawberries are found through blob analysis.
5) The algorithm determines if the waterjet cutting system should attempt to de-calyx the imaged strawberry or move out of the way to reject the strawberry. A strawberry will be rejected if the assigned cut-line leaves less than 2/3 of the original berry.
6) If the algorithm chooses to cut the strawberry, a subroutine uses the extracted blob features to determine the cut-line coordinates for calyx removal.
7) These coordinates are then converted to a parameter representing a physical location on the machine's roller rod.
8) This parameter is then sent via Ethernet to the waterjet positioning motor.
9) The waterjet positioning motor uses the cut-line coordinate parameter to reference an internal lookup table of pre-defined rotational degrees.
10) The waterjet cutting stream is then positioned accordingly.

### 5.3.3 AVID Machine Output

The AVID machine produces four outputs: Sliced Fruit, Calyx & White Shoulder, Residual, and Return Fruit. The Sliced Fruit output consists of whole and partial berries, as seen in Figure 12. The Calyx & White Shoulder output includes both the separated calyx leaf and the white-colored fruit region located near the calyx of some strawberries. The Residual output consists of strawberries with parts of the calyx still remaining following a removal attempt. Finally, the Return Fruit output includes strawberries identified as unable to be cut. These strawberries are misshapen, significantly damaged, un-oriented, or discolored. The AVID system is capable of diverting Return Fruit output to a separate stream to be fed through the system once again.

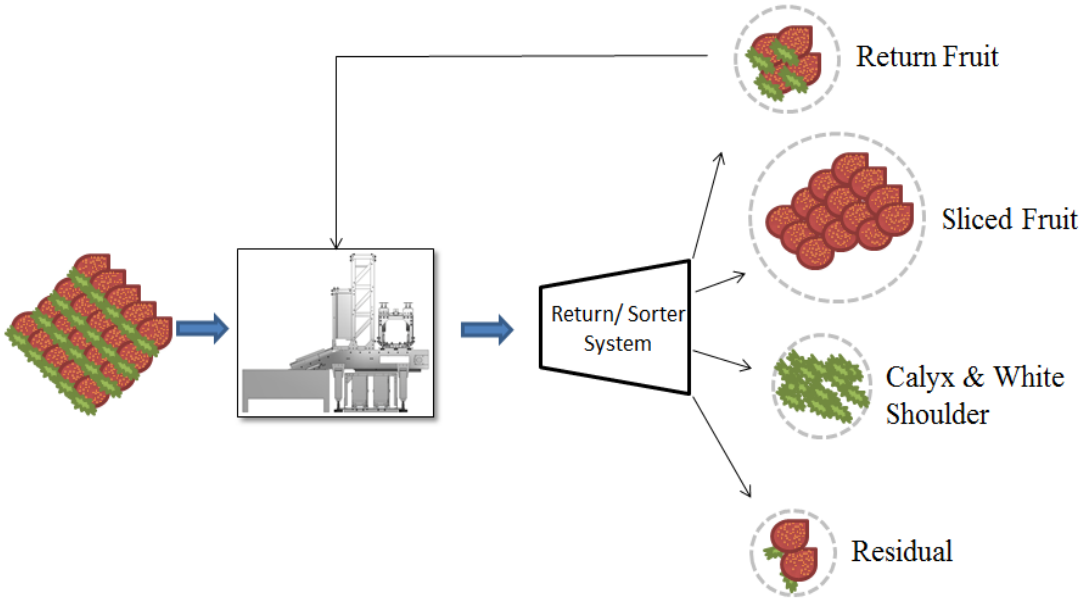


**Figure 12.** The four output products of the machine are shown. The Return Fruit can be cycled back into the machine for another opportunity for calyx removal.

### 5.4 Machine Iterations

The AVID machine is currently on its third generation. The first generation was a galvanized steel prototype used for proof-of-concept. The second generation was a stainless steel version of the prototype that utilized a UHMW material handling system. This system was later upgraded to be fully stainless steel in the current iteration of the machine.

#### 5.4.1 Initial Prototype

A running prototype was developed and demonstrated for CSC representatives in February 2013. This basic prototype consisted of a handling system, vision system, and a waterjet knife actuation system, as shown in Figure 13. The demonstration proved: the handling system could singulate and orient conical strawberries, the vision system was able to identify and track the location of each strawberry calyx, and the actuation system could position the waterjet knives appropriately.

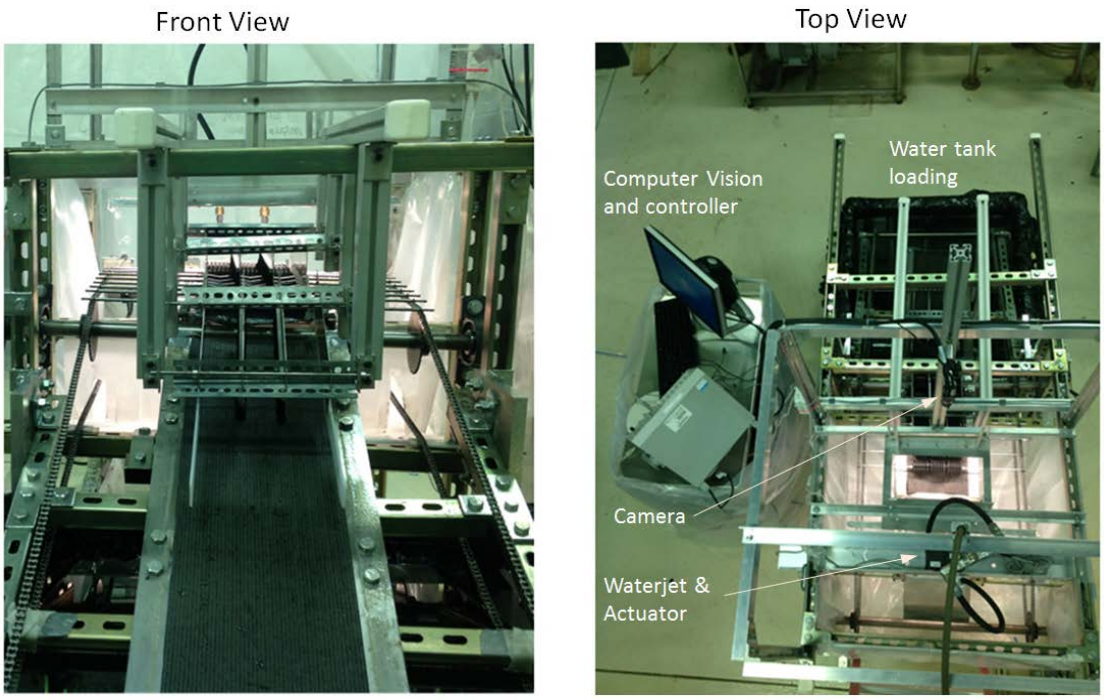


**Figure 13.** Initial prototype of the automated calyx removal system is shown. Strawberries are loaded from the water tank and travel to the waterjet cutting area.

Although the proof of concept was successful, the orientation system needed further optimization to account for more variations in strawberry dimensions. Additionally, the vision system's algorithms were not as robust as needed for a field system, and the waterjet actuation system was not fully synchronized with the rest of the components. These areas were addressed in the second iteration of the machine.

### 5.4.2 Second Generation

The second generation AVID machine's structure was fabricated with all stainless steel components, and UHMW was used for all wear surfaces. A computer-automated rendering of the completed machine is shown in Figure 14. A picture of the second generation AVID machine is shown in Figure 15. All surfaces were food contact compliant and able to withstand the daily sanitation procedures of a typical

strawberry processing facility. Particular attention was placed on creating an easy-to-maintain system. This included designing roller components that could be interchanged within seconds and creating a chassis-like frame that allowed for easy attachment and detachment of sub-components.

The material handling system utilized blue UHMW roller rods press-fit over a stainless steel shaft. The color blue was chosen in order to assist the machine vision system in subtracting background noise. Unfortunately, over long periods of testing, the waterjet knives were shown to delaminate the UHMW material. This caused UHMW flakes to be found in the output product stream. This issue was addressed in the third iteration of the machine.

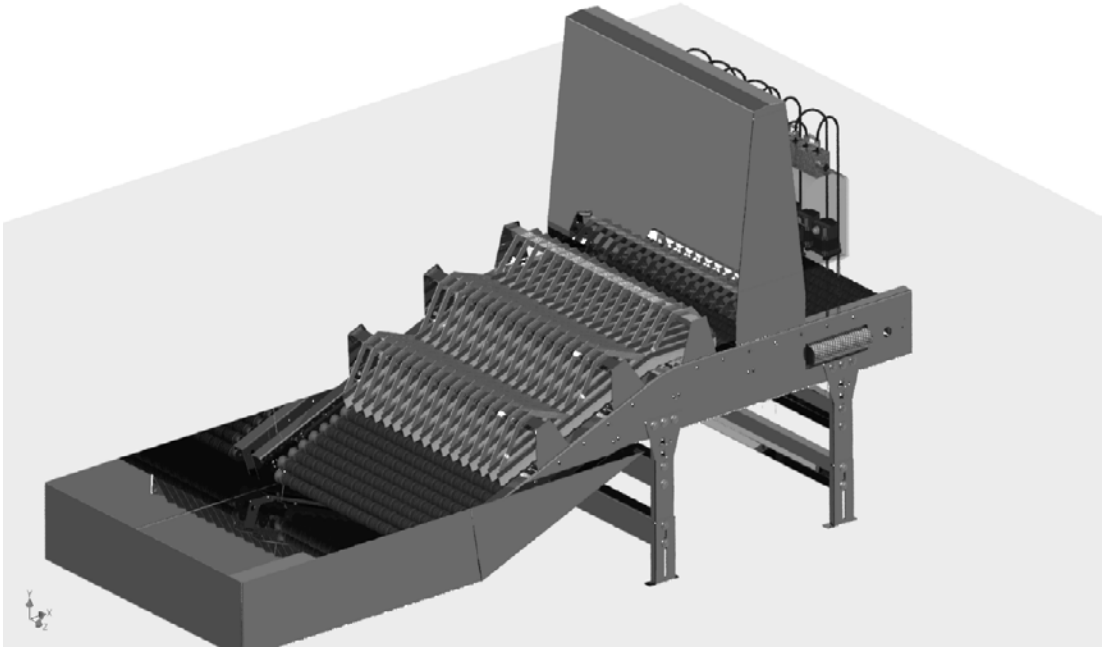

**Figure 14.** Machine rendering of the second generation AVID system. This version was a wash-down capable stainless steel IP67 / NEMA4X model designed to meet the USDA/FDA requirements for food safety and sanitation of food processing equipment (Tao, Lin, Chen, & Seibel, 2014).

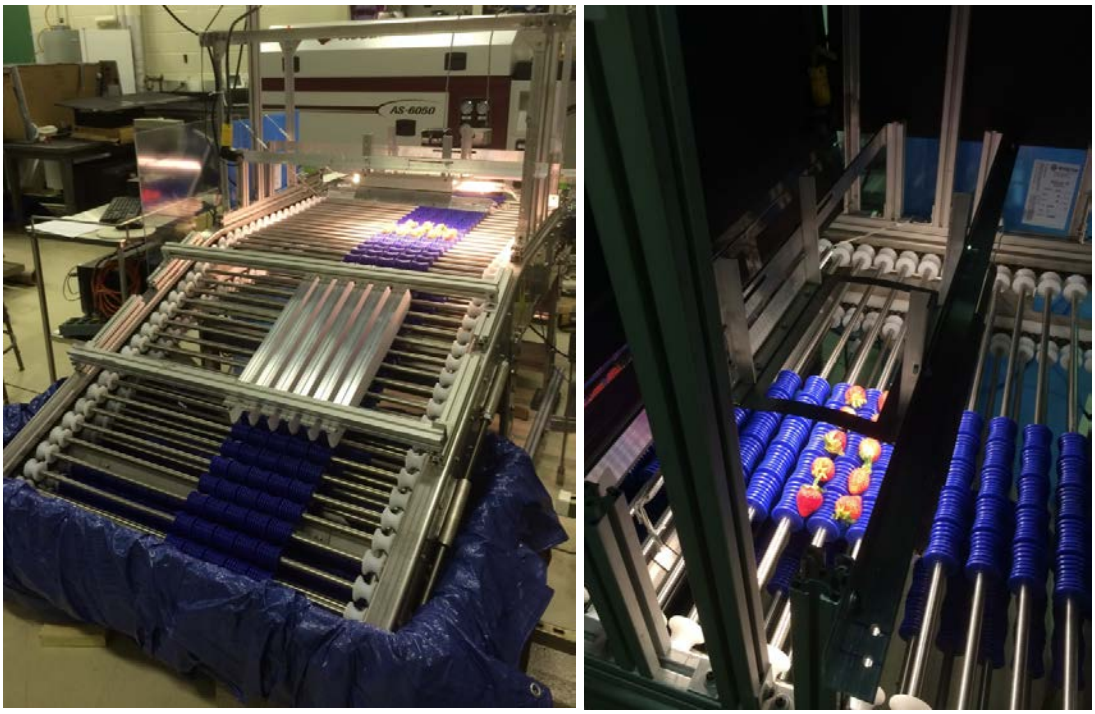

**Figure 15.** A working construction of the second generation AVID machine is shown. An isometric view of the AVID machine with lighting chamber removed is shown on the left, and a top-down isometric view within the lighting chamber is shown on the right (Tao, Lin, Chen, & Seibel, 2014).

### 5.4.3 Third Generation

The third generation machine was a full-scale AVID machine. It was capable of withstanding daily wash-down procedures as well as 24-hour operation. In addition, it could be easily positioned via forklift and transported across the country to the California pilot study location. Furthermore, the footprint of the machine was small enough so that it could be retrofitted into existing processing facility production lines. A computer-automated rendering of the completed machine is shown in Figure 16. A picture of the third generation AVID machine is shown in Figure 17.

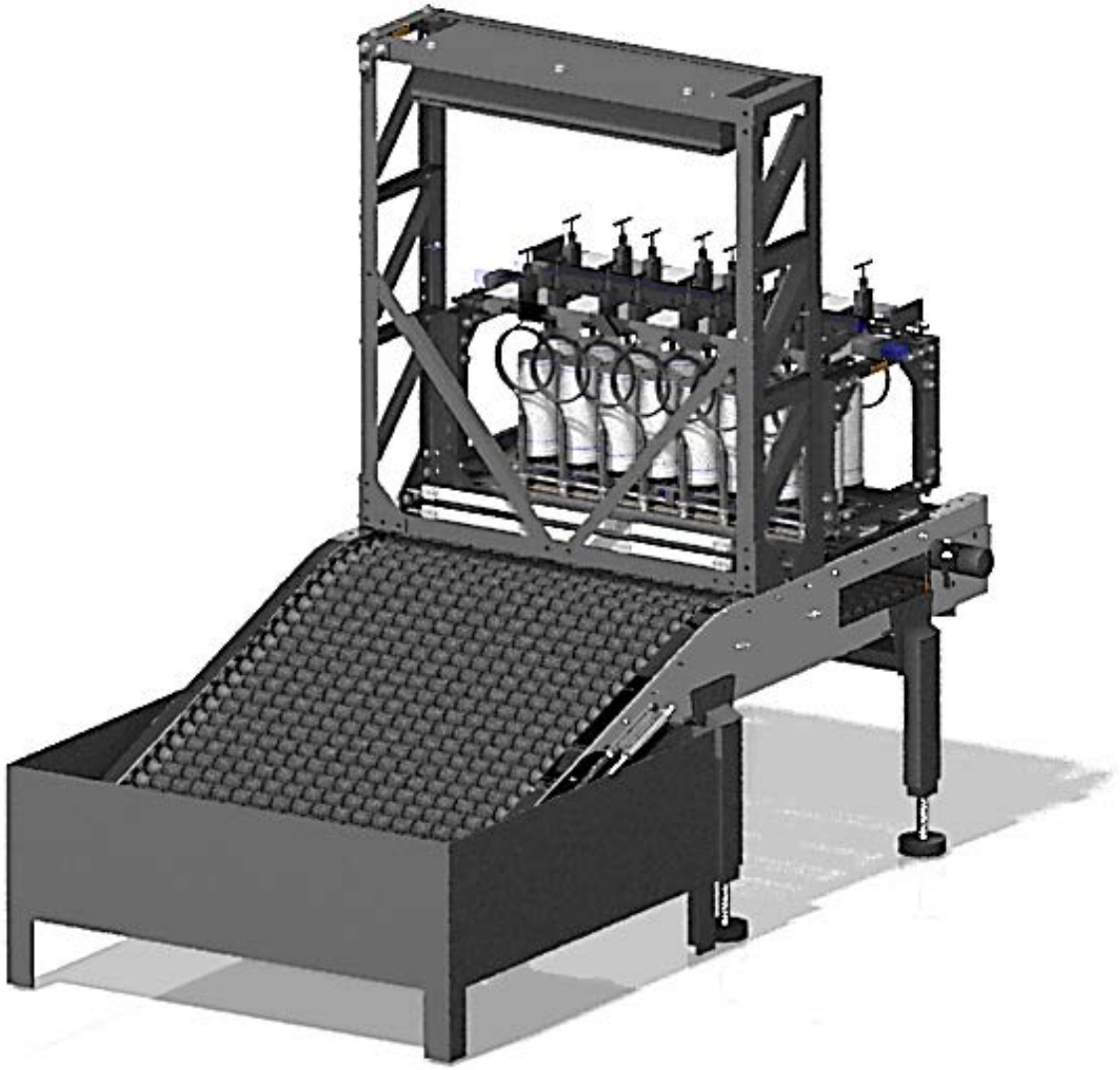

**Figure 16.** Machine rendering of third generation AVID machine. This version was a wash-down capable stainless steel IP67 / NEMA4X model designed to meet the USDA/FDA requirements for food safety and sanitation of food processing equipment.

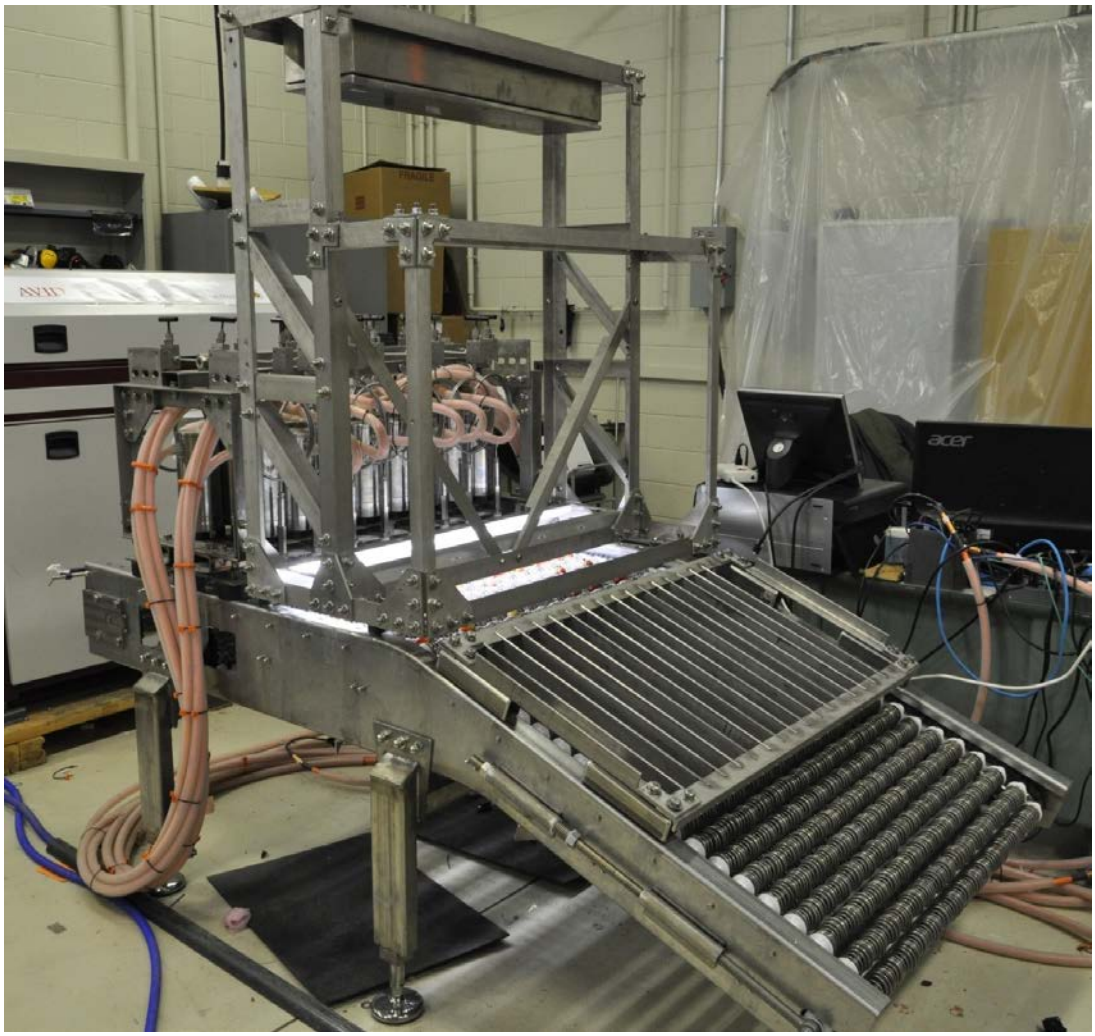


**Figure 17.** An isometric view of the third generation AVID machine with lighting chamber enclosure removed is shown.

The UMD's agricultural machine shop, along with local fabricators, manufactured the frame and components of the system. The results discussed in Chapters 6, 7, 8, and 9 were obtained from this machine.

# Chapter 6: Pilot Study

The purpose of this study was to examine three areas of the AVID machine: 1) the Sliced Fruit weight yield efficacy, 2) the reliability of the hardware and software, and 3) the ease of installation and use of the machine.

## 6.1 Introduction

A full-scale third generation AVID machine was tested at California's Cal Pacific Specialty Foods (CPSF) Watsonville location (see Figure 18). In 2015, CPSF accounted for more than 15 percent of California's processed strawberry production (Noncitrus Fruits and Nuts 2014 Summary, 2015). The study lasted 12 weeks, starting from mid-February of 2016, and used over 70 tons of strawberries.

**Figure 18.** The AVID machine is seen installed in a food processing plant. The strawberries are loaded from the right. The output of the machine is transported to the white bin on the left via the white takeout conveyor.

### 6.2 Materials and Methods

The first two weeks of arrival were dedicated to installation and calibration of the machine. The water, electricity, and compressed air requirements were specified and provided by the facility. The following eight weeks were used to run performance tests. Each week, three days were dedicated to operating the machine. The other two days were used to update software and make hardware improvements. The last two weeks were used to perform stress tests, which were performed on the AVID machine as a whole and its three subcomponents individually.

A performance test day consisted of running approximately 5,000 pounds of strawberries. The varieties used were Portola, San Andreas, Monterey, Fronteras, and Cabrilo. These strawberries were provided by CPSF and were selected from their daily product arrivals. The strawberries were then sized into three groups: small, medium, and large. This corresponded to groups of strawberries with diameters ranging from 5/8 – 1.00, 1.00 – 1.50, and 1.50+ inches, respectively. The sizing was performed with a bar shaker. Three separate sets of bars were used, spaced at 5/8, 1.00, and 1.50 inch intervals, respectively. The sizing efficacy depended on the strawberries received. For example, if the strawberries were more wedge-like, large strawberries would be mixed with the small and medium groups.

Due to weather and growing conditions, it was seen that of the 5,000 pounds received per test day, a majority of the strawberries were of one size. However, on average, a minimum of 2,000 pounds of each size group could be accumulated over three weeks.

The AVID machine was operated at three speeds: 0.50, 1.00, and 1.50 feet per second. To optimize operating parameters, the strawberry size and conveyor speed were varied. This produced nine combinations of speed and size. Through three weeks' worth of test days, a minimum of ~600 pounds of strawberries were used to test each size-speed case.

For each test day, the size-speed case to be tested was randomly chosen from the available strawberry sizes received. For each test case, the percent weight yield of each of the four AVID machine outputs was collected: percent weight yield of Sliced Fruit, Calyx & White Shoulder, Residual, and Return Fruit. The sample size was roughly 2 pounds and was evenly spaced throughout the test case. Approximately one sample was taken per minute. This data was used to determine the AVID machine's de-calyxing efficacy.

The operating parameters, including speed, calibration settings, and lighting conditions, were saved for each test case. In addition, strawberry size, variant, and physical conditions were noted. Furthermore, for each size grade, the percentage of conical strawberries by count was also noted.

A two-factor analysis of variance (ANOVA) was performed between strawberry size and conveyor speed to determine the effect each parameter had on Sliced Fruit weight yield. A multiple comparison test was then used to identify significant differences between Sliced Fruit weight yields within the levels of each parameter. Both analyses were preformed using MATLAB Statistics and Machine Learning toolbox (Mathworks)

The AVID machine was sanitized daily. At the beginning of each test, an Adenosine triphosphate swab was performed to verify that the machine was properly sanitized.

## 6.3 Results and Discussion

### 6.3.1 Sliced Fruit Efficacy

The two-factor ANOVA analysis over the eight weeks of performance tests indicated that Sliced Fruit weight yields depended primarily on strawberry size, as seen in Table 1. The strawberry variant, human operator, and length of runtime showed no significant difference in machine percent weight yield efficacy.

**Table 1.** The results of a two-factor ANOVA analysis between size (columns) and speed (rows) are shown. The size *p*-value of 0.0849 is considered significant. This analysis was performed using MATLAB Statistics and Machine Learning toolbox (Mathworks).

| Source | SS | df | MS | F | Prob>F |
|---|---|---|---|---|---|
| Size | 627.1 | 2 | 313.55 | 2.54 | 0.0849 |
| Speed | 45.7 | 2 | 22.87 | 0.19 | 0.831 |
| Interaction | 157.2 | 4 | 39.31 | 0.32 | 0.8646 |
| Error | 9985.7 | 81 | 123.28 | | |
| Total | 10815.8 | 89 | | | |

The multiple comparison test within the size parameter showed Sliced Fruit weight yields did not vary significantly between size groups, as seen in Figure 19. The Sliced Fruit weight yields of small, medium, and large strawberries were 39.5, 45.9, and 41.6 percent, respectively. Although the standard errors between each size overlapped, it should be noted that the average medium sized strawberry Sliced Fruit weight yield was roughly 5 percent larger than any other size group. This is understandable, considering the material handling system was optimized for medium sized strawberries.

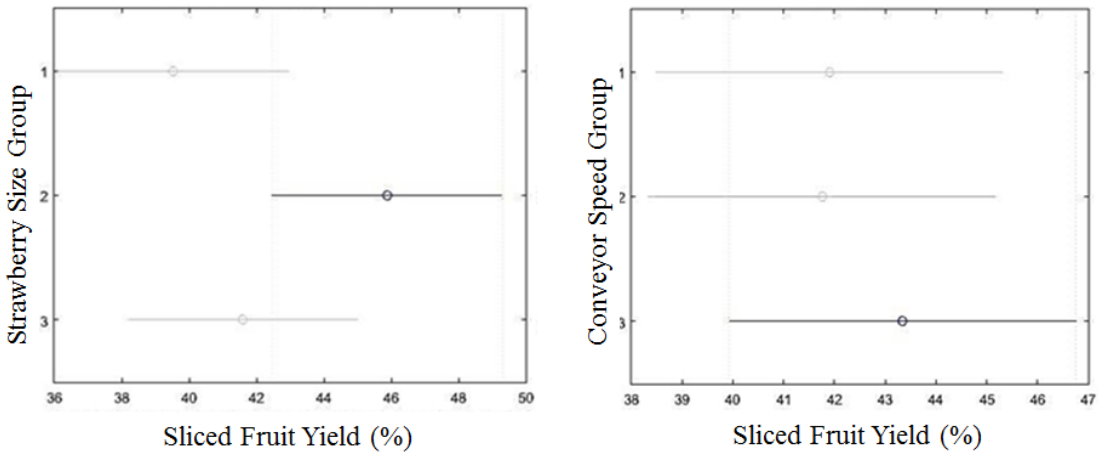


**Figure 19.** A multiple comparison test within the size and speed parameters is shown from left to right, respectively. The group numbers 1 through 3 within the size figure correspond to small, medium, and large. The group numbers 1 through 3 within the speed figure correspond to slow, medium, and fast. The standard error bars for both figures are 2 percent. The highlighted groups (2 and 3 for the size and speed parameters, respectively) produce the largest Sliced Fruit yield. This analysis utilizes the Tukey-Kramer multiple comparison approach provided by MATLAB Statistics and Machine Learning toolbox (Mathworks).

The optimal operating conditions were medium sized fruit of 1.00 to 1.50 inches in diameter running at 1 foot per second, as seen in Figure 20. The average optimal Sliced Fruit weight percentage was 43.2 percent, with a margin of error

(MOE) of 4.5 percent at a 95 percent confidence interval (CI). Of the Sliced Fruit portion, 70 percent was IQF whole, and 30 percent was IQF partial.

The study noted that the strawberries became larger and more spherical in the second half of the test period. To better understand the effect of shape on Sliced Fruit efficacy, the data collected was split into two 4-week periods: the first half and the second half. The first half of the trial period, with higher proportions of medium sized conical shaped fruit, produced a Sliced Fruit weight yield of 49.5 percent with a MOE of 4.2 percent at 95 percent CI. The second half of the trial period, with higher proportions of larger sized spherical fruit, produced a Sliced Fruit weight yield of 31.0 percent with a MOE of 4.8 percent at 95 percent CI.

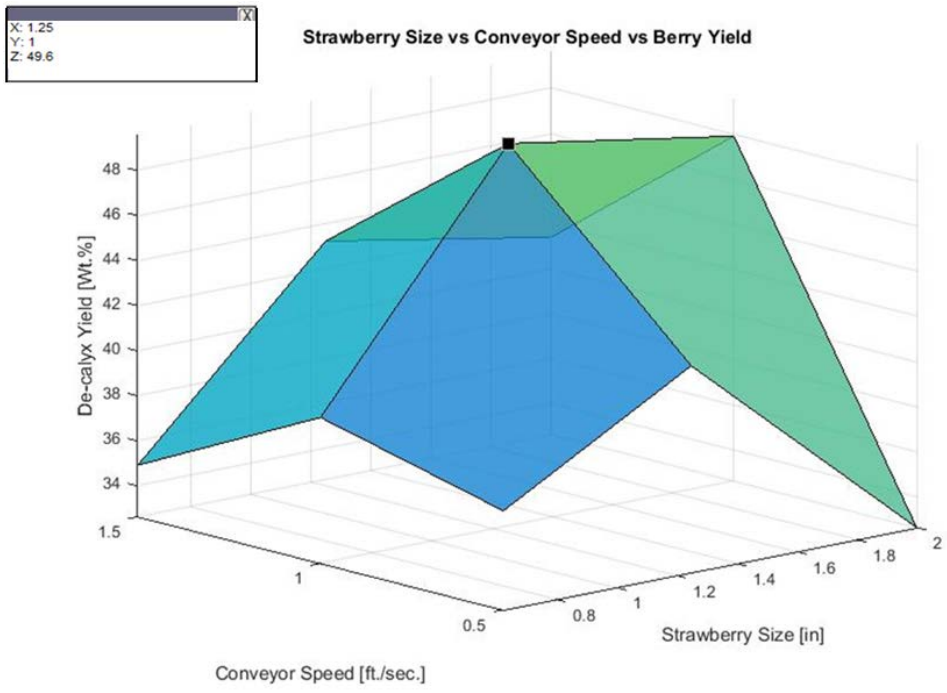


**Figure 20.** The relation between conical strawberry size and conveyor speed on Sliced Fruit percent weight yield is shown. The strawberry size ranges are 5/8 – 1.25, 1.25 – 1.50, and 1.50+ inches. The conveyor speeds are 0.50, 1.00, and 1.50 feet per second. The data shows that optimal Sliced Fruit percent weight is with a medium sized strawberry running at 1 foot per second. This optimization point is indicated by the black marker. These parameters are shown in the text box located at the top left corner.

### 6.3.2 Reliability

Over the 12-week pilot study, a maintenance log was recorded for both the hardware and software. In terms of hardware, multiple points of minor failure occurred. Specifically, the water treatment equipment used to supply the high-pressure pump with 50 tds water malfunctioned. The lighting system of the machine vision component failed as a result of corrosion from sanitation chemicals, while the conveyor encoder and AVID computer failed due to humidity damage. In addition, the material handling rollers became less effective throughout the testing period due to a wear component prematurely failing. However, all failures encountered were fixable on site, with no delay to the pilot study.

The software was iteratively improved during the pilot study. These enhancements included widening the range of detectable strawberry fruit and leaf colors, as well as improving the time complexity of the feature identification algorithms. Furthermore, software bugs were continuously removed throughout the trial period.

### 6.3.3 Installation and Operation

Five days were required for machine installation. The waterjet intensifier was installed roughly 50 feet away from the AVID machine. The utilities used were a 10 gpm line of city water, an 80 amp 460 volt 3 phase power line, and a 100 SCFM at 70 psi compressed air source. These were standard utilities for CPSF. Local staff found the machine easy to use and clean. Additional guards and interlocks were necessary to

meet Occupational Safety and Health Administration (OSHA) standards. Based on this installation, a suggested layout of multiple machines is shown in Figure 21.

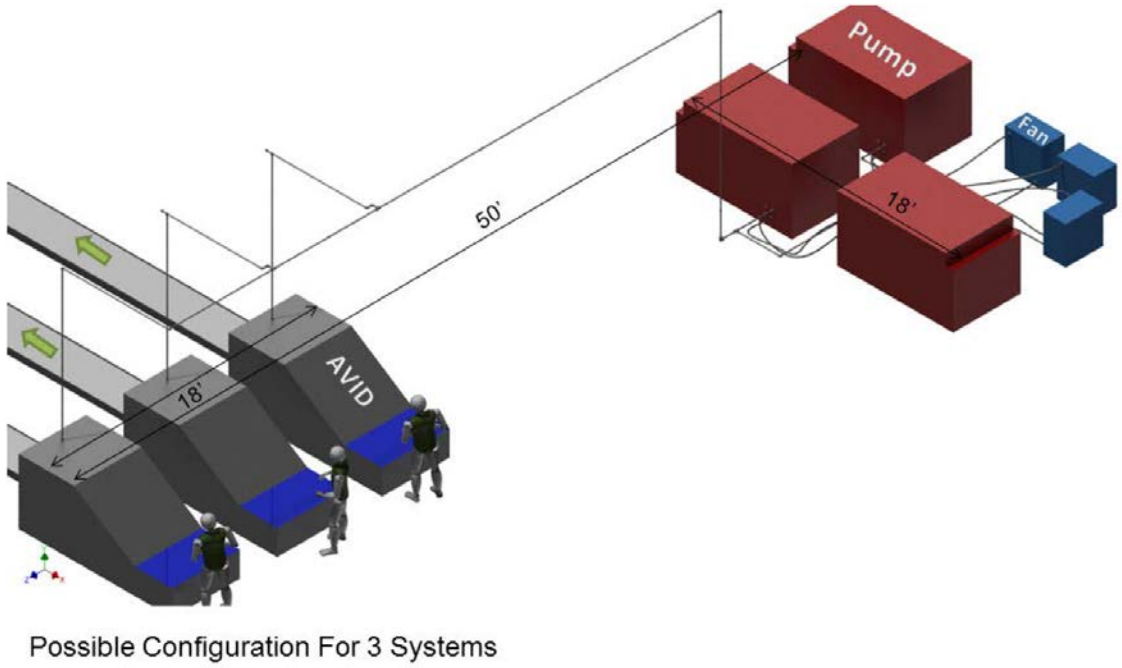


**Figure 21**. A suggested floorplan for multiple AVID machines is shown. The AVID machines are shown to the left and the waterjet intensifier pumps are shown to the right.

# Chapter 7: Efficacy of Strawberry Handling Technique

A rotational energy-driven conical strawberry orientation method was developed to order the initial randomly oriented strawberry input. A rotational force is applied to the strawberry through the use of a custom-designed roller. This causes the typical strawberry to uniformly orient itself into one of two positions due to its conical-like shape.

## 7.1 Introduction

Automated high-throughput strawberry calyx removal first requires mechanization of strawberry handling. Humans may be adept at de-calyxing strawberries of random orientations, but machine processes require carefully positioned parts in consistent orientation. Typically, randomly arranged items are oriented and sorted by first imparting motion through gravity, centrifugal force, tumbling, air pressure, or vibration, and then passed through a cleverly designed mechanical device (Mechanization Of Parts Handling, 2008). However, the orientation of fruits can be especially difficult due to their inherent variability in size, shape, and fragility. In fact, the best method for orientating strawberries for calyx removal has been a 50-year-old unanswered question. There have been many attempts to solve this problem, ranging from vibrating tables to elaborate vacuum suction devices (Ortega & Ortega, 2001), (Hayashi, et al., 2010). However, none of these systems have been economically feasible or robust enough to handle current levels of strawberry demand. This project offers a possible solution to this problem. Recent advances in waterjet cutting techniques allows for a dynamic cutting process to be

performed over the conveyor system. Therefore, the strawberries only need to be oriented along their axes, and the cutting nozzle can be directed to appropriate locations. This enables us to use the established technique of applying rotational energy to conical shapes to cause orientation. When a conical shape is placed between two rotating rollers, its axis will self-align to the direction of the roller axis. The effectiveness of this technique has been demonstrated in both the egg and pepper industries (Niederer, 1980), (Rose & Thornton, 1975).

### 7.2 Material and Methods

When designing the strawberry orienting roller rods of the material handling system, a distribution of strawberry sizes and geometries was first determined in order to appropriately size the rods. Samples were provided by the CSC during the months of July and August 2012. From these samples, roughly 400 strawberries were hand-inspected to determine width, length, and weight distributions. A chi-squared test indicated that a Gaussian distribution could adequately represent variation in all three characteristics. The physical appearance and geometry of the strawberries were also noted. Additionally, strawberries were collected from local stores from a variety of brands such as Dole, Driscoll, Wish Farms, etc. throughout the year to verify that the distributions could provide a rough estimate of a typical strawberry. Given a distribution of sizes and geometries, the roller rods were developed to orient over 95 percent of strawberries. This correlates to strawberries within approximately 1.00 – 2.50 inches in length. Both empirical and dynamic simulations were used to optimize

design. The resultant roller rod geometry resembles an hourglass figure, which creates a pseudo-cup in between the valley of adjacent roller rods.

In order to singulate the strawberries, they were first placed in a water tank. The lower density of the strawberries compared to the water caused them to float and form a single sheet of strawberries on the surface. Next, the conveyor of roller rods picked the top layer of strawberries up from the water tank in the cup created between the adjacent rollers. The roller rods then began to rotate due to friction forces between the ends of the rods and the AVID frame. The rotation imparted energy to the strawberries, which caused the haul of strawberries to settle into their individual cups. Excess strawberries would fall back into the water tank and wait for the next empty cup. The rotation also caused strawberries within their cups to orient themselves so that their axes were parallel to the roller rod's axes, as seen in Figure 22.

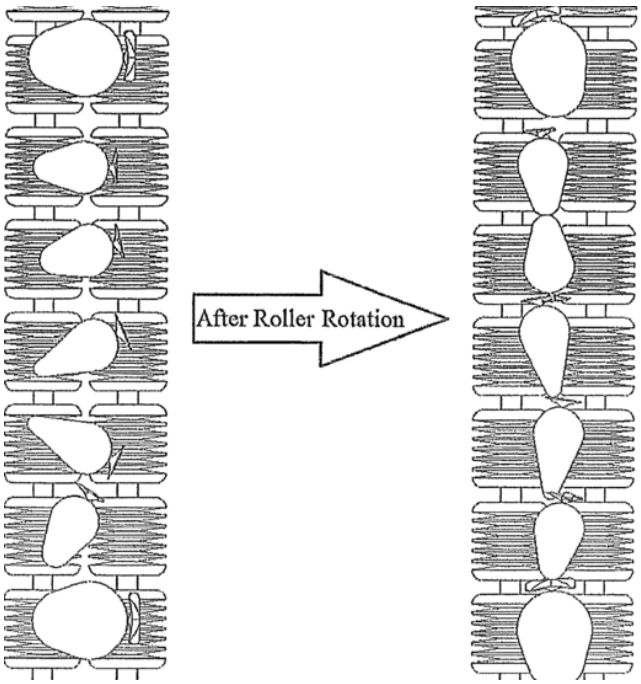


**Figure 22.** An illustration of the roller rod orientation method is shown. Randomly oriented strawberries are shown on the left. After roller rotation, the strawberries are significantly more oriented, as shown on the right.

In addition, separating fins were used in the first few feet of the conveyor in order to prevent strawberries that had settled into their respective cups from jumping into neighboring cups. The result was a uniform grid of strawberries, as illustrated in Figure 23.

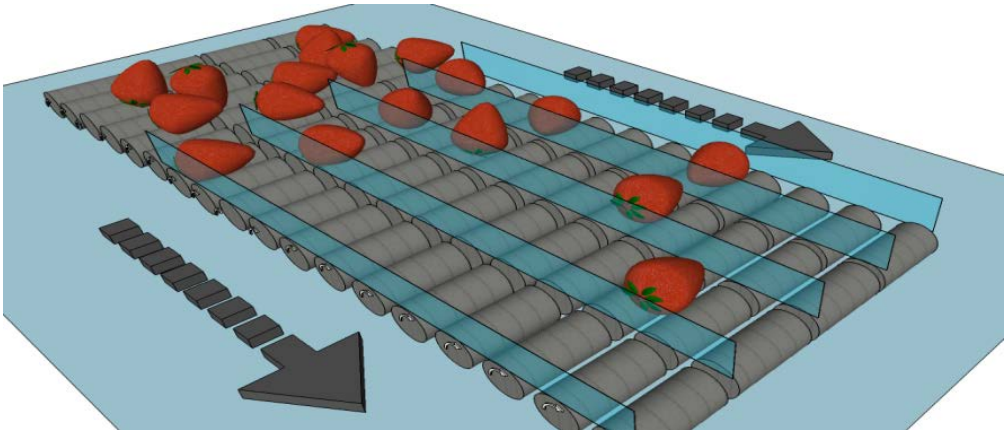

**Figure 23.** Orientation and singulation of strawberries as a result of rotating roller rods. A cylindrical roller rod can be used (as shown). However, hourglass roller rods have achieved better results.

Many variations of the roller rod were investigated. The initial roller rod consisted of CNC machined UHMW press-fit on a stainless steel rod. The UHMW was easy to clean and could be colored to assist the machine vision system in noise reduction. The second generation roller rod replaced the UHWM material with a completely stainless steel spring design, which could better withstand the forces of the waterjet cutting stream. Finally, the third generation roller rod improved upon the spring design by adding structural support disks evenly spaced throughout the rod. This design allowed for more uniformity between roller rods and was easier to assemble. The final roller design took into account strawberry size and shape as well as roller material, and was optimized to achieve the highest percentage of strawberry orientation and singulation.

### 7.3 Results and Discussion

#### 7.3.1 Strawberry Size Distributions

Strawberry width and length distributions were taken from roughly 400 samples provide by the CSC during the months of July and August 2012. The distributions are shown in Figure 24. These results were then compared to random samples of locally purchased strawberries from a variety of brands. From these observations, we developed a specially designed roller rod capable of properly orienting and positioning conical strawberries for the subsequent vision and cutting section. This data was also used to assist the vision system in appropriately defining the calyx removal cutting path.

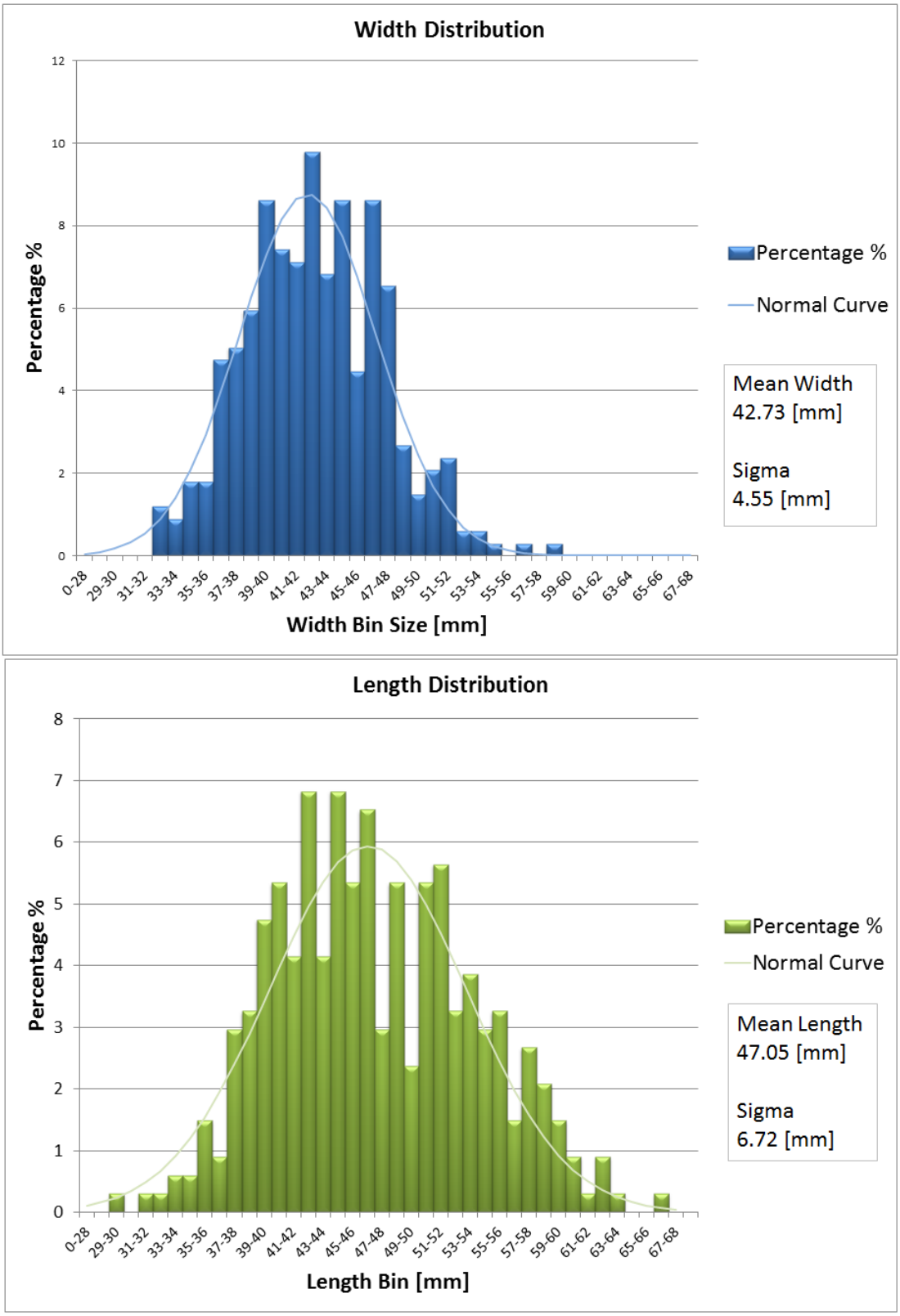


**Figure 24.** Strawberry width and length distributions from 400 samples collected from July – August 2012. A Gaussian curve is plotted over each distribution.

### 7.3.2 Strawberry Abnormality

Strawberry geometry and abnormalities were also noted, as shown in Figure 25. The results indicate that roughly 90 percent of strawberries selected were ideal for automatic calyx removal. This number will be significantly higher if minor presorting is performed on the grower or processor side. However, the machine will automatically separate abnormal strawberries for alternative use.

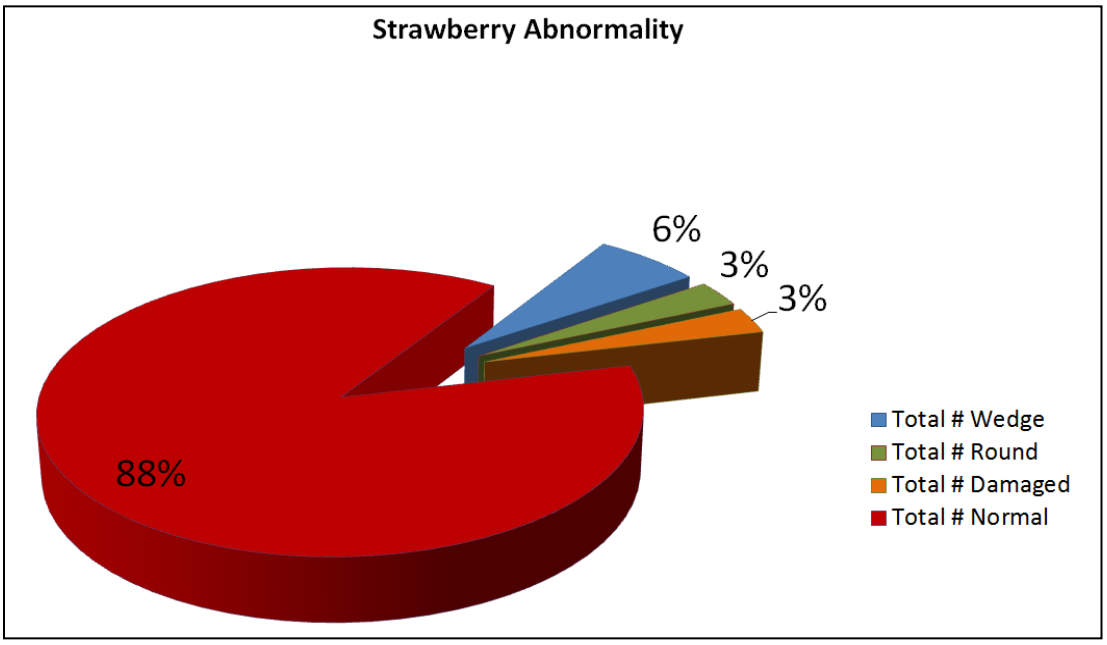


**Figure 25.** The data shows strawberry abnormalities in 400 samples collected from July – August 2012. Roughly 90 percent of strawberries are ideal for orientation and singulation.

The optimal strawberry orientation roller design was determined using both empirical and dynamic simulation data. The result was an hourglass figure that created a pseudo-cup to pick up strawberries from the water tank (see Figure 26). Once out of the water tank, the rotation of the roller oriented and singulated strawberries into a uniform grid. Through testing, it was found that V-grooves or gaps

were necessary to prevent the waterjet stream from ricocheting off the roller surface and moving surrounding strawberries during the calyx removal process.

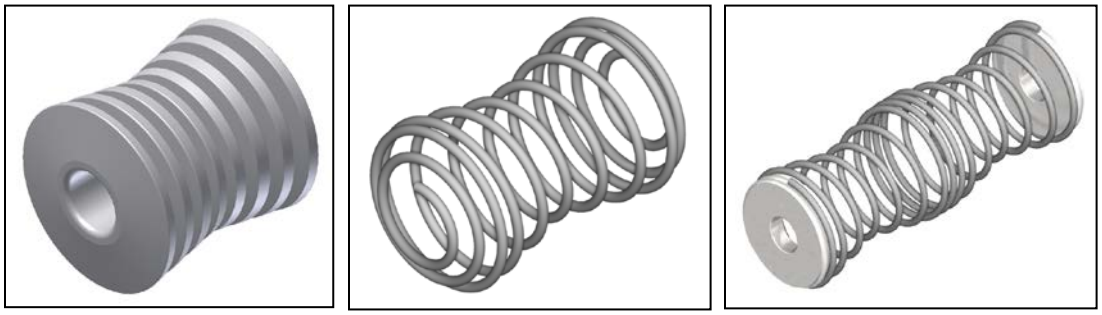

**Figure 26.** The three generations of the roller portion of the orientation roller rod are shown from left to right. The first generation is fabricated using UHWM. The second generation utilizes a stainless steel spring design. The third generation contains end structures that increase fabrication efficiency. The dimensions and geometry of the roller are optimized to orient the largest variety of strawberries (Tao, Lin, Chen, & Seibel, 2014).

### 7.3.3 Dynamic Simulations

The custom roller rod was then modeled in Autodesk Inventor 2012 dynamic simulator, as seen in Figure 27. This kinematic analysis was used to determine the optimal geometry and rotational speed needed for strawberry orientation. The simulations indicated that optimal strawberry orientation took place at conveyor speeds of 1 foot per second. It should be noted that the simulation parameters were adjusted so as to best replicate empirical data.

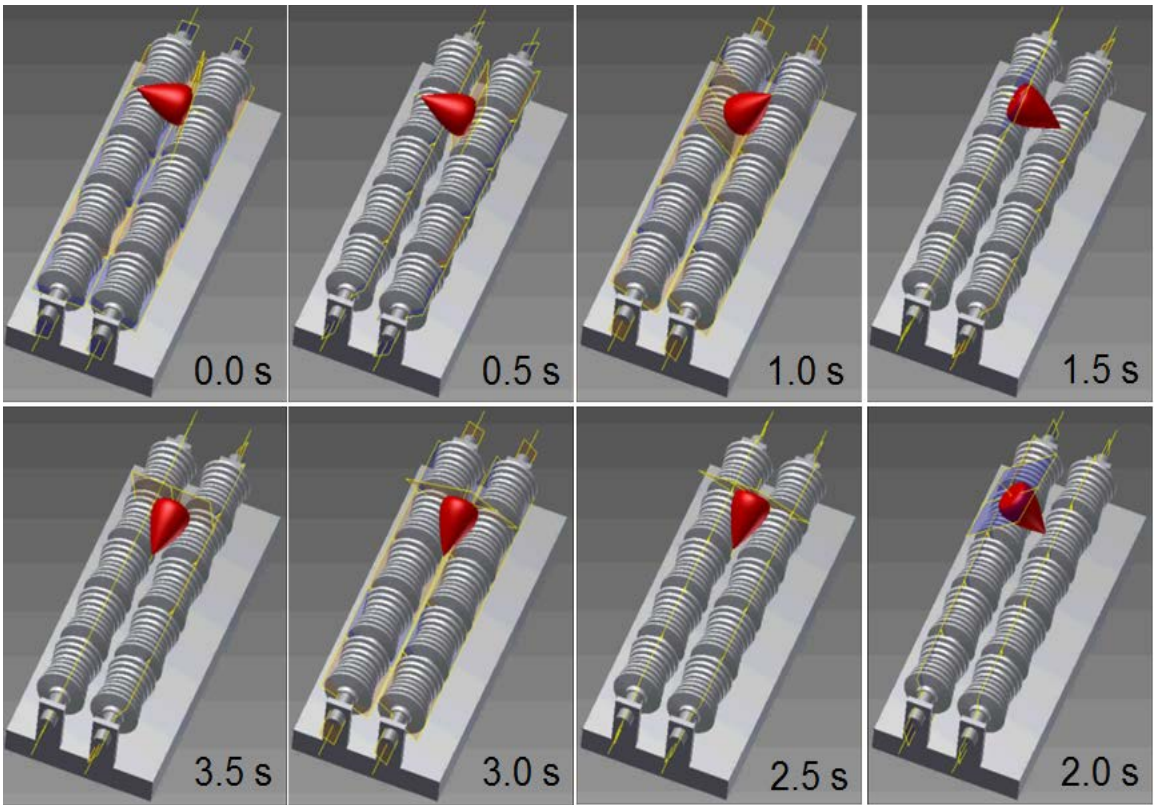


**Figure 27.** Simulation of orientated roller rods' effect on randomly placed strawberries. The kinematic analysis was performed by Autodesk Inventor 2012 dynamic simulator. This analysis software uses the Newton-Raphson method to solve constraint equations to determine strawberry position at an instant in time.

Although the first generation roller was depicted in this simulation, all three generations of rollers showed similar results.

### 7.3.4 Live Orientation and Singulation

The strawberry orientation roller rods were tested by randomly loading strawberries onto the rods and inspecting the imaged results (see Figure 28). Of 150 randomly sampled strawberries, 96.7 percent were oriented and 98.7 percent were singulated.

**Figure 28.** Strawberries are randomly loaded onto the roller rods using a vibration shaker. The strawberries are shown to be more oriented as they travel along the rollers from right to left. After roughly 3 seconds, a majority of strawberries are oriented so that their axes are parallel to the roller rod.

However, it was noted that approximately 5 – 10 percent of strawberries would rest tip down within the rollers. As the rollers began to rotate, these tip-down strawberries would not orient in a manner in which their calyxes could be removed by the waterjet system. A preliminary attempt to decrease the occurrence of this case was made.

### 7.4 Ongoing Improvements

The current third generation rollers are designed specifically for small, medium, and large conical strawberries. Further research and development is needed to account for spherical and rectangular shaped strawberries. In addition, further improvements in hygienic design should be made.

An attempt to decrease the occurrence of tip-down strawberries is currently being made. A custom designed sprocket was used to engage with the orientation roller so as to lift or dislodge tip-down strawberries. Figure 29 shows a rendering of this orientation sprocket.

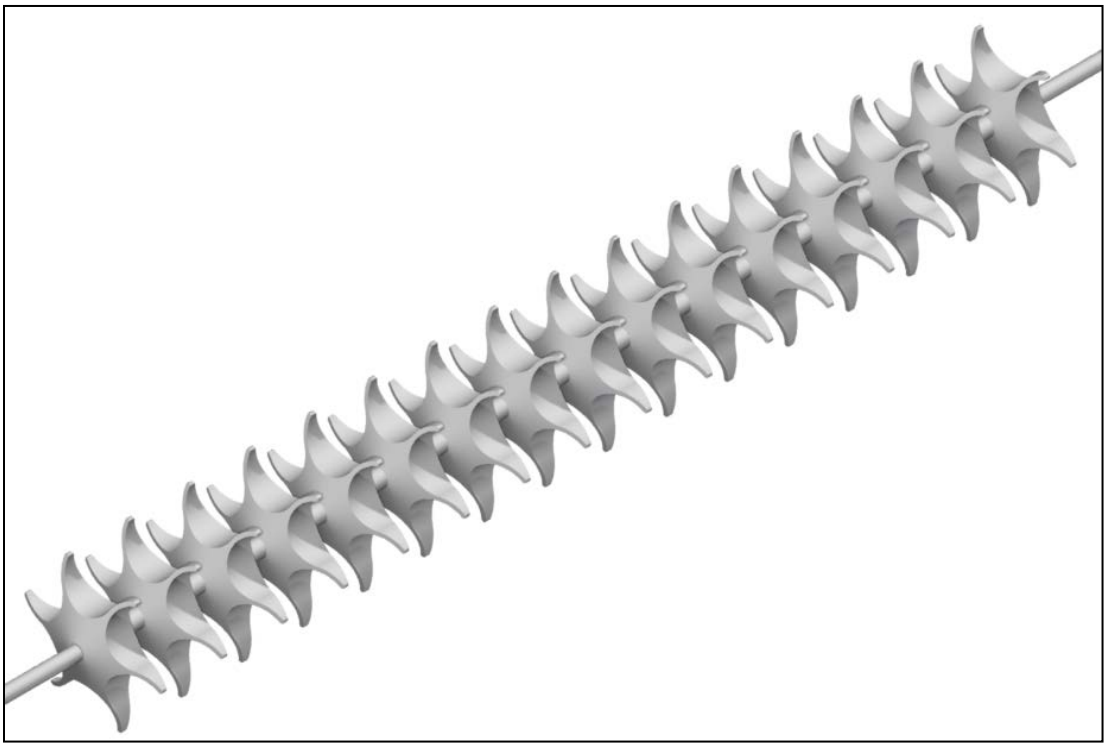

**Figure 29.** A rendering of the orientation sprocket is shown.

Preliminary studies indicate that the orientation sprocket is able to significantly decrease the occurrence of tip-down strawberries. Further research is needed to optimize the design and use of this system.

# Chapter 8: Quantitative Assessment of Machine Vision System

The high production speed of the AVID machine requires machine vision automation. This non-contact sensing approach is able to provide accurate identification of strawberry features for assigning cut-line location. In addition, this method allows for future improvements in speed and accuracy with minimal to no hardware adjustments. A simple and efficient calyx identification algorithm has been developed that is linear in complexity with low constant factors. A colored image of the strawberry provides lightness and color values that allow for feature detection. These features are then used to decide between attempting to remove the calyx or flagging the strawberry for a return loop cycle.

## 8.1 Introduction

The main challenge in calyx identification is to cope with a wide variety of variations within and between strawberry cultivars. These variations include a strawberry's orientation, geometric shape, and color. External factors such as dirt, complex backgrounds, and inconsistent illumination conditions may also contribute to the overall problem.

Throughout the last decade, there has been increased research in strawberry segmentation algorithms for use in robotic harvesters (Feng, Qixin, & Masateru, 2008), (Hayashi, et al., 2010). Although there is an abundance of methods and approaches, most techniques use a pixel-based color cue method to identify a strawberry's fruit and calyx location. This is where each pixel is classified as

background, strawberry fruit, or strawberry calyx, individually and independently from its neighbors. Depending on the algorithm's implementation and how the results are used, this can be a fast and reliable solution. There have also been attempts to use more complex algorithms that rely on neural networks to solve this segmentation problem; however, due to their computational expense, their use for real-time automation is limited.

In this project, a pixel-based color cue method is used to identify calyx location and the appropriate cutting position for its removal. The CIELAB color space is used because it possesses lower variance overlap between background, fruit, and calyx pixels. A user-defined set of thresholds is used to classify each pixel as one of the three regions.

## 8.2 Material and Methods

The main components of the machine vision system are illustrated in Figure 30 below.

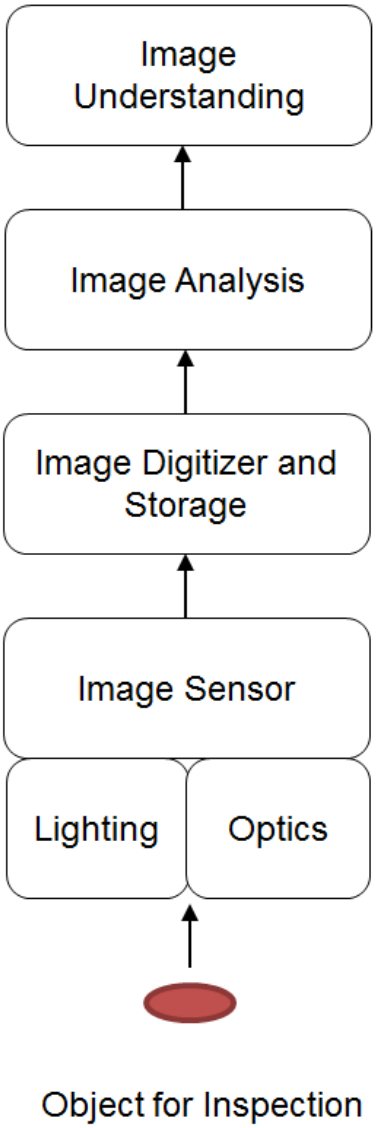


**Figure 30.** Basic components of a machine vision system as adopted by Pinder (Pinder & Godfrey, 1993).

Specific attention has been placed on the design of the strawberry image formation. The machine vision components have been optimized to minimize the

complexity of the cut-line identification algorithm while still being reliable enough to withstand a food processing environment.

### 8.2.1 Lighting

The strawberries were lit with ten Patlite IP69K LED light bars; six were 1200mm in length and four were 100mm in length. The color of each light was 4800K, and illuminance was approximately 1600lx and 140lx with respect to length. The lights were mounted in a rectangular fashion, where three 1200mm lights were used for each of the side lengths and two 100mm lights were used for each of the side widths. The elevation of the lights was approximately 6 inches above the strawberry. This provided a fairly uniform lighting condition for each strawberry that passed under the rectangular light arrangement. In addition, this height highlighted strawberry features while obscuring the background.

### 8.2.2 Optics

A fixed 8mm Navitar lens designed for 1/3 inch format CCD chips was used. The object area at minimum object distance of this lens was approximately 183mm x 136mm. Two of these lenses were used, each viewing eight lanes of potential strawberries. The spherical aberration of the 8mm lens was sufficiently small for our application. It should be noted that a larger focal length would have improved image quality; however, this would have increased vision chamber dimensions significantly.

### 8.2.3 Image Sensor

A Sony XCL-C130C camera with 1/3 inch format CCD was used to segment strawberry features from one another based on color. The camera's region of interest (ROI) was set to 1068 by 200 pixels. The ROI was centered with the CCD center to minimize spherical aberration, and the camera exposure time was set to 0.2ms to minimize motion blur. The camera was positioned approximately 42 inches above the strawberry conveyor zone, which provided a resolution of $0.5mm^2$ per pixel.

### 8.2.4 Image Digitizer

The image signal was fed to a Matrox Solios eV-CL frame grabber. The frame grab was then triggered through an interrupt signal from the conveyor's encoder, and the image was stored as three separate monochrome component images.

### 8.2.5 Image Analysis

Matrox Imaging Library 9 (MIL9) (Matrox) was used for developing the image analysis algorithms. MIL9 contained built-in toolboxes for blob analysis. In addition, this software package was optimized for speed and supported the C++ language. A flow chart of the image analysis and image understanding is shown in Figure 31.

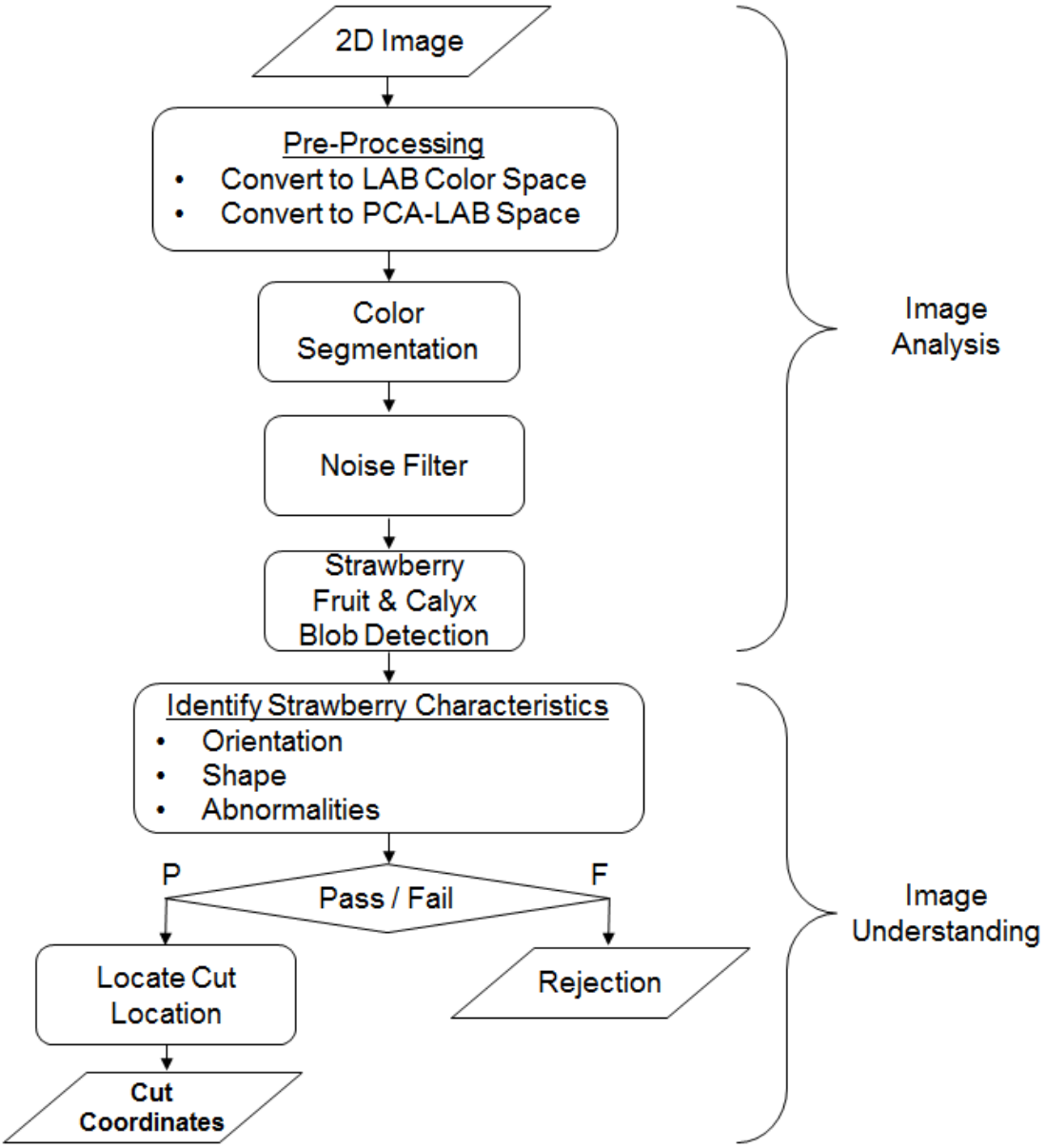


**Figure 31.** Flow chart of how the calyx removal cut-line is determined is shown.

#### 8.2.5.1 Pre-Processing

Initially, the input signals for the red, green, and blue channels were converted to CIELAB color space to take advantage of its uniform distribution and device-independent characteristics. Furthermore, CIELAB color space separated color from intensity, allowing the reflective gray metal background to be isolated and subtracted

from the image. This also made the acquired image less vulnerable to lighting and white balance imperfections. The CIELAB conversion was optimized for speed by replacing commonly used float computations with integer-based calculations. The transformation process consisted of an RGB to XYZ, then to CIELAB color space through the use of lookup tables (Leo´n, Mery, Pedreschi, & Leo´n, 2006).

A pairwise correlation analysis between the channels of the CIELAB color space was performed to measure the independence of each channel. This analysis utilized CIELAB data from ten randomly selected images. The study was then replicated three times. The Pearson linear correlation coefficient was calculated for each combination of CIELAB channels, which is described by the equation below.

$$\rho(A,B) = \frac{1}{N-1}\sum_{i=1}^{N}\left(\frac{A_i - \mu_A}{\sigma_A}\right)\left(\frac{B_i - \mu_B}{\sigma_B}\right)$$

Where,

$\rho(A,B)$ = Pearson correlation coefficient between random variables *A* and *B*
$N$ = Number of observations
$\mu_A$ = Mean of random variable *A*
$\mu_B$ = Mean of random variable *B*
$\sigma_A$ = Standard deviation of *A*
$\sigma_B$ = Standard deviation of *B*

A correlation coefficient matrix was then created for the three channels of the CIELAB color space. This is represented by the matrix *C*, as seen in the following.

$$C = \begin{bmatrix} \rho(L,L) & \rho(L,A) & \rho(L,B) \\ \rho(A,L) & \rho(A,A) & \rho(A,B) \\ \rho(B,L) & \rho(B,A) & \rho(B,B) \end{bmatrix}$$

Where,

$\rho(A,B)$ = Pearson correlation coefficient between random variables *A* and *B*

The *C* matrix consisted of Pearson correlation coefficients for each pairwise variable combination of the *L*, *A*, and *B* channels.

Principle component analysis (PCA) was then used to rotate the CIELAB axis in order to maximize each axis's variance. The analysis accomplished this by setting the new axis as the unit eigenvectors of the CIELAB covariance matrix. This process is referred to as PCA-LAB transformation. The CIELAB data of ten randomly selected images were used to create the covariance matrix. The covariance matrix Σ is shown below.

$$\Sigma = \begin{bmatrix} \sigma(L,L) & \sigma(L,A) & \sigma(L,B) \\ \sigma(A,L) & \sigma(A,A) & \sigma(A,B) \\ \sigma(B,L) & \sigma(B,A) & \sigma(B,B) \end{bmatrix}$$

Where,

$\sigma(A,B)$ = Covariance between random variables *A* and *B*
*L* = *L*-channel
*A* = *A*-channel
*B* = *B*-channel

The solutions of the principle component analysis satisfy the equation below.

$$\Sigma\nu = \lambda\nu$$

Where,

$\lambda$ = A column vector containing the eigenvalues of matrix $\Sigma$
$\nu$ = Eigenvector of matrix $\Sigma$

Once this was completed, a CIELAB to PCA-LAB space transformation matrix was found. This matrix was then used to create lookup tables to minimize the time complexity of the transformation.

It should be noted that an HSI approach was also attempted when using first generation rollers (Hughes, et al., 2014). This approach took advantage of the blue colored roller to create a high fidelity fruit and leaf binary blob image. However, this approach could not be used with the third generation rollers due to the reflections from the stainless steel.

#### 8.2.5.2 Segmentation

The strawberry was first segmented into color features using a user-defined knowledge-based thresholding method. These segmented colors were then classified as strawberry fruit or strawberry calyx. The fruit classification consisted of the following colors: red, dark red, yellowish red, and bright red. The calyx classification consisted of the following colors: green, dark green, and light green. Once the fruit and leaf portions of a strawberry had been identified, the image was converted to a

binary image. The associated noise for each image was minimized through the use of open and close operations, which used two pixels as their filter criteria. Furthermore, to reduce artifacts, smaller blobs were ignored. Through user inspection, we discovered that blob sizes beneath 40 pixels and 30 pixels for fruit and leaf binary images, respectively, worked well.

#### 8.2.5.3 Blob Analysis

A blob-based recognition algorithm was developed to account for the many scenarios of strawberry shape and pose on the rollers. Each blob provided information on pixel area, center of gravity (*cog*) location, *x*-axis projection, and bounding box coordinates. These features were then used to identify strawberry characteristics such as orientation, shape, and abnormalities. An area threshold filter was used to ignore fruit and leaf blobs of underneath a certain threshold.

### 8.2.6 Image Understanding

The cut-line assignment was designed to maximize capped fruit weight. This assignment would vary depending on the strawberry's orientation, shape, and abnormalities. Based on many observations of strawberries that passed through the AVID's material handling section, ten cases were identified: aligned, diagonal, perpendicular, tip-up, calyx-up, round, wedged, multi-berry, overlap, and white shoulder. To help differentiate the cases, a statistical analysis was performed using MATLAB's Machine Learning and Statics toolbox (Mathworks) to identify unique blob features for each case.

#### 8.2.6.1 Case Identification

Each of the ten cases was identified using statistically significant fruit and calyx blob features. An aligned case occurred when a conical strawberry sat axially parallel with the roller rods. This case included all features extracted from both the fruit and leaf binary image; these features from the aligned case serve as the reference for all other orientations and shapes. The diagonal and perpendicular cases used the fruit *cog* as an origin and found the average vector between fruit *cog* and leaf pixels (*BcLp*). The *cog* was calculated using the equation below.

$$(x_{cog}, y_{cog}) = \left\{ \frac{\sum_{x=0}^{M-1}\sum_{y=0}^{N-1} x \cdot I(x,y)}{\sum_{x=0}^{M-1}\sum_{y=0}^{N-1} I(x,y)}, \frac{\sum_{x=0}^{M-1}\sum_{y=0}^{N-1} y \cdot I(x,y)}{\sum_{x=0}^{M-1}\sum_{y=0}^{N-1} I(x,y)} \right\}$$

Where,

$x_{cog}, y_{cog}$ = $x$ and $y$ coordinates of the center of gravity
$M$ = Column dimension of the image
$N$ = Row dimension of the image
$I(x,y)$ = 1 for a white pixel and 0 for a black pixel

The fruit binary image would assign a white color pixel for the object of interest and a black color pixel for the image background. Given the coordinates of the center of gravity, the *BcLp* vector could be determined as follows.

$$(x_{BcLp}, y_{BcLp}) = \left\{ \frac{\sum_{x=0}^{M-1} \sum_{y=0}^{N-1} (x - x_{cog}) \cdot I(x,y)}{\sum_{x=0}^{M-1} \sum_{y=0}^{N-1} I(x,y)}, \frac{\sum_{x=0}^{M-1} \sum_{y=0}^{N-1} (y - y_{cog}) \cdot I(x,y)}{\sum_{x=0}^{M-1} \sum_{y=0}^{N-1} I(x,y)} \right\}$$

Where,

$x_{BcLp}, y_{BcLp}$ = $x$ and $y$ end coordinates of the *BcLp* vector
$M$ = Column dimension of the image
$N$ = Row dimension of the image
$I(x,y)$ = 1 for a white and 0 for a black pixel

The magnitude and direction of the *BcLp* vector determined if the strawberry was diagonal or perpendicular, as seen in Figure 32.

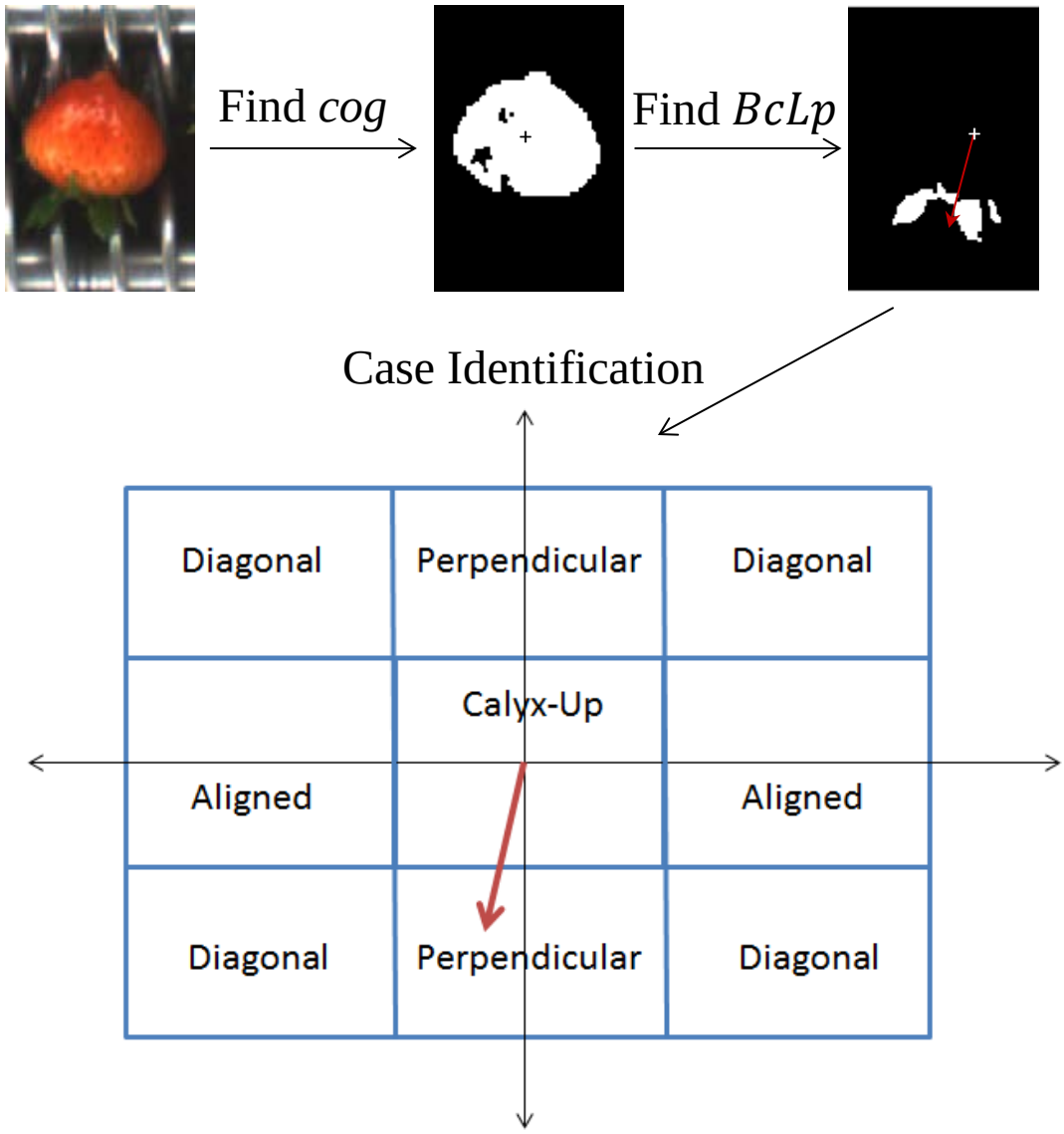


**Figure 32.** A visual representation of case identification through use of the *BcLp* vector is depicted. The *cog* is shown as a cross symbol and the *BcLp* vector is shown as a red vector. The location of the vector's end coordinate is used to help identify the strawberry case.

Tip-up cases were detected if there was a lack of calyx pixels present beneath a minimum threshold. Calyx-up cases were identified through any of three characteristics: 1) a large amount of leaf pixels was present and few fruit pixels present, 2) the number of blobs per lane was greater than 1, or 3) the *BcLp* vector's magnitude and direction were beneath a certain threshold. Round cases were

identified through the comparison of the four values of fruit *cog*, location of peak *x*-projection, variance of *x*-projection, and bounding box coordinates. Wedge cases were found in a similar fashion as round cases, but with different thresholds used. Multi-berry cases were identified through any of two characteristics: 1) the number of blobs per lane was greater than 1, or 2) the *BcLp* vector's magnitude and direction were outside of the aligned case's threshold. Overlap cases were identified as a fruit blob shared between two lanes. This can be seen in Figure 33.

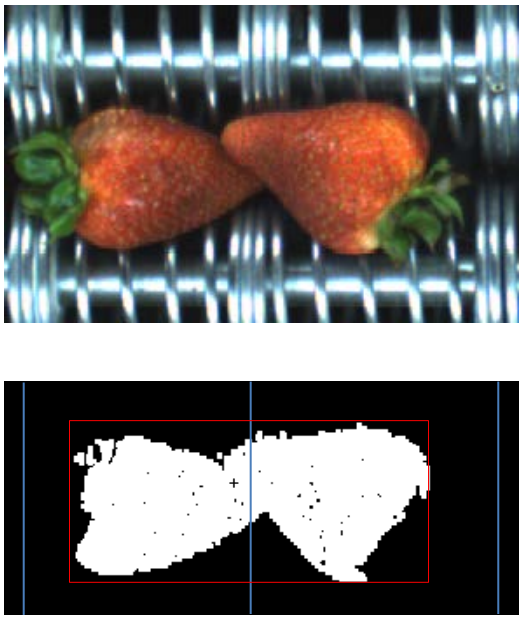

**Figure 33.** An example of an overlap case identification is shown. The top image is of two overlapping strawberries. The bottom image shows the fruit binary image, which contains the fruit blob bounding box (shown in red) and the lane borders (shown in blue). The *cog* is shown as a cross symbol.

The *cog* of an overlap case would be far offset from the center of a lane, and the bounding box coordinates would crossover a lane's dividing line. Finally, white shoulder cases were inherently considered and appropriately adjusted for by selecting

color thresholds that did not include the white shoulder portion. The cut-line adjustment of this case resembled that of round cases.

#### 8.2.6.2 Algorithm Development

Two algorithms were developed for the AVID machine vision system: a rejection algorithm and a cut-line assignment algorithm. The rejection algorithm identified strawberries that were not ideally oriented for calyx removal. The cut-line assignment algorithm first considered the strawberry shape and pose, and then determined a cutting location that would minimize fruit loss while fully removing the unwanted calyx and white shoulder region. The algorithms were both optimized using a user-defined ground truth cut-line coordinate.

##### 8.2.6.2.1 Ground Truth Comparison

The orientation and shape of the imaged strawberry affected the cutting location. For example, a diagonal case required the cutting location to be moved closer to the center of the strawberry in order to remove the calyx completely. In order to account for each strawberry's orientation and shape, a case-based algorithm was developed. Each case's algorithm was calibrated using a ground truth database that included a set of 100 pictures of each of the following cases: aligned, wedged, round, diagonal, white shoulder, and overlap. Each image contained strawberries with user-defined cut-line coordinates. These cut-lines were used as the ground truth in calibrating the case-based algorithm. Cases that were considered unfavorable for calyx removal were actively avoided by the waterjet cutting stream. These

strawberries were labeled as “rejected” and would be diverted to a return loop cycle for another opportunity for calyx removal.

#### 8.2.6.2.2 Cut or Reject Decision

In order to improve yields of IQF whole berry, the most valuable output, a rejection algorithm was implemented. This allowed for strawberries that were not ideally aligned or were in other ways defective to be actively avoided by the waterjet cutting stream. This fruit would then be sent into a return cycle for a second chance at orientation and calyx removal. In terms of output product, this strawberry would be considered Return Fruit.

Six of the ten most common observed strawberry cases were accepted for calyx removal and four were selected for rejection. The acceptable cases were aligned, diagonal, round, wedge, overlap, and white shoulder. The rejection cases were multi-berry, perpendicular, tip-up, and calyx-up. Sensitivity and specificity data were collected on the rejection algorithm.

#### 8.2.6.2.3 Cut-Line Assignment

The cut-line determination algorithm was designed in a manual iterative error-correcting procedure in which an initial prediction was made and then modified to more accurately fit the given strawberry case. The initial prediction was a length value between fruit *cog* and cut-line location (*BcCl* length).

The *BcCl* length was calculated using the following equations below.

$$G_r = \frac{\sum_{y=0}^{N-1} I(x_{cog}, y)}{2}$$

$$\overrightarrow{BcCl} = (K)\left(\frac{H}{W}\right)(G_r)$$

Where,

$K$ = Case constant
$H$ = Fruit blob bounding box height
$W$ = Fruit blob bounding box width
$G_r$ = Fruit blob gravity radius
$N$ = Row dimension of image
$x_{cog}$ = $x$-coordinate of the center of gravity location
$I(x, y)$ = 1 for a white pixel and 0 for a black pixel

This $BcCl$ equation was applied to the aligned strawberry case and was considered the default cut-line assignment algorithm. This length value was then either extended or contracted through the *K* constant depending on the strawberry case. This is referred to as a shortening or lengthening correction. For example, this value was extended for strawberries that were conical and more elongated, and contracted for strawberries that were more spherical. The accuracy was determined as a measure of absolute error between the ground truth cut-coordinates and those calculated by each respective case-based algorithm.

Although the absolute values of the errors were used for measuring accuracy, positive and negative errors were still tracked because each had different implications in the context of the resultant output product. A positive error was defined as when

the algorithm predicted a *BcCl* length value shorter than the ground truth, and a negative error was when the prediction was longer than the ground truth. In this setting, positive errors were preferred, since the cut strawberry would still be free of any leaf or residual calyx, whereas a negative error case would not cut off enough of the undesirable part of the strawberry. Specifically, any negative error greater than three pixels, or about 1.5mm, was considered a "miss" and counted separately as an alternative measure of accuracy. In terms of output product, a negative error would be either a Residual or a Return Fruit.

## 8.3 Results and Discussion

### 8.3.1 Image Analysis

The imaging system was capable of identifying the precise calyx location based on the CIELAB differences between strawberry fruit and calyx, even under noisy environments. In addition, the calyx location was identified within 50ms upon image capture. Figure 34 shows the typical results of each step of the image analysis. The descriptions of the steps are discussed in Sections 8.2.5.1 through 8.2.5.3.

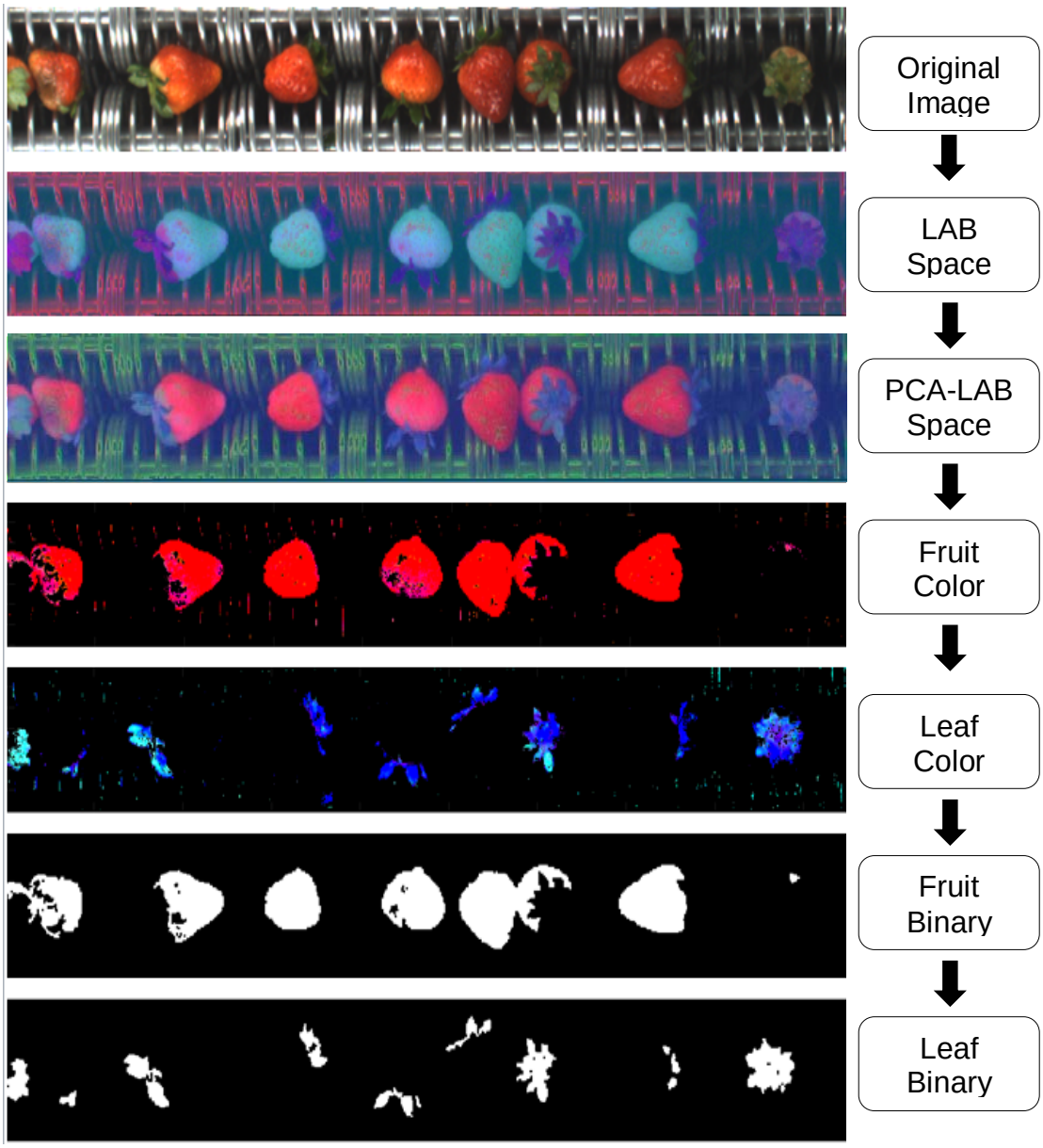


**Figure 34.** The steps of the AVID machine vision's image analysis are shown in order from top to bottom. The original image is first captured and converted to LAB space. The covariance matrix's eigenvectors are then found and used to convert the image to PCA-LAB space. A user-defined knowledge-based thresholding method is used to identify fruit and leaf portions through color segmentation. Both the fruit and leaf portions are then filtered to remove noise and converted to binary images.

#### 8.3.1.1 Pre-Processing

The PCA-LAB transformation allowed for increased signal-to-noise ratios beyond 10 percent when compared to the CIELAB color space approach. This

increase in strawberry fruit and leaf blob fidelity was seen consistently over a wide range of strawberry types and lighting conditions. This was predictable considering the pairwise correlation between channels of the CIELAB color space of one dataset were as follows.

$$C = \begin{bmatrix} 1.0000 & 0.1166 & 0.2748 \\ 0.1166 & 1.0000 & 0.7573 \\ 0.2748 & 0.7573 & 1.0000 \end{bmatrix}$$

Where, *C* is the correlation matrix among CIELAB channels. The correlation among some CIELAB channels was as high as 0.76. It should be noted that although this result was from one dataset, all replications of this study showed a similar *C* matrix.

The transformation matrix used to map the CIELAB space to PCA-LAB space is shown below.

$$H = \begin{bmatrix} 0.3126 & 0.9376 & -0.1525 \\ 0.6561 & -0.3292 & -0.6791 \\ 0.6869 & -0.1122 & 0.7180 \end{bmatrix}$$

Where, *H* is the transformation matrix. This result utilized a dataset of CIELAB points from ten randomly selected strawberry images. It was seen that ten samples were sufficient in creating a general *H* matrix that could be applied to all acquired images to enhance color segmentation. The new image coordinates were found using the following equation.

$$PCALAB = [LAB][H]$$

Where,

*PCALAB* = Transformed image matrix set in PCA coordinate system
*LAB* = Matrix containing column vectors of *L*, *A*, and *B* channels of image
*H* = CIELAB space to PCA-LAB space transformation matrix

The *PCALAB* matrix consisted of column vectors of the original coordinates set in the principle component coordinate system. Furthermore, it was seen that the *H* transformation matrix described above could be used for a wide range of strawberry types and lighting conditions. This allowed the time consuming calculations of the covariance matrix to be performed offline.

#### 8.3.1.2 Threshold Selection

The PCA-LAB color space allowed strawberry fruit and leaf portions to be identified through color segmentation. A user-defined knowledge-based threshold selection method produced the best results. Through the manual analysis of hundreds of randomly sampled pictures over the eight weeks of performance tests, it was found that both the fruit and leaf portions needed to include multiple color regions in order to reliably classify strawberries of different color intensities and degrees of damage. The fruit classification consisted of the following colors: red, dark red, yellowish red, and bright red. The calyx classification consisted of the following colors: green, dark green, and light green. These hand-selected regions are seen in Figure 35.

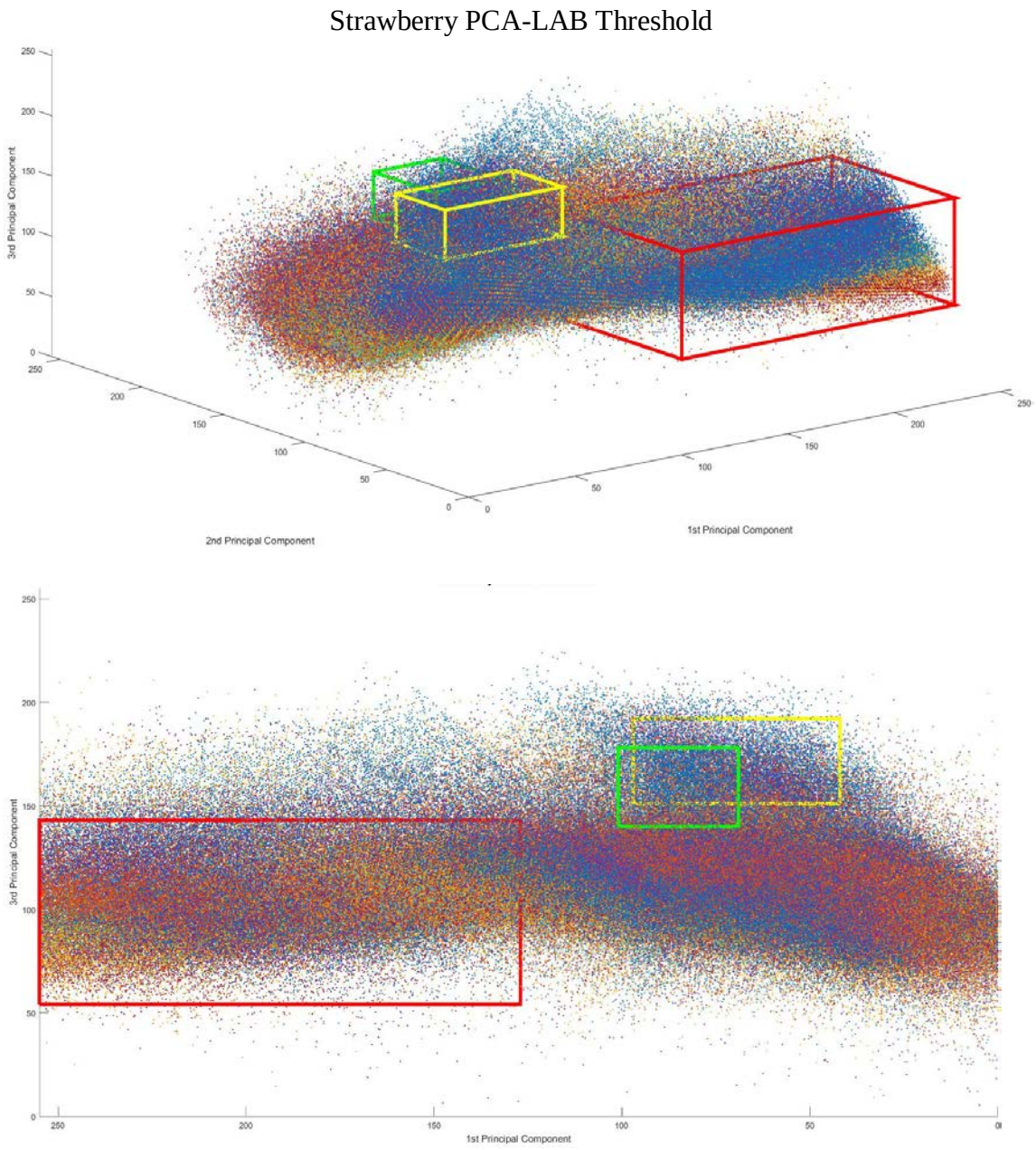


**Figure 35.** The PCA-LAB coordinates of 12 randomly selected strawberry images are plotted in three-dimensional space. Each strawberry image's coordinates are represented by a different color dot. The colored square region represents the hand-selected thresholds used to classify fruit from leaf. The red region consists of fruit pixels, and the green and yellow regions consist of leaf pixels.

Although there was not a distinct visual separation between PCA-LAB regions of fruit and leaf, the binary image fidelity was sufficient for the AVID machine application.

#### 8.3.1.3 Blob Detection Sensitivity vs. Specificity Analysis

During the eight weeks of performance tests, 55 images acquired by the AVID machine vision system were randomly selected to test the vision system's ability to correctly identify strawberry fruit and calyx. These images were selected during times when the conveyor was moving at 1 foot per second. A sensitivity and specificity analysis of the data is shown in Table 2. The analysis indicated that the strawberry calyx specificity was high at 99.7 percent; however, at 92 percent, the sensitivity could be improved. This indicated that the majority of calyxes identified by the algorithm were identified correctly. Given the high specificity, it is possible to increase the sensitivity by lowering the threshold of what *L*, *A*, and *B* values are considered a calyx. This could be implemented by slightly widening the fixed calyx threshold ranges.

**Table 2.** Sensitivity and specificity data for the vision system's strawberry calyx identification is shown.

| Calyx Blob Sen. vs. Spec. | | Strawberry Calyx | | |
|---|---|---|---|---|
| | | Present | Absent | Total |
| AVID Vision System | Positive | 127 (a) | 1 (b) | 128 |
| | Negative | 11 (c) | 301 (d) | 312 |
| | Total | 138 | 302 | 440 |

$$Sensitivity = \frac{a}{a+c} = \frac{127}{138} = 92\%$$

$$Specificity = \frac{d}{b+d} = \frac{301}{302} = 99.7\%$$

$$Predictive\ value\ of\ a\ positive\ test = \frac{a}{a+b} = \frac{127}{128} = 99.2\%$$

$$Predictive\ value\ of\ a\ negative\ test = \frac{d}{c+d} = \frac{301}{312} = 96.5\%$$

The strawberry fruit identification was more accurate than calyx identification. The specificity was 100 percent and the sensitivity was 95.2 percent (see Table 3). The sensitivity can also be increased with the same approach, as described previously with the calyxes.

**Table 3.** Sensitivity and specificity data for the vision system's strawberry fruit identification is shown.

| Fruit Blob Sen. vs. Spec. | | Strawberry Fruit | | |
|---|---|---|---|---|
| | | Present | Absent | Total |
| AVID Vision System | Positive | 140 (a) | 0 (b) | 140 |
| | Negative | 7 (c) | 293 (d) | 300 |
| | Total | 147 | 293 | 440 |

$$Sensitivity = \frac{a}{a+c} = \frac{140}{147} = 95.2\%$$

$$Specificity = \frac{d}{b+d} = \frac{293}{293} = 100\%$$

$$Predictive\ value\ of\ a\ positive\ test = \frac{a}{a+b} = \frac{140}{140} = 100\%$$

$$Predictive\ value\ of\ a\ negative\ test = \frac{d}{c+d} = \frac{293}{300} = 97.7\%$$

During the eight weeks of performance tests and two weeks of stress tests, the correct identification of strawberry fruit and leaf was shown to be fairly accurate. This demonstrates the ability of the PCA-LAB approach to produce a high fidelity fruit and leaf binary image.

### 8.3.2 Image Understanding

It was found that fruit and leaf blob features could provide sufficient information to determine strawberry orientation and shape. This allowed the rejection algorithm to accurately identify which strawberries to cut and which to divert to a return loop cycle. Furthermore, these features were shown to be effective in optimizing the cut-line assignment algorithm to minimize fruit loss over a range of strawberry cases during the calyx removal process.

#### 8.3.2.1 Feature Analysis

Three unique features were found to be statistically useful for identifying strawberry orientation and shape: fruit and calyx area, fruit height-width ratio, and fruit gravity radius. This is shown in Figure 36

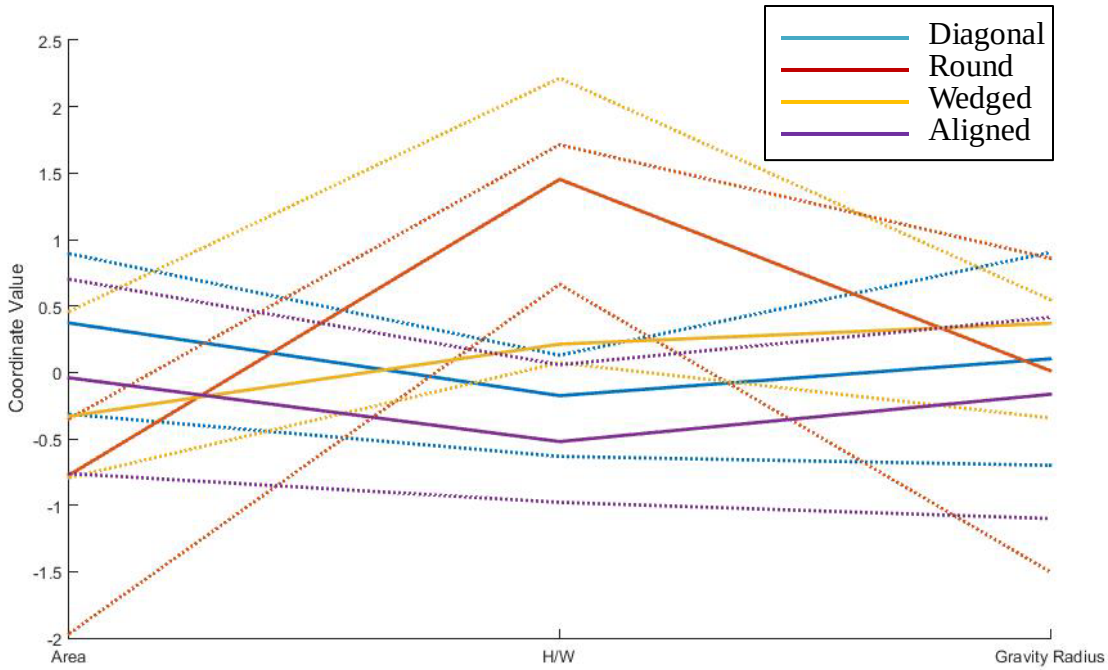


**Figure 36.** The features of fruit area, height-width ratio (H/W), and gravity radius are compared between the orientation and shape cases of diagonal, round, wedged, and aligned strawberries. These cases are represented by the colors blue, red, yellow, and purple, respectively. The coordinate value is a standardized value, where each variable has been standardized to have zero mean and unit variance. Approximately 300 strawberries were sampled. The solid colored lines represent the mean value, and the dotted lines represent the $40^{th}$ and $60^{th}$ quantiles. This analysis was performed using MATLAB Machine Learning and Statics toolbox (Mathworks).

The analysis indicated that for the fruit blob, the following data was necessary: *cog*, pixel area, *x*-axis projection, and bounding box coordinates. It was later determined that the number of fruit blobs per lane could help identify additional cases. For the leaf blob, only the pixel area and pixel location were critical. The binary features used to identify each case are summarized in Table 4.

**Table 4.** The fruit and leaf blob parameters used to identify strawberry cases are listed. The decision to either attempt a calyx removal procedure (accept) or actively avoid cutting the strawberry (reject) is indicated in brackets under each case.

| Strawberry Case | Fruit Binary Feature | Leaf Binary Feature |
|---|---|---|
| **Aligned (Reference) [Accept]** | *Cog*<br>Pixel Area<br>*x*-Axis Projection<br>Number of Blobs Per Lane<br>Bounding Box Coordinates | Pixel Area<br>Pixel Location |
| **Multi-Berry [Reject]** | *Cog*<br>Number of Blobs Per Lane | Pixel Location |
| **Perpendicular [Reject]** | *Cog* | Pixel Location |
| **Tip-Up [Reject]** | N/A | Pixel Area < 50 |
| **Calyx-Up [Reject]** | *Cog*<br>Pixel Area < 500<br>Number of Blobs Per Lane | Pixel Location<br>Pixel Area > 2500 |
| **Diagonal [Accept]** | *Cog* | Pixel Location |
| **Round [Accept]** | *Cog*<br>*x*-Projection<br>Bounding Box Coordinates | N/A |
| **Wedge [Accept]** | *Cog*<br>*x*-Projection<br>Bounding Box Coordinates | N/A |
| **Overlap [Accept]** | *Cog*<br>Bounding Box Coordinates | N/A |
| **White Shoulder [Accept]** | N/A | N/A |

#### 8.3.2.2 Rejection Algorithm Sensitivity vs. Specificity Analysis

During the last two weeks of the pilot study, 200 imaged strawberries were randomly selected to test the rejection algorithm's accuracy. A sensitivity and specificity analysis of the data is shown in Table 5. The analysis indicated that the rejection algorithm's sensitivity was high at 93.0 percent; however, at 74.1 percent, the specificity could be improved. This indicated that the majority of ideally oriented strawberries were identified correctly. Given the high sensitivity, it is possible to increase the specificity by raising the threshold of what is considered an ideally oriented strawberry.

**Table 5.** Sensitivity and specificity data for the strawberry rejection algorithm is shown.

| Rejection Sen. vs. Spec. | | Human-Defined | | |
|---|---|---|---|---|
| | | Accept | Reject | Total |
| AVID Vision System | Accept | 107 (a) | 22 (b) | 129 |
| | Reject | 8 (c) | 63 (d) | 71 |
| | Total | 115 | 85 | 200 |

$$Sensitivity = \frac{a}{a+c} = \frac{107}{115} = 93.0\%$$

$$Specificity = \frac{d}{b+d} = \frac{63}{85} = 74.1\%$$

$$Predictive\ value\ of\ a\ positive\ test = \frac{a}{a+b} = \frac{107}{129} = 83.0\%$$

$$Predictive\ value\ of\ a\ negative\ test = \frac{d}{c+d} = \frac{63}{71} = 88.7\%$$

In terms of output production, the strawberries in cell (b) of Table 5 are considered Residual fruit, while the strawberries in cell (c) of Table 5 are considered Return Fruit. Depending on the end-user's production requirements, the rejection algorithm can be optimized accordingly.

#### 8.3.2.3 Cut-Line Assignment

The most accurate algorithm for the aligned case strawberry had a mean absolute error of 4.07 pixels, or about 2mm (see Figure 37). The algorithm utilized both a shortening and lengthening correction factor to adjust the initial predicted *BcCl* length.

**Figure 37.** A bar graph of the average absolute error is shown for multiple cut-line improvement methods. The features used in each method are shown along the *x*-axis. The standard error is shown for each method.

In addition, the shortening and lengthening correction showed a tight error distribution amongst the many different aligned case strawberry images, as seen in Table 6.

**Table 6.** Descriptive statistics describing the absolute error distribution of the cut-line prediction algorithm implementing the shortening and lengthening correction factors are shown. This analysis was generated using Excel 2010.

| Descriptive Statistics for Aligned Case | |
|---|---|
| Mean | 4.07 |
| Median | 4 |
| Mode | 1 |
| Standard Deviation | 2.97 |
| Minimum | 0 |
| Maximum | 20 |
| MOE at Confidence Level (95.0%) | 0.34 |

Furthermore, the miss rate of the aligned case algorithm was seen to be minimal with the use of both a shortening and lengthening correction factor to adjust the initial predicted *BcCl* length (see Figure 38).

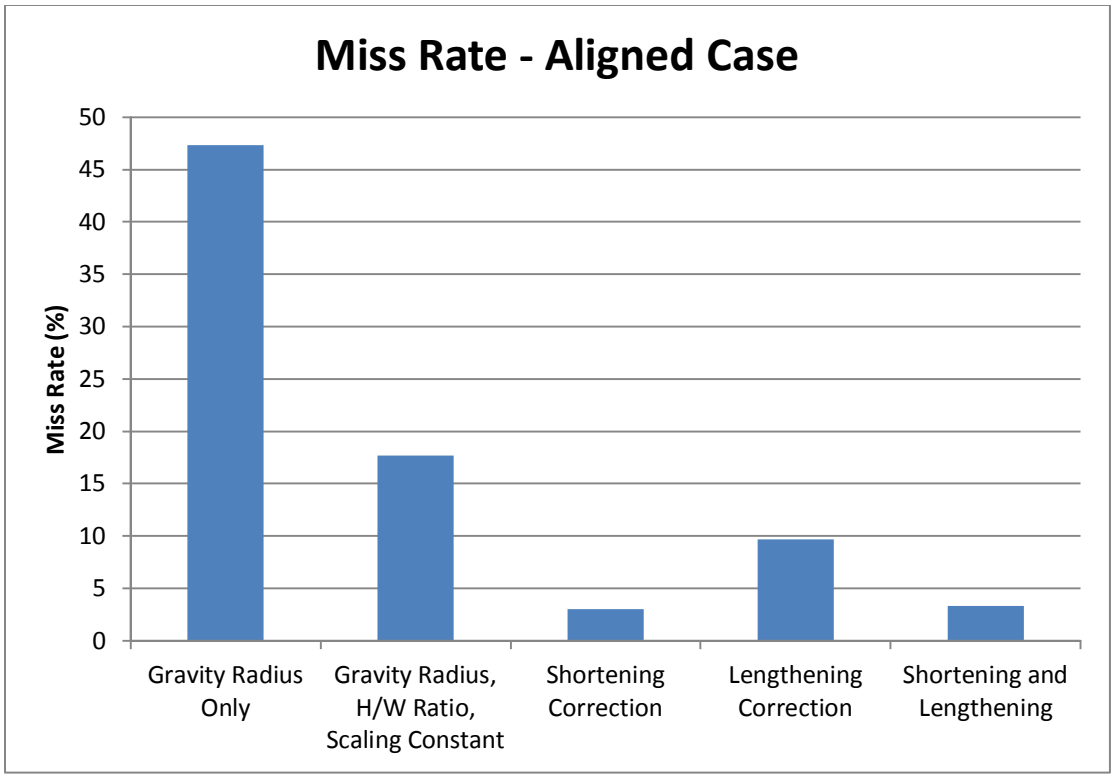


**Figure 38.** The number of negative error (miss) occurrences is shown for the aligned case. The sample size is 300 strawberries.

The cases for wedge, diagonal, and round also showed that including the shortening and lengthening parameters were optimal in both cut accuracy and miss rate. The coefficients for these parameters differed significantly from case to case.

### 8.3.3 Previously Performed HSI Results

The first generation blue rollers allowed for an HSI approach, where H is Hue, S is Saturation, and I is Intensity. However, this approach was found to be ineffective when stainless steel rollers were used in the final iteration of the machine, because the steel's gray color caused severe noise in the Hue channel of the HSI domain. Figure 39 shows the preliminary results of the achievable fidelity in identifying fruit and leaf blobs. The row containing the two strawberries is the region of interest; the

strawberry in the top right corner was neglected during image processing and analysis. The image's RGB data is shown in Figure A, and subsequent Hue, Saturation, and Intensity data is shown in Figures B, C, and D, respectively. These figures clearly illustrate that the Hue and Saturation pixel data provided a significant distinction between strawberry fruit, strawberry calyx, and surrounding background. However, when using the Intensity data, it was more difficult to distinguish these regions.

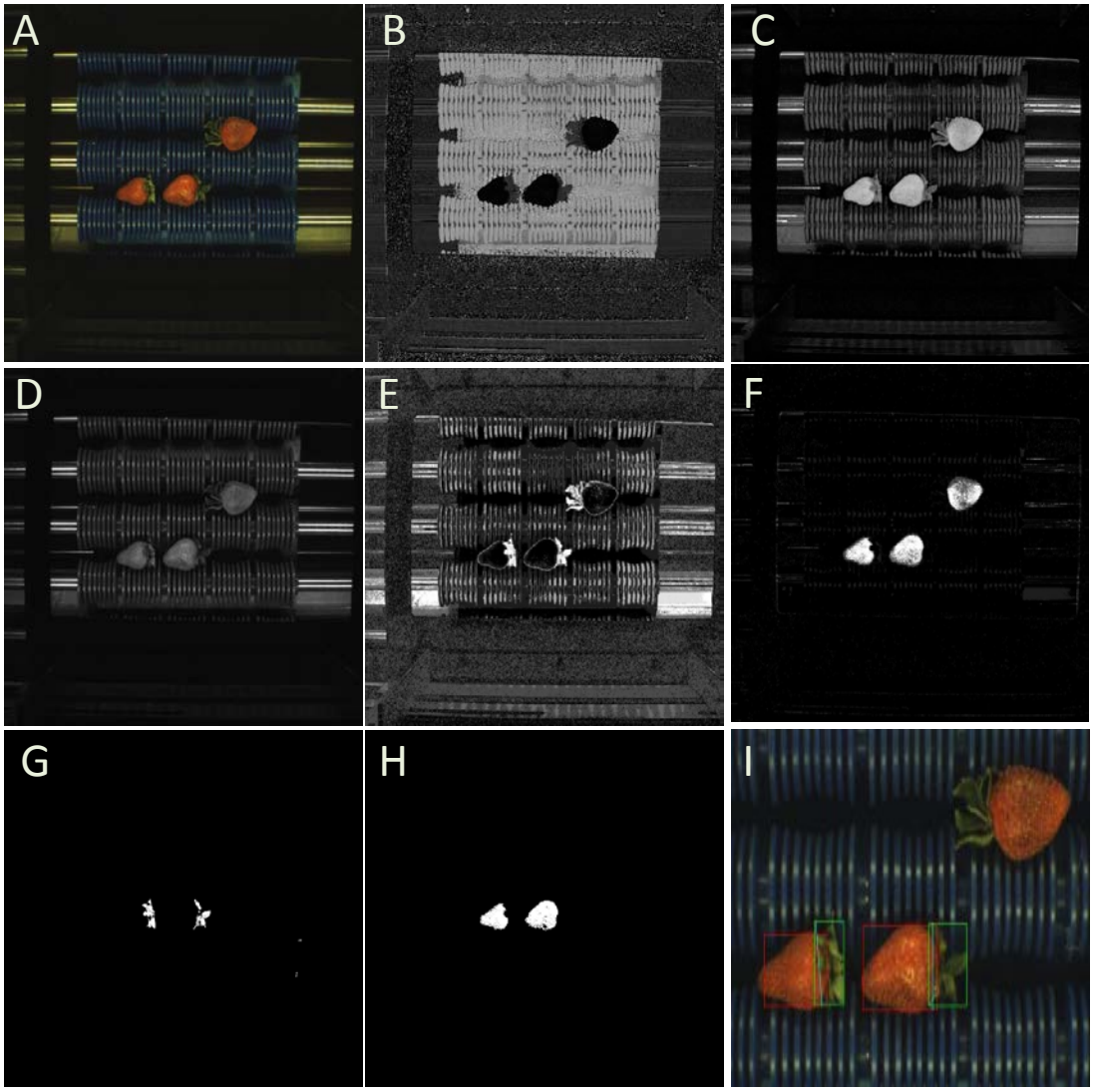


**Figure 39.** The steps of the HSI image processing are shown. (A) Initial image acquired from camera. (B) The Hue space of the initial image. (C) The Saturation space of the initial image. (D) The Intensity space of the initial image. (E) User-defined calyx color is compared to the Hue, Saturation, and Intensity information to display whiter pixels as calyx. (F) A user-defined strawberry color is compared to the Hue, Saturation, and Intensity information to display whiter pixels as strawberry fruit. (G) The results of a threshold on Figure E to identify calyx regions. (H) The results of a threshold on Figure F to identify fruit regions. (I) An image of the real-time vision algorithm identifying the calyx location and the strawberry fruit. The line indicates the cutting coordinates that will be sent to the cutting actuation system.

The histograms of the Hue, Saturation, and Intensity values are shown in Figure 40. Histogram values indicating strawberry fruit and calyx are distinguished by a red or green double arrow sign, respectively. These ranges were based on user-defined regions of a training image. The data confirmed the initial visual inspection that Hue and Saturation data could more easily distinguish between strawberry fruit and calyx. In particular, the Hue data was almost bimodal, with little cross-variance between fruit and calyx.

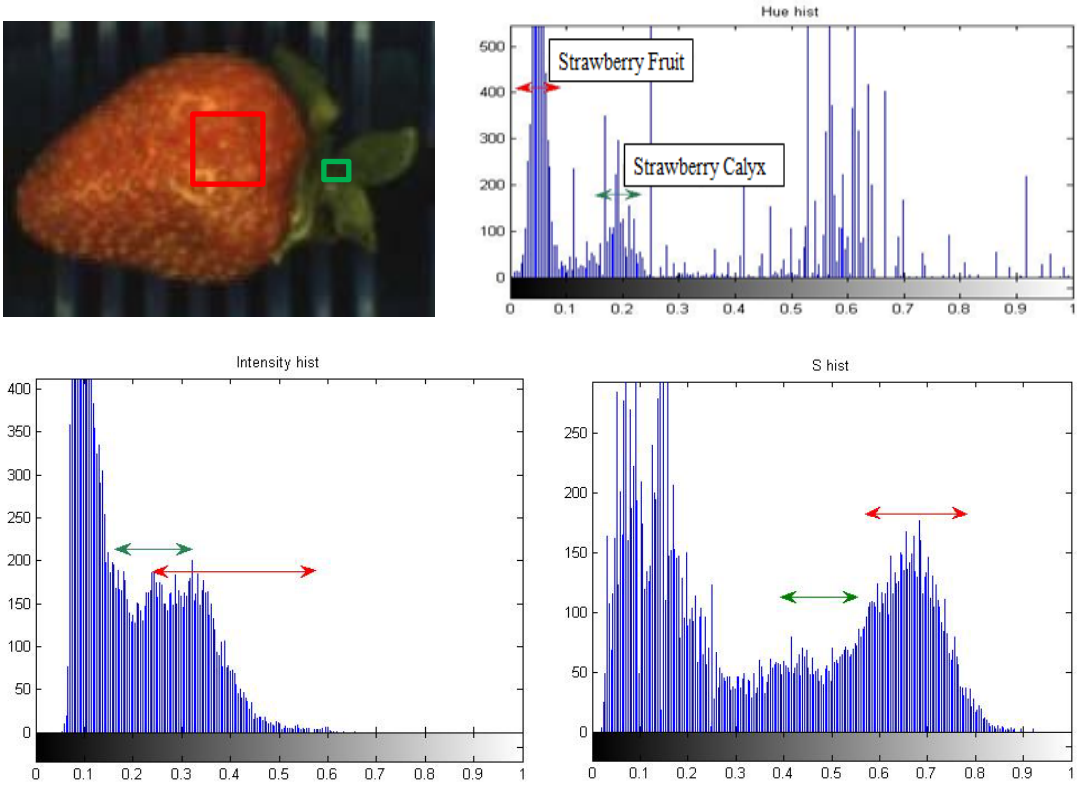


**Figure 40.** Hue, Saturation, and Intensity histograms of an image captured during a live run. A depiction of how a user defines the strawberry fruit and calyx region is shown on the top left. An average value for each Hue, Saturation, and Intensity space is determined based on these regions and a fixed range is set. The ranges for strawberry fruit and calyx are shown in red and green, respectively.

Although the HSI approach could not be used for this current version of the AVID machine, the high fidelity strawberry fruit and leaf binary images produced are

notable. This image analysis method required little noise reduction and was computationally low cost.

### 8.4 Ongoing Improvements

More advanced algorithms are being investigated to improve calyx identification accuracy and to better determine optimal calyx removal coordinates. We are exploring simple graph-based algorithms to identify the calyx location. This may be able to account for more image scenarios. Concurrently, we are further developing a decision tree where we can manually program the current algorithm to recognize problem image scenarios. The decision tree will allow for improved calyx removal coordinate identification. Overall, this will make the vision system more adaptive. However, any approach we implement must be within the computational complexity limitations necessary for cost effective real-time high-throughput calyx identification.

# Chapter 9: Evaluation of Waterjet Cutting Technology Used for Calyx Removal

Waterjet cutting technology is combined with servomotors to create a high-speed calyx removal actuation system. A high-pressure waterjet pump produces a powerful thin stream of water able to produce knife-like cut quality for calyx removal. Servomotors are used to position the water stream in the appropriate location, as determined by the vision system.

## 9.1 Introduction

In the last two decades, interest in waterjet cutting for food applications has grown significantly due to its benefits in overall cost and quality (Corp, 2001). The standard blade cutting of food products, especially fruit, injures or even "cooks" cells at the cut surface and below as a result of friction (FlowCorp, 2001). Such damage is not always apparent to the naked eye, but can result in a significant reduction of the product's shelf life. In contrast, the precise, low-temperature operation of a waterjet cutting system cuts with very little cell damage and thus can extend the product's shelf life (Tatsumi, Watada, & Ling, 1993). In addition, knives and saws need to be cleaned, sharpened, and replaced frequently. However, a nozzle orifice in a waterjet system commonly lasts over 500 hours and can be replaced in less than a minute. Furthermore, the danger of product contamination from broken saw blades or knives is eliminated with the waterjet.

## 9.2 Materials and Methods

### 9.2.1 Waterjet Positioning System

The waterjet calyx removal system consists of a custom high-pressure water pump and a servomotor-driven nozzle positioning unit. The AVID system used a 50 horsepower intensifier pump that was factory-limited to 30,000 psi in order to increase the maximum pressurized water output. The lower pressure also extended the maintenance cycle of all water-facing components. Furthermore, at this pressure, the risk of occupational hazards was decreased. A diamond orifice nozzle was used to concentrate the high-pressure water into a thin stream. This waterjet stream would remove the calyx off each strawberry with knife-like cut quality. The pressure and nozzle orifice size were optimized to increase cut quality, decrease water consumption, and extend the pump maintenance cycle. Each water nozzle was stationed over a lane of strawberries formed by the material handling system, as seen in Figure 41. Given the precise coordinates of the calyx from the vision system, actuators would position the water knife accordingly.

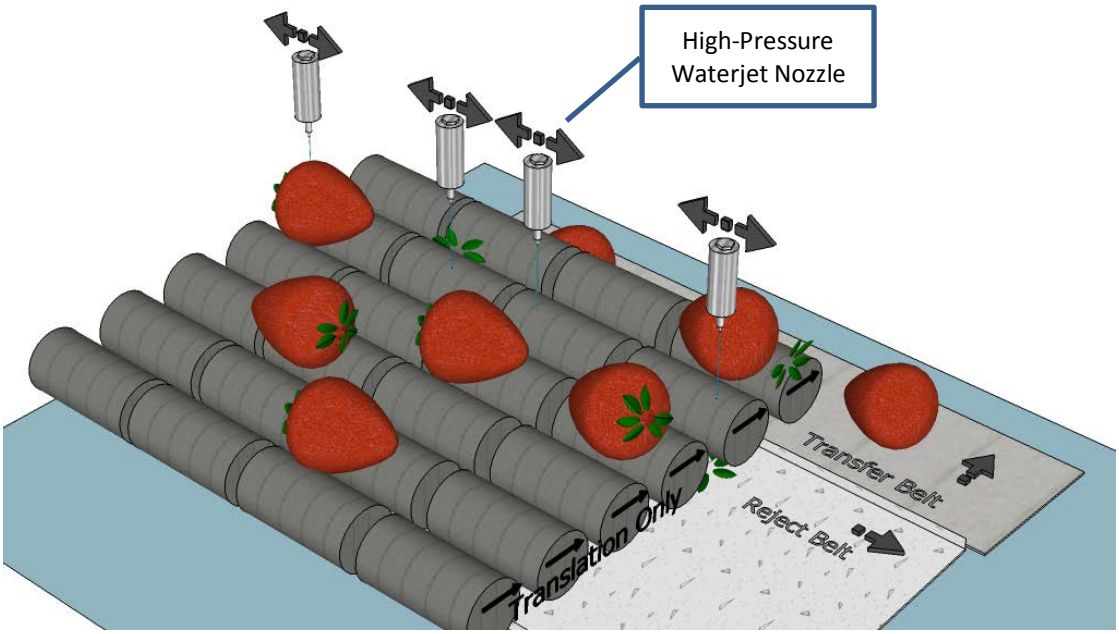


**Figure 41.** High-pressure waterjet cutting system for strawberry calyx removal. Only the waterjet nozzles are shown here for clarity. One nozzle is stationed over one lane of strawberries. Servomotor-driven actuators will position the nozzles in the correct location depending on strawberry calyx position.

The positioning system consisted of three main components: the controller, drive, and servomotor. In general, the controller sends the positioning data to the drive, which then powers the servomotor to the correct position. In this machine, the controller was a Dell Precision T7600 computer running Windows 7 Professional 64-bit, the drive was a Kollmorgen AKD-P00606, and the servomotor was a Kollmorgen AKMH44E. The vision system identified calyx removal cutting coordinates as described previously. For each lane, the calyx coordinate was then discretized into one of 128 cutting positions that spanned the lane's width. The computer sent the selected cutting position to the drive over Modbus TCP/IP communication protocol. After the drive determined the best motion profile to reach the desired position from the nozzle's current position, the selected motion task was sent to the servomotor.

This would move the directly coupled nozzle arm to its appropriate position. A control diagram of the actuation system is shown in Figure 42.

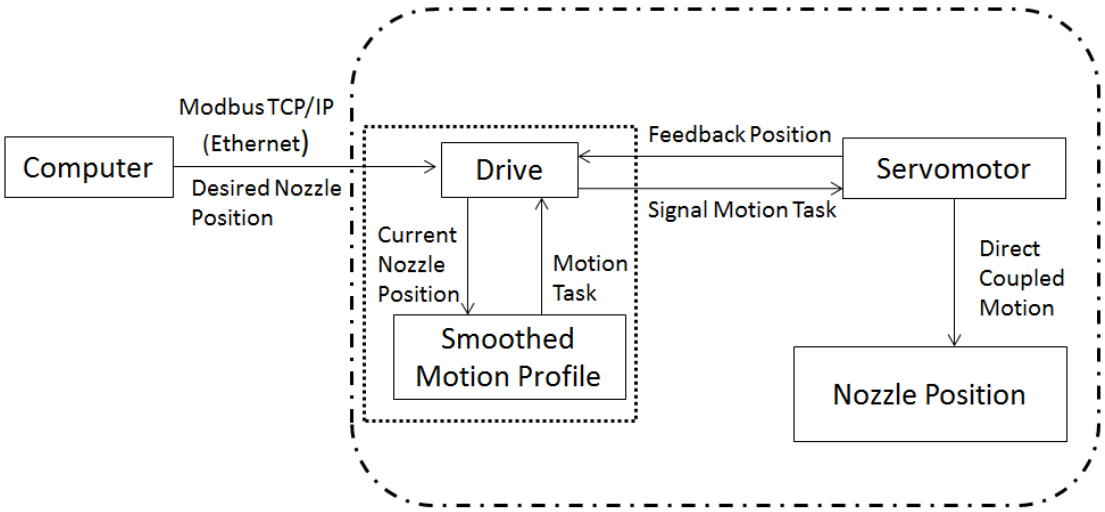


**Figure 42.** A control diagram of the waterjet calyx removal actuation system is shown. The computer only needs to provide the desired cutting position; the drive will find how to position the nozzle accordingly.

The drive created the smoothed motion profile by applying a Gaussian curve to the starting and stopping motion ramps. This method of using the drive to create the motion profile significantly decreases the computation cost on the computer, allowing more processing power to be allocated to the vision algorithms.

### 9.2.2 Strawberry Stabilization

In order to maintain an accurate high-quality calyx removal cut, the strawberry was first stabilized through pressured air jets before entering the waterjet cutting stream. The air jets were constantly on and were provided by two parallel air manifolds positioned symmetrically on either side of the nozzle above the strawberry, as seen in Figure 43.

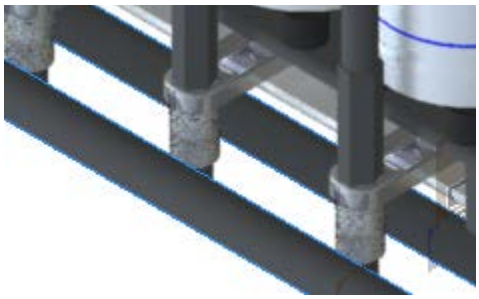

**Figure 43.** A rendering of the air manifold position respective to the waterjet cutting nozzles is shown. The air manifold is highlighted in blue. The manifold consists of two pipes that symmetrically surround the waterjet cutting nozzle. This allows for air jets to stabilize the strawberry before it enters the waterjet cutting stream.

To find the optimal air pressure, flow rate, and angle of impact, simulations were developed using ANSYS FLUENT. This computational fluid dynamics software utilizes finite elements and finite volume techniques to solve for complex physical models. It does this by subdividing the flow domain into a large number of finite elements or control volumes, then solving the governing fluid flow equations. In addition, this software allows for object mesh to be imported through computer automated design files. This provides a more uniform reference for creating simulations across different simulation software (www.fluent.com, 2016).

The parameters that were varied and optimized for peak resultant stabilization force were air pressure, orifice diameter, and height above strawberry. To see the effect the air jets had on strawberries entering the cutting stream, two time points were inspected. For the first time point, the strawberry plane of symmetry was offset 1/4 inch from the air manifold's plane of symmetry. This simulated the position of the strawberry entering the waterjet cutting stream. For the second time point, the strawberry plane of symmetry was flush with the air manifold's plane of symmetry.

This provided further insight into the air jet's impact on strawberry stabilization during waterjet cutting.

### 9.3 Results and Discussion

#### 9.3.1 Waterjet Knife Optimization

The waterjet knife pressure was optimized to increase cut quality, decrease water usage, and increase time between maintenance cycles. Examples of cut quality produced from a range of 25,000 psi to 35,000 psi with a 0.005-inch orifice nozzle are shown in Figures 44 and 45. The tests were performed on strawberries with widths ranging from 1.25 to 1.75 inches. At low pressures, the strawberry cut was visibly striated, signifying poor cut quality. At pressures below 25,000 psi, the strawberry was not fully severed.

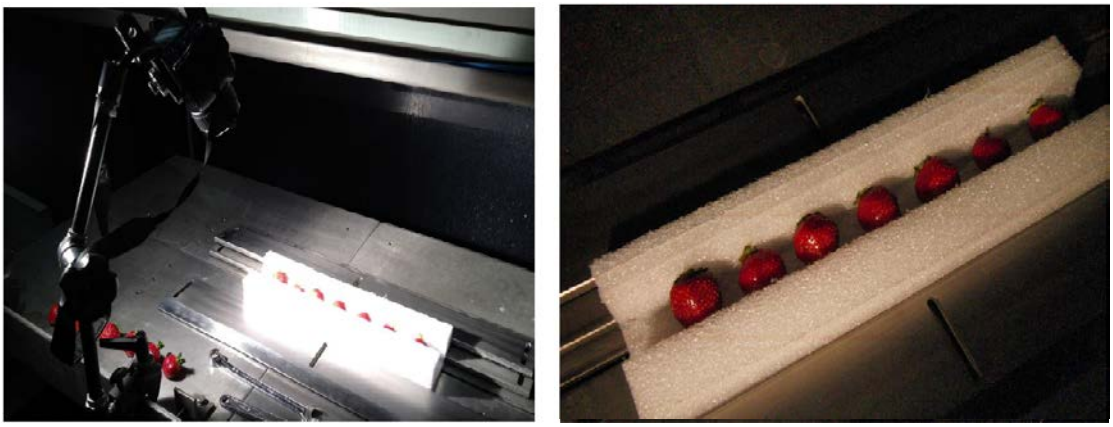

**Figure 44.** The experimental setup for waterjet cut quality optimization. The strawberries are placed in a foam container to prevent rolling. The waterjet nozzle then cuts the calyxes off the strawberries at 1 foot per second. The pressure and nozzle orifice size are varied.

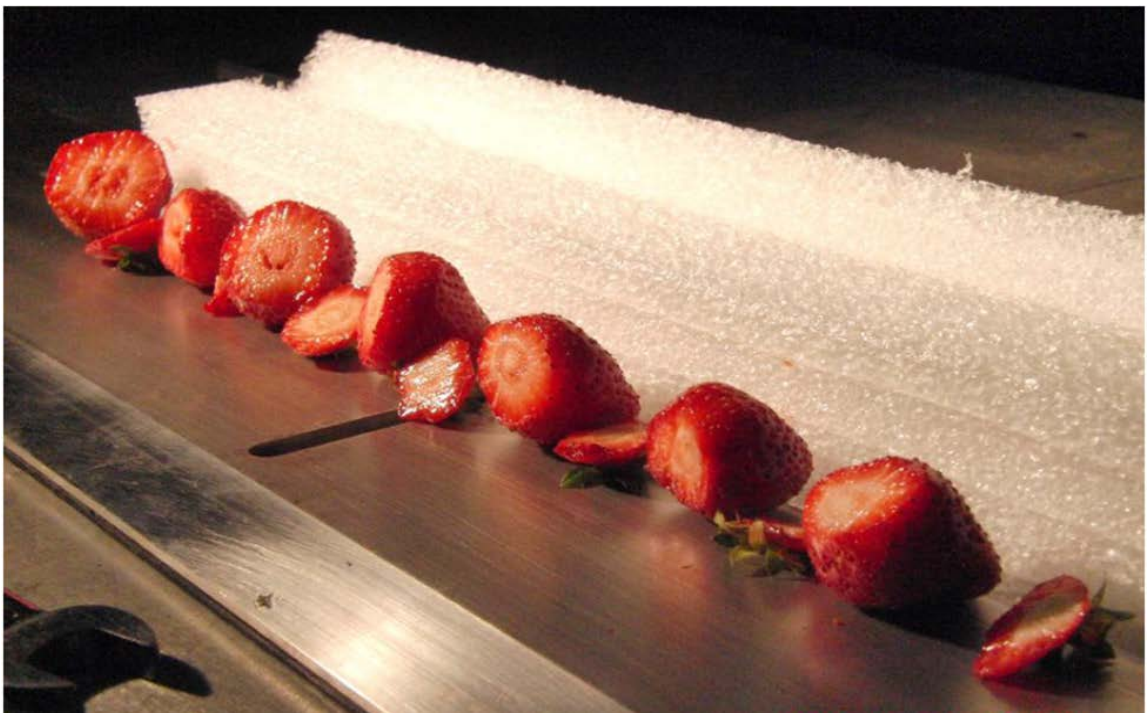

**Figure 45.** The de-calyxed strawberries of the waterjet cut quality optimization experiments using a 0.005-inch orifice nozzle are shown. The strawberry widths range from 1.25 to 1.75 inches. Strawberries cut with water pressure ranging from 25,000 psi to 35,000 psi are placed from left to right. The lowest pressure cut (leftmost strawberry) shows distinct striation. However, as the pressure increases, so does the cut quality. The rightmost strawberry has a knife-like cut quality.

The optimal cutting parameters were determined through varying orifice size and water pressure. These two parameters effectively determined the amount of power that was generated by the nozzle's cutting stream. Increasing either orifice size or water pressure would increase the waterjet stream's cutting abillity. The results of the optimzation are shown in Figure 46.

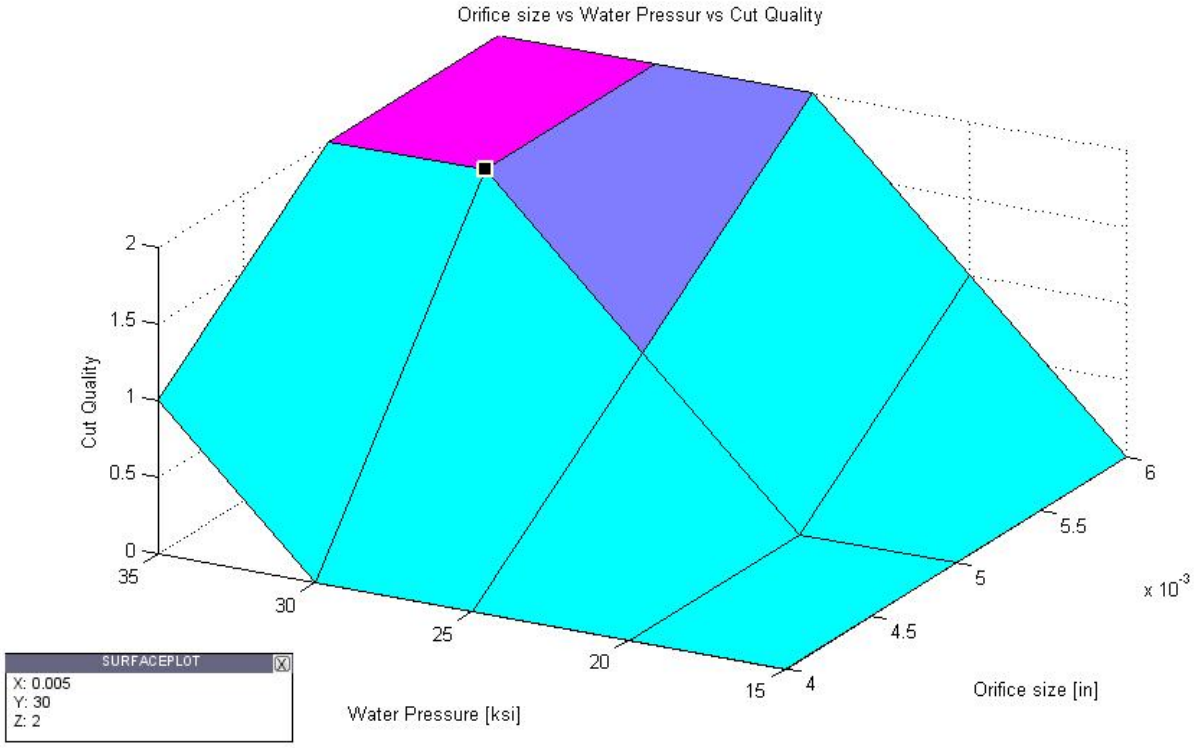


**Figure 46.** The relation between orifice size and water pressure on cut quality is shown. The cut quality is broken up into three grades: 0, 1, and 2. Grade 0 indicates that the strawberry's calyx was not fully separated. Grade 1 indicates the calyx was removed; however, there was a significant amount of striation associated with the cut surface. Grade 2 indicates the cut showed a knife-like quality. The data shows that as water pressure and orifice size increases, the cut quality also increases. The selected cut quality optimization point is indicated by the black marker. These parameters are shown in the text box located in the lower left corner.

The 0.005-inch orifice size and 30,000 psi pressure parameters were selected due to their resultant high cut quality, cut consistency, and relatively low water usage. Additionally, the tests found that there was a limitation to how high the water pressure level could be set. At higher pressures, the waterjet stream would cause the strawberry and its neighbors to jostle within their roller rod cups. This was a result of the water stream's increased speed moving a more significant amount of air due to the Venturi effect. This would occasionally cause the nozzle to miss its targeted location. This limitation was accounted for when selecting the orifice size and pressure setting.

Furthermore, when operating at these cutting parameters, the calyx removal actuation system was able to run at full capacity using only 2.1 gallons of water per minute.

### 9.3.2 Waterjet Positioning System

The separation of the controller from the drive and servomotors was seen to be an effective method for providing quick response times with accurate positioning results (see Figure 47). The limiting factor within the response time was the Modbus TCP/IP communication. The baud rate was seen to be roughly 10,000 bits per second. This produced a response time of approximately 40ms, starting from when the control signal was sent, at the falling edge of the conveyor encoder pulse, to when the waterjet nozzles began to move. It should be noted that when the control signal was passed through up to four Ethernet switches, the response time increased by roughly 5ms.

The time necessary to perform a full swing from one end of the strawberry lane to the other, within an error of 10 percent, was approximately 100ms. Although this reaction time was sufficient for the current version of the AVID machine, the speed could be easily improved by increasing controller gains.

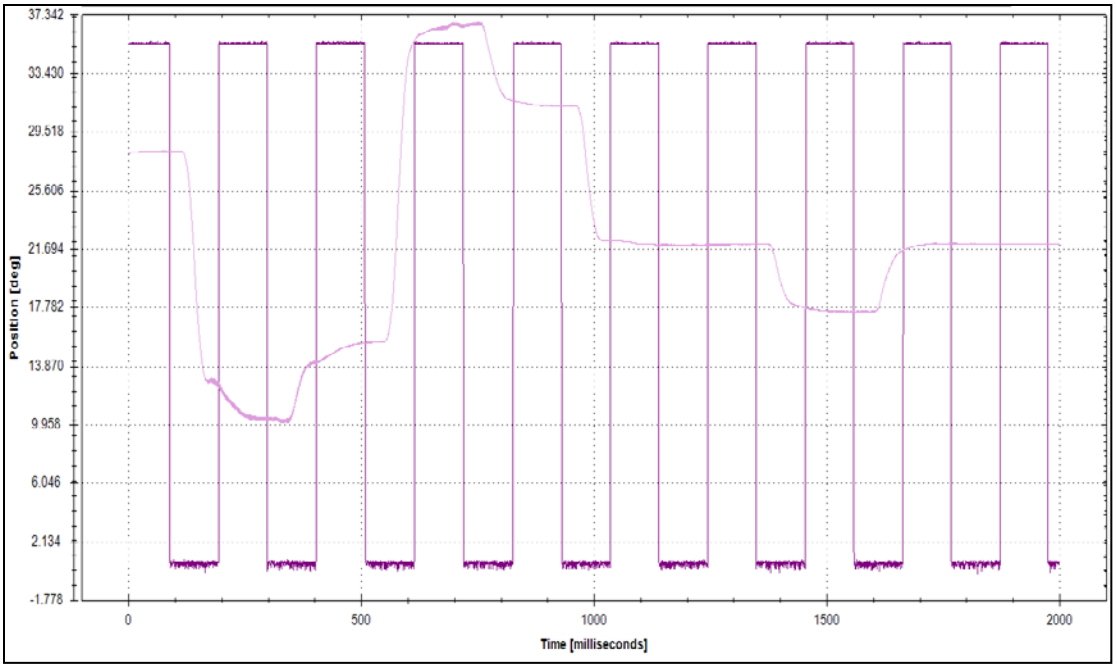


**Figure 47.** A trace of the waterjet cutting nozzle position in relation to conveyor encoder pulse is shown. The AVID machine's conveyor encoder pulse is seen as the square purple signal train. The position of the waterjet cutting nozzle is seen as the pink trace. If a strawberry is present in the lane, the control signal will be sent to the positioning system on the falling edge of the encoder pulse. If no strawberry is present, the nozzle position will remain near degree 22.

During live runtime of the AVID machine, the drive would produce a periodic high frequency noise. This has been attributed to the servomotors attempting to maintain a fixed position during the waterjet calyx removal process. The high controller gains caused the motor to dither around the fixed position, which in turn caused the high frequency noise (see Figure 48). It should be noted that the noise could be mitigated through better tuning of the control loop gains.

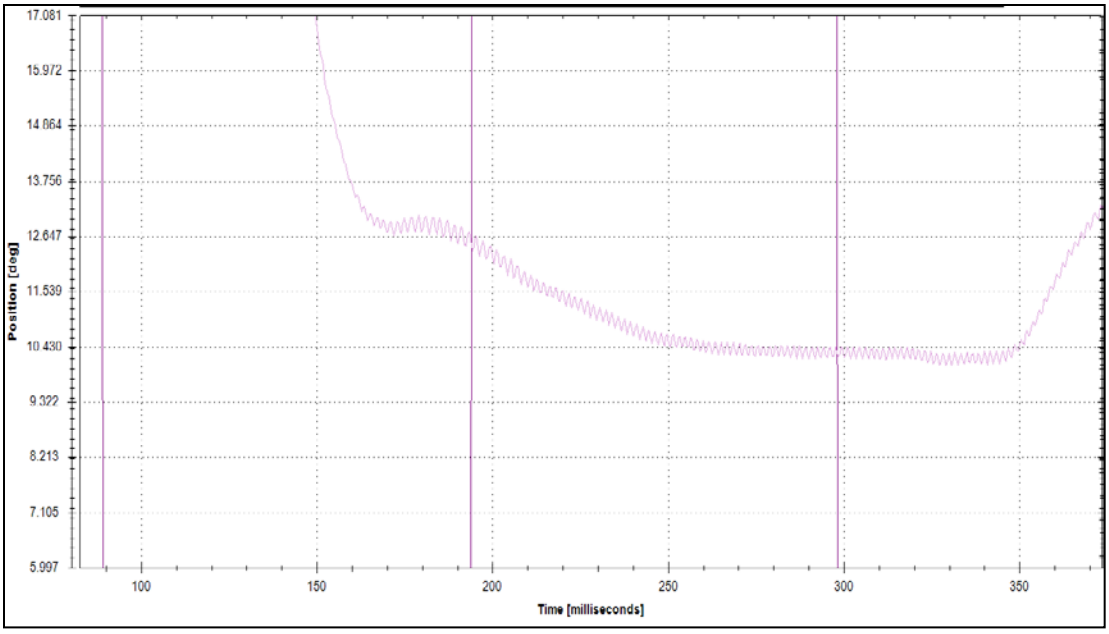


**Figure 48.** A magnified image of the waterjet cutting nozzle position trace is shown. The sharp tooth-like structure of the trace indicates vibration.

Overall, the actuation system was able to precisely position the waterjet nozzle toward the vision guided target location. There were no computing or signaling errors found during the eight weeks of testing. However, the repetitive fast movements of the nozzles did cause vibrations in the AVID frame. This will be accounted for in the future design.

### 9.3.3 Air Jet Stabilization

The air jets used to stabilize the strawberry during the waterjet calyx removal process were optimized to apply the maximum downward force while utilizing the least amount of high-pressure air. The multi-physics simulations indicated that two sets of four nozzles of 0.042-inch orifice diameter positioned above the strawberry could supply enough stabilizing force (see Figure 49). The spacing of the nozzles was set to 0.75 inches to evenly cover one strawberry lane. These simulations further

suggested that at 70 psi air pressure, the nozzles could be fabricated from a pair of cylindrical tubes where the nozzles are directed at the strawberry 120 degrees apart from one another.

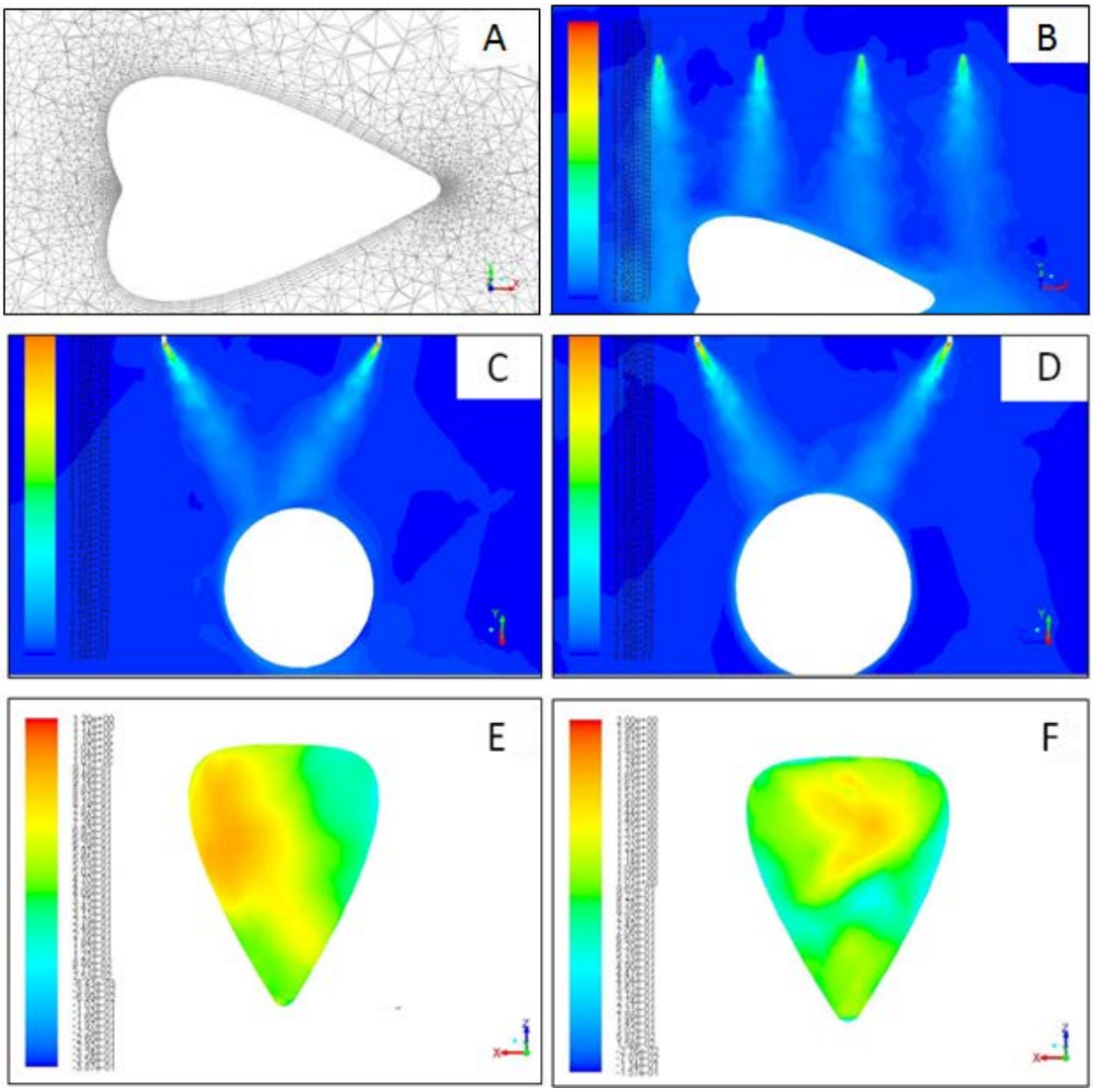


**Figure 49.** The resultant velocity and pressure contours of the air manifold are shown. (A) The geometric mesh used for the simulation. (B) A velocity profile of the plane bisecting one of the air manifold's nozzle streams when the strawberry is directly under the waterjet cutting stream. (C) A front view of the air velocity contour profile of a strawberry entering the waterjet cutting stream. (D) A front view of the air velocity contour profile of a strawberry directly under the waterjet cutting stream. (E) The resultant pressure contours on a strawberry entering the waterjet cutting stream. (F) The resultant pressure contours on a strawberry directly under the waterjet cutting stream. The simulations were created using ANSYS Fluent 15.0.

The nozzle angle and height position of 120 degrees apart and 1.1 inches high were seen to provide optimal stability during both simulated stages of the calyx removal process. This included when the strawberry entered the waterjet cutting stream and when the strawberry was directly underneath the waterjet cutting stream.

The results of the simulated force components on the strawberry are shown in Table 7. The effect of strawberry diameter, nozzle orientation and position, and air pressure are seen on resultant strawberry stabilization forces.

**Table 7.** The simulated air manifold strawberry stabilization force results are shown. The parameters that were varied are: strawberry diameter, air manifold angle and position, and air supply pressure. Cases 1 through 8 are of the strawberry first entering the waterjet cutting stream, and cases 9 through 16 are of the strawberry when it is directly under the cutting stream. This simulation was completed using ANSYS Fluent 15.0.

| Case | Strawberry OD | Angle | Height (in) | Orifice OD (in) | Pressure (psi) | Force Y (lbf) | Force X (lbf) | Force Z (lbf) |
|---|---|---|---|---|---|---|---|---|
| ***Strawberry Entering Waterjet Cutting stream*** | | | | | | | | |
| **1** | 1.25" | min | 0.725 | 0.042 | 100 | 0.320 | 0.033 | 0.128 |
| **2** | 1.25" | 120 | 1.107 | 0.042 | 100 | 0.227 | 0.013 | 0.204 |
| **3** | 1.25" | min | 0.725 | 0.03 | 100 | 0.200 | 0.017 | 0.120 |
| **4** | 1.25" | 120 | 1.107 | 0.03 | 100 | 0.211 | 0.024 | 0.093 |
| **5** | 1.25" | min | 0.725 | 0.042 | 70 | 0.232 | 0.027 | 0.130 |
| **6** | 1.25" | 120 | 1.107 | 0.042 | 70 | 0.264 | 0.051 | 0.094 |
| **7** | 1.25" | min | 0.725 | 0.03 | 70 | 0.119 | 0.019 | 0.069 |
| **8** | 1.25" | 120 | 1.107 | 0.03 | 70 | 0.084 | 0.012 | 0.010 |
| ***Strawberry Directly Underneath Waterjet Cutting Stream*** | | | | | | | | |
| **9** | 1.25" | min | 0.7 | 0.042 | 100 | 0.529 | 0.182 | 0.083 |
| **10** | 1.25" | 120 | 1.1 | 0.042 | 100 | 0.423 | 0.171 | 0.016 |
| **11** | 1.25" | min | 0.7 | 0.03 | 100 | 0.200 | 0.002 | 0.015 |
| **12** | 1.25" | 120 | 1.1 | 0.03 | 100 | 0.194 | 0.014 | 0.006 |
| **13** | 1.25" | min | 0.7 | 0.042 | 70 | 0.347 | 0.007 | 0.075 |
| **14** | 1.25" | 120 | 1.1 | 0.042 | 70 | 0.316 | 0.143 | 0.030 |
| **15** | 1.25" | min | 0.7 | 0.03 | 70 | 0.167 | 0.028 | 0.024 |
| **16** | 1.25" | 120 | 1.1 | 0.03 | 70 | 0.186 | 0.021 | 0.007 |

The air manifold design was verified empirically with a wide range of strawberry shapes and sizes. The air pressure was varied between 50 – 100 psi. It was seen that 70 psi air supply could sufficiently prevent the strawberry from moving during the waterjet cutting process. A comparison between the calyx removal results with and without the use of air jet stabilization is shown in Figure 50.

**Figure 50.** The results of attempted calyx removal without any attempt at strawberry stabilization (left) and with the use of air jet stablization (right) are shown.

It was seen that without any form of strawberry stabilization, the majority of strawberries would rock within the material handling's roller cup. This would create a V-shape or wave-shape cut pattern. This movment was seen to also significnatly decrease accuracy of the calyx removal procedure and would result in residual leaf being left on the strawberry.

### 9.4 Ongoing Improvements

The design of the actuation system is currently being optimized to decrease power usage and frame vibration, and improve ease of maintenance. The nozzle mass will be lowered to decrease the power consumption of the servomotors and also lower frame vibration. Passive dampeners will be installed between the actuator system and frame, which will further lower vibrations. In addition, an automated maintenance data acquisition protocol is being developed. This will allow for easier remote diagnosis of problems once installed in the field.

# Chapter 10: Conclusion

Based on our results and on-going progress, we believe an automated calyx removal system is highly feasible within the near future. Our material handling system has shown that strawberries can be oriented and positioned appropriately for efficient processing. The vision system can identify calyx locations with relatively high accuracy in real-time. The waterjet actuation system has been able to produce quick and reliable nozzle positioning consistently over a 10-week period. The results of our high-pressure waterjet cutting experiments allowed us to design an optimized system to produce excellent calyx removal results while decreasing the overall cost of the machine. Commercial manufacturers, distributors, and fabricators of the machine components have been found and relationships developed. The current progress has significantly advanced us to the goal of bringing calyx removal out of the fields and into an automated, controlled, and reliable environment.

# Chapter 11: Economic Impact

## 11.1 Cost Savings

The AVID machine is expected to reach a point of economic viability within the next two years. At this time, a commercial machine that is ready to be installed in a wide range of processing plants will have been developed. With an input of 1WC strawberries, this machine will be capable of producing an estimated output yield of 60 percent IQF whole berry, 15 percent IQF partial berry, and 25 percent juice berry at a rate of 5, 1, and 2 thousand pounds per hour, respectively. Given that the cost per pound of 1WC strawberries, IQF whole berries, IQF partial berries, and juice berries are roughly 22, 55, 45, and 18 cents, respectively, the profit and cost can be calculated from the equations below.

Profit

$$\left(0.6 * 55 \frac{Cents}{lb\ IQF\ W}\right) + \left(0.15 * 45 \frac{Cents}{lb\ IQF\ P}\right) + \left(0.25 * 18 \frac{Cents}{lb\ Juice}\right) = 40.55 \frac{Cents}{lb}$$

Cost

$$= 22 \frac{Cents}{lb\ 1WC}$$

Net Profit

$$(40.55 - 22) \frac{Cents}{lb} = 18.55 \frac{Cents}{lb\ 1WC} - Cost\ of\ AVID\ machines$$

As a hypothetical example, if there were high demand for IQF whole, IQF partial, and juice berries such that prices were to stay constant on average, regardless of the supply of each quantity, then using the AVID machine to process the 600 million pounds of California strawberries produced in 2014 (Noncitrus Fruits and

Nuts 2014 Summary, 2015) would have created over $110 million in profit, minus the annual cost of the AVID machines.

### 11.2 Field Labor Savings

An automated strawberry calyx removal system could significantly reduce field labor, improve management and logistics, and increase annual yield, while producing a better product. Given that the U.S. harvested 600 million pounds of strawberries for processing in 2014 (Noncitrus Fruits and Nuts 2014 Summary, 2015), and manual pickers take about 1 second to remove a calyx, we conservatively estimate the labor savings for 2014 as follows.

$$(600\ million\ lb)x\left(15\frac{Strawberries}{lb}\right)x\left(\frac{1.0}{3600}\right) = 2.5\ million\ field\ labor\ hours$$

Overall savings could be significant if the reclaimed 2.5 million field labor hours were used to harvest more strawberries for the fresh and processed markets. It should also be noted that this savings does not account for the savings from management and logistics, inconsistent field labor, or product loss due to spoilage and contamination.

# Chapter 12: Suggestions for Future Work

The AVID machine's 12-week pilot study in a food processing environment revealed many improvements that could be made. These improvements can be separated into two categories: efficacy and reliability. Based on a survey from a large portion of California strawberry processers, the throughput and yields of the output streams should be better optimized to meet market demands. Specifically, increased output yield of IQF whole berries is desired. This may require a higher level of cutting accuracy than can currently be provided. As a result, all three components of the AVID machine should be optimized. The material handling system should be redesigned to account for spherical and rectangular shaped strawberries. The machine vision system could further develop a database of strawberry images that would provide the basis for more advanced algorithms and possibly three-dimensional feature predictions. The waterjet cutting system could be upgraded to include an additional cutting axis. All of these improvements would increase calyx removal accuracy.

In terms of reliability, the material handling system and the machine vision system should be reinforced to better withstand daily sanitation procedures. In addition, the full AVID system must be redesigned for easier maintenance and repair. This will prepare the machine for the ever-increasing demands of food processing equipment. Furthermore, interlocks, guards, and sound barriers should be installed to meet OSHA standards.

## Bibliography

(2015). Retrieved from 3-A Sanitary Standards, Inc.: http://www.3-a.org.

(2016). Retrieved from PND Fruit Processing Machinery: http://www.pndsrl.it.

(2016). Retrieved from Seditec S.A.: http://www.seditec-sa.com.

Ara, T., Haydar, A., Mahmud, H., Khalequzzaman, K. M., & Hossain, M. M. (2009). Analysis Of The Different Parameters For Fruit Yield And Yield Contributing Characters In Strawberry. *Int. J. Sustain. Crop Prod., 4*(5), 15-18.

*AS-6050*. (2014). Retrieved from Accustream, a Hypertherm Company: https://www.accustream.com/products/waterjet-machines/as-series/as-6050.html.

Brosnan, T., & Sun, D. W. (2002). Inspection and grading of agricultural and food products by computer vision systems - a review. *Computers and Electronics in Agriculture, 36*, 193-213.

Chase, C. (2012, Nov). *Whole Farm Financial Analysis*. Retrieved 9 14, 2015, from Iowa State University Extension and Outreach: https://www.extension.iastate.edu/agdm/wholefarm/html/c3-65.html.

Corp, F. (2001). Waterjet Cutting In The Food Industry. Kent, WA, USA: Flow International Corporation.

Daming Dong, C. Z. (2013). Analyzing Strawberry Spoilage via its Volatile Compounds Using Longpath Fourier Transform Infrared Spectroscopy. *Nature*, 2585.

Daugovish, O., Klonsky, K. M., & De Moura, R. L. (2011). *Sample Costs To Produce Strawberries.* Oxnard: University Of California Cooperative Extension.

ERS. (2013). *U.S. Strawberry Industry (95003)*. Retrieved from Economic Research Service U.S. Department of Agriculture: http://usda.mannlib.cornell.edu/MannUsda/viewDocumentInfo.do?documentID=1381.

FAOSTAT. (2013). *Production Crops*. Retrieved from Food And Agriculture Organization Of The United Nations: http://faostat.fao.org/site/567/DesktopDefault.aspx?PageID=567.

Feng, G., Qixin, C., & Masateru, N. (2008). Fruit Detachment and Classification Method for Strawberry Harvesting Robot. *International Journal of Advanced Robotic Systems, 5*(1), 41-48.

FlowCorp. (2001). Ultrahigh-pressure Waterjets from FLOW offer many advantages over traditional food cutting methods. USA: Flow International Corporation.

(1992). *Grading Manual for Frozen Strawberries.* Washington DC: USDA.

Hartman, K. R., & Gerrans, A. W. (1963). *Patent No. 3092160.* USA.

Hayashi, S., Shigematsu, K., Yamamoto, S., Kobayashi, K., Kohno, Y., Kamata, J., & Kurita, M. (2010). Evaluation of a strawberry-harvesting robot in a field test. *b i o s y stems e n g i n e e r i n g, 105*, 160-171.

*How a Water Jet Machine Works.* (2013). Retrieved from Jet Edge Waterjet Systems: http://jetedge.com/content.cfm?fuseaction=dsp_applications_101.

Hughes, J. F., Van Dam, A., Mcguire, M., Sklar, D. F., Foley, J. D., Feiner, S. K., & Akeley, K. (2014). Computer Graphics Principles and Practice Third Edition. Boston: Addison-Wesley.

Iowa State University. (2014). *Commodity Strawberry Profile*. Retrieved from Agricultural Marketing Resource Center: http://www.agmrc.org/commodities__products/fruits/strawberries/commodity-strawberry-profile.

Janick, J., Brecht, J. K., & Saltveit, M. E. (2010). Fresh-Cut Vegetables and Fruits. *Horticultural Reviews*, 185-251.

Jordan, R. (1988). Water Jet Cutting at 20,000 PSI. *Society of Manufacturing Engineers*, 1-9.

Kress-Rogers, E., & Brimelow, C. J. (2001). Instrumentation and Sensors for the Food Industry. Sawston: Woodhead Publishing.

*Labor: US Fruits and Vegetables.* (2011, January). Retrieved from Rural Migration News: http://migration.ucdavis.edu/rmn/more.php?id=1596_0_5_0.

Leban, E. (1976). *Patent No. 3952646.* USA.

Ledebuhr, R. L., Hansen, C. M., & Patterson, R. J. (1978). *Patent No. 4122766.* USA.

Leo´n, K., Mery, D., Pedreschi, F., & Leo´n, J. (2006). Color measurement in L*a*b* units from RGB digital images. *Food Research International*, 1084-1091.

Liming, X., & Yanchao, Z. (2010). Automated strawberry grading system based on image processing. *Computers and Electronics in Agriculture, 715*, 532-539.

Mathworks. (n.d.). Natic, Massachusetts.

Matrox. (n.d.). Quebec, Canada.

*Mechanization Of Parts Handling*. (2008). Retrieved from http://www.eng.morgan.edu: http://www.eng.morgan.edu/~galexan/IEGR/Parts.htm.

Mohammad Ali Sahari, F. M. (2004). Effect of low temperature on the ascorbic acid content and quality characteristics of frozen strawberry. *Food Chemistry*, 357–363.

Niederer, T. O. (1980). *Patent No. 4382501*. USA.

(2015). *Noncitrus Fruits and Nuts 2014 Summary.* Washington DC: USDA, National Agricultural Statistics Service.

(2015). *Noncitrus Fruits and Nuts 2015 Summary.* Washington DC: USDA, National Agricultural Statistics Service.

Omid, M., Khojastehnazhand, M., & Tabatabaeefar, A. (2010). Estimating volume and mass of citrus fruits by image processing technique. *Journal of Food Engineering, 100*, 315-321.

Ortega, E., & Ortega, C. (2001). *Patent No. 0029825.* USA.

Pinder, A., & Godfrey, G. (1993). Food Process Monitoring Systems. Chapman & Hall.

Robertson, G. H. (1974). Liquid-Jet Penetrometry For Physical Analysis: Application To Bread Aging. *Journal of Food Science, 39*(6), 1247-1253.

Rose, B. W., & Thornton, G. W. (1975). *Patent No. 3894631.* USA.

Schlosser, E. (1995). In the Strawberry Fields. *The Atlantic Online*.

Shin, Y., Liu, R. H., Nock, J. F., Holliday, D., & Watkins, C. B. (2007). Temperature and relative humidity effects on quality, total ascorbic acid, phenolics and flavonoid concentrations, and antioxidant activity of strawberry. *Postharvest Biology and Technology*, 349–357.

Tao, Y. (2013). *California Strawberry Commission Annual Report 2012-2013.* Watsonville: California Strawberry Commission.

Tao, Y., Lin, J., Chen, X., & Seibel, G. (2014). *Patent No. 028602.* USA.

Tatsumi, Y., Watada, A. E., & Ling, P. P. (1993). Sodium Chloride Treatment or Waterjet Slicing Effects on White Tissue Development of Carrot Sticks. *Journal of Food Science, 58*(6), 1390-1392.

Turatti. (2013). *Machines for fruit: Strawberry capper*. Retrieved from Turatti the Future Today: http://www.turatti.com/index.php/sections-en/machinery/machines-for-fruit/frazer-en-US.

Wahl, C., Liegel, L., & Seavert, C. F. (2014). *Strawberry Economics: Comparing the Costs and Returns of Establishing and Producing Fresh and Processed Market June Bearing Strawberries in a Perennial Matted Row System to Day-Neutrals in a Perennial Hill, Plasticulture System, in the Willamette Valley.* Corvallis: OSU Extension Service.

Walker, J. T., & Bansal, R. (1999). A Study of High Pressure Water Jets For Cutting Chicken Breast Meat. *Journal of Food Process Engineering, 22*(4), 307-318.

Wu, F., Guan, Z., & Whidden, A. (2012). *Strawberry Industry Overview and Outlook.* University of Florida.

*www.fluent.com*. (2016). Retrieved from www.fluent.com.

Zhang, Y. (1996). A Survey on Evaluation Methods for Image Segmentation. *Pattern Recoynition, 29*(8), 1335-1346.